IRE Transactions on ANTENNAS and PROPAGATION

Volume AP-8 SEPTEMBER, 1960 Number 5

Published Bimonthly

In This Issue

PUBLISHED BY THE

Professional Group on Antennas and Propagation

IRE TRANSACTIONS® PGAP IS A PUBLICATION DEVOTED TO EXPERIMENTAL AND THEORETICAL PAPERS ON RADIO ANTENNAS, ON GUIDED OR UNGUIDED PROPAGATION OF RADIO WAVES, AND ON ALLIED FIELDS OF RADIO PHYSICS SUCH AS RADIO ASTRONOMY

MANUSCRIPTS should be submitted to Sidney A. Bowhill, Editor, 222 Electrical Engineering, Pennsylvania State University, University Park, Pa. Manuscripts should be original typewritten copy, double spaced, plus one carbon copy and two sets of copies of illustrations. Original illustrations will be called for if the paper is accepted. References should appear as footnotes and include author's name, title, journal, volume, initial and final page numbers, and date. Each paper must have a summary of not more than 200 words. News items concerning PGAP members and group activities should be sent to the News Editor, R. C. Hansen, Space Technology Laboratories, P.O. Box 95001, Los Angeles 45, Calif.

ORIGINAL ILLUSTRATIONS should be submitted as follows: All line drawings (graphs, charts, block diagrams, cutaways, etc.) should be inked uniformly and ready for reproduction. If commercially printed grids are used in graph drawings, author should be sure printer's ink is of a color that will reproduce. All halftone illustrations (photographs, wash, airbrush, or pencil renderings, etc.) should be clean and ready to reproduce. Photographs should be glossy prints. Call-outs or labels should be marked on a registered tissue overlay, not on the illustration itself. No illustration should be larger than 8 x 10 inches.

Copies can be purchased from **THE INSTITUTE OF RADIO ENGINEERS, 1 East 79 St., New York 21, N.Y. PRICE PER COPY:** members of the Professional Group on Antennas and Propagation, $1.50; members of the IRE $2.25; nonmembers, $4.50. **ANNUAL SUBSCRIPTION PRICE:** PGAP members, included in PGAP fee of $4.00; IRE members, $8.50; Colleges and public libraries, $10.00; nonmembers, $17.00. IRE TRANSACTIONS ON ANTENNAS AND PROPAGATION. Printed in U.S.A. Printed by George Banta Co., Inc., Curtis Plaza, Menasha, Wisconsin.

Second-class postage paid at MENASHA, WISCONSIN, and additional mailing offices under the act of August 24, 1912. Acceptance for mailing at a special rate of postage is provided for in the act of February 28, 1925, embodied in Paragraph 4, Section 412, P. L. & R., authorized October 26, 1927.

IRE Transactions on Antennas and Propagation

Volume AP-8 SEPTEMBER, 1960 Number 5
Published Bimonthly

TABLE OF CONTENTS

CONTRIBUTIONS

COMMUNICATIONS

contributions

Comparison of Experimental with Computed Tropospheric Refraction*

W. L. ANDERSON†, MEMBER, IRE, N. J. BEYERS‡, AND R. J. RAINEY†, STUDENT MEMBER, IRE

Summary—Limits of applicability of ray tracing in computing tropospheric refraction at White Sands Missile Range have been further explored. 286 comparisons were made, all for a path from radar to fixed beacon of about 45 miles and an elevation angle of 17.99 milliradians. A horizontally stratified atmosphere was assumed. Refractive index profiles were prepared from a variety of weather data, and classified A, B, C, or R, in descending order of reliability prior to ray-tracing calculations.

Angle observations were made with an FPS-16 C-band radar having a quoted instrumental accuracy of 0.14 milliradian rms. Angle readings varied from 18.36 to 20.54 milliradians, with mean of 19.01 milliradians and standard deviation of 0.41 milliradians.

The rms deviation of computed from experimental angles ranges from 0.28 to 0.41 milliradian for different classes of data. The ratio of this deviation to the deviation from over-all mean varies from 0.68 for Class A to 1.00 for Class R. Thus the improvement over a "standard atmosphere" varies from 32 per cent to 0, and correlates directly with quality of weather information.

For this experiment it is concluded that most of the rms elevation angle error is contributed by atmospheric conditions. Although ray tracing methods provide a significant correction when sufficiently good weather information is available, there still remains a large uncertainty not accounted for by equipment.

* Received by the PGAP, December 4, 1959; revised manuscript received, March 12, 1960. This work was performed under Contract No. DA-29-040-ORD-1238.

† Elec. Engrg. Dept., University of New Mexico, Albuquerque, N. M.

‡ Missile Geophysics Division, White Sands Missile Range, N. M.

INTRODUCTION

DURING the period July, 1958–July, 1959, a considerable amount of data was obtained at WSMR for the purpose of comparing computed with observed tropospheric refraction. Some results obtained prior to July, 1958 and presented in a previous report[1] are not presented here, because the recent data involves a different ray path and a more accurate radar. However, conclusions of the two reports are compared. On the basis of present information, it is possible to define more definitely the magnitude of the elevation angle errors to be expected from meteorological uncertainties in the WSMR area.

RADAR PATH AND TOPOGRAPHY

The White Sands Missile Range is situated in the Tularosa Basin in southern New Mexico. The basin is oriented with its major axis north-south and is about 140 miles long and 40 miles wide (Fig. 1). It is sharply bounded by mountain ranges which average 7500 to 9000 feet MSL while the basin floor is about 4000 feet

[1] W. L. Anderson, N. J. Beyers, and B. M. Fannin, "Comparison of computed with observed atmospheric refraction," IRE TRANS. ON ANTENNAS AND PROPAGATION, vol. AP-7, pp. 258–260; July, 1959.

MSL. The sandy soil on the basin floor supports desert vegetation such as mesquite, greasewood, cactus, and so forth.

The radar unit used in this experiment is situated on the basin floor as shown in Fig. 1. All radar observations were taken over a path extending from the radar site to a beacon target, equipped with a horn antenna, located in the Sacramento Mountains northeast of the radar. The slant range is 79,060 yards with the target altitude 5610.5 feet above that of the transmitter, and the resulting elevation angle is 17.99 milliradians. Except for the mountains at the beacon end of the path, most of the terrain between transmitter and target is quite flat. The topography is shown in cross section in Fig. 2, where the altitude scale has been multiplied by a factor of 7.5.

Climatology

The high plains region of southern New Mexico is characterized by short, mild winters and long hot summers. Average temperatures range from 23°F low to 61°F high in the winter and from 59°F low to 98°F high in the summer. The arid climate of the Tularosa Basin yields an average annual rainfall of about 8 inches, much of which is the result of the numerous thunderstorms occurring in late summer and early fall. These thunderstorms cause the formation and dissipation of convective cells which disrupt the horizontal stratification picture during this time of year. Clear skies generally prevail during the winter months, while the spring is characterized by frequent winds averaging 20 to 30 miles per hour.

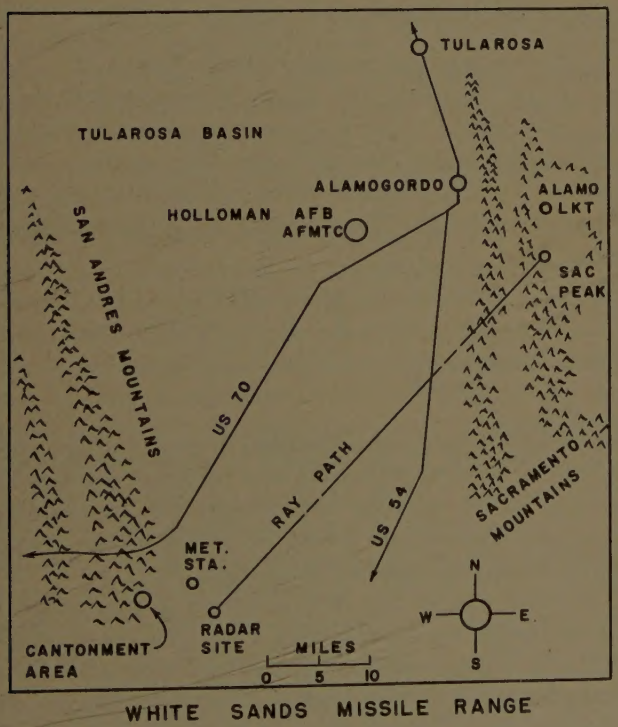

Fig. 1.

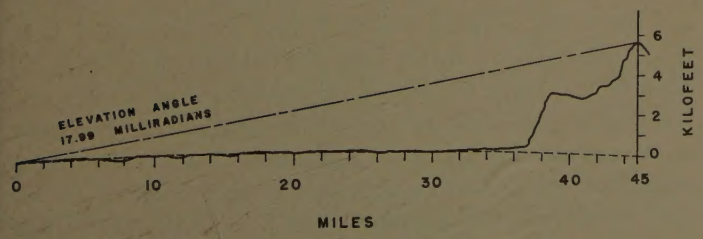

Fig. 2—Terrain profile along ray path.

Meteorological Data

The refractive index profiles used in computing expected bending were prepared by personnel of the WSMR Missile Geophysics Division, U. S. Army Signal Missile Support Agency. The data used in making up the profiles were obtained from radiosonde, wiresonde, surface observations, and helicopter mounted refractometer. At the time of preparing each profile, and before bending calculations were performed, a classification was assigned. The criteria for classification involved the following:

Class A

1) use of at least two observational methods,
2) close agreement between observations made by different methods,
3) obtaining all data within two hours of radar observation,
4) a stable synoptic situation,
5) sounding made within 5 miles of propagation path.

Class B

1) one sounding available,
2) obtaining data within two hours of radar observation,
3) a stable synoptic situation,
4) soundings within 5 miles of propagation path,
5) use of supplementary data more than two hours old if in good agreement.

Class C

1) data which did not qualify for Class A or B, but were still considered to be a fair representation of existing conditions.

Class R

1) This category includes all profiles prepared solely from radiosonde, although in every case at least part of a radiosonde profile was also used in making up the Class A, B, or C profiles. The reason for this type of classification is to give a comparison between the Class A, B, or C results and those which would be obtained if the only available information were radiosonde data, sometimes taken at times differing up to several hours from times of radar observations, and taken with no factor of meteorologist's judgment entering the picture. Thus there are cases, for example, when the Class R profiles are the same as the B or C profiles.

TABLE I

Class	Time of Day	Number of Comparisons	α_Y	ϵ_{rms}	$\frac{\epsilon_{rms}}{\alpha_Y}$	Per Cent Improvement
A	A.M.	21	0.663 milliradian	0.426 milliradian	0.643	35.7 per cent
	P.M.	16	0.288 milliradian	0.273 milliradian	0.948	5.2 per cent
	Both	37	0.534 milliradian	0.368 milliradian	0.689	31.1 per cent
B	A.M.	55	0.408 milliradian	0.307 milliradian	0.752	24.8 per cent
	P.M.	56	0.292 milliradian	0.261 milliradian	0.894	10.6 per cent
	Both	111	0.354 milliradian	0.285 milliradian	0.805	19.5 per cent
C	A.M.	8	0.482 milliradian	0.339 milliradian	0.703	29.7 per cent
	P.M.	9	0.319 milliradian	0.333 milliradian	1.044	−4.4 per cent
	Both	17	0.404 milliradian	0.336 milliradian	0.832	16.8 per cent
A, B, & C combined	A.M.	84	0.491 milliradian	0.344 milliradian	0.701	29.9 per cent
	P.M.	81	0.294 milliradian	0.272 milliradian	0.925	7.5 per cent
	Both	165	0.406 milliradian	0.311 milliradian	0.766	23.4 per cent
R	A.M.	75	0.478 milliradian	0.470 milliradian	0.983	1.7 per cent
	P.M.	68	0.272 milliradian	0.330 milliradian	1.213	−21.3 per cent
	Both	143	0.394 milliradian	0.409 milliradian	1.038	−3.8 per cent

Ray-Tracing Method

The procedure used in ray-tracing has been fully described in previous reports,[2] and will not be further discussed except for the remark that the computational accuracy is conservatively estimated to be within about 0.03 milliradian.

Radar Readings

The internal precision of the FPS-16 radar is quoted at 0.10 milliradian rms, but since additional fixed error or "bias" can occur, the over-all internal accuracy of the radar is quoted at 0.14 milliradian rms. This is considered a conservative figure.

A total of 165 observations were made during the period July, 1958 to July, 1959. Of these, 84 were taken at around 0900 and 81 around 1400 local time. Mean observed angle was 19.01 milliradians, representing an average bending of 1.02 milliradian. Extremes in observed angles were 18.36 and 20.54 milliradians. Standard deviation was 0.406 milliradian.

In nearly all cases the so-called "observed angle" is the mean of 5 readings taken at 1-minute intervals. The maximum difference between extremes during any single 4-minute period was 0.58 milliradian, but this was quite unusual. There were no other cases in which the difference exceeded 0.25 milliradian. The mean difference between extremes was 0.07 milliradian, and the rms was 0.16 milliradian. Since bias is probably constant during a 4-minute interval, the internal radar precision figure, 0.10 milliradian, can be used to arrive at a value for the rms contribution of random atmospheric fluctuations, or scintillations,

$$\sqrt{0.16^2 - 0.10^2} = 0.125 \text{ milliradian rms.}$$

This should be considered a very tentative figure only, since at present there is no way of knowing how much of the change during an observation period is contributed by random fluctuations about a mean, and how much by sudden shifts in the refractive index profile.

Comparison, Observed with Computed Values

An evaluation was made of 165 Class A, B, and C profiles. In addition, 143 Class R comparison profiles were considered. Table I gives a breakdown of the results, subdivided in various ways. The quantity ϵ is defined as $(X - Y)$, where X is the computed angle and Y the observed angle. The quantity α_Y is introduced and defined as

$$\alpha_Y = \sqrt{\frac{\sum_{i=1}^{N} (Y_i - 19.01)^2}{N}},$$

where 19.01 is the mean observed angle for all 165 cases studied. α_Y is used primarily as a measure of departure of any group of recorded angles from the over-all mean, and in the special case where all 165 readings are considered, α_Y is the standard deviation.

The ratio ϵ_{rms}/α_Y has been adopted as a criterion for judging results for two reasons. First, it tells at a glance whether any improvement was gained over a "standard atmosphere" correction, and second, it makes different samples of data directly comparable, whether or not the samples differed among themselves in their statistical properties. Thus, although in footnote 1 the value of ϵ_{rms} for Class A data was 0.17, and in this report it is 0.37, the ratio to α_Y in each case shows that approximately the same degree of improvement was effected, namely, a reduction of rms error to about 30 per cent to 40 per cent below α_Y. Considering both reports, the reduction for Class B lies in the neighborhood of 20 per cent to 40 per cent, and for Class C, −40 per cent to 20

[2] *Ibid.;* and B. M. Fannin and K. H. Jehn. "A study of radar elevation-angle errors due to atmospheric refraction," IRE Trans. on Antennas and Propagation, vol. AP-5, pp. 71–77; January, 1957.

per cent. Since the number of Class C cases is quite small in both reports, probably the safest conclusion is that Class C gave no improvement. Nor was there improvement from Class R data.

It will be noted from Table I that the rms values for ϵ_{rms} are considerably higher in the morning than in the afternoon. This fits the pattern of the diurnal meteorological cycle, as discussed by various investigators.[2,3] Day and Trolese conducted experiments in the Arizona desert during winter months, and obtained averaged profiles of refractive index hourly over 24 hours. At 1400, the atmosphere was nearly standard with time rate of change near minimum. On the other hand, when observed at 0900, the refractive index near the surface was high, owing to existence of a temperature inversion formed during the night, but it was beginning to decrease quite rapidly due to heating of the ground by the sun. In the desert type terrain of the Tularosa Basin, in the WSMR area, the same general conditions prevail. During periods of time instability, there is almost certainly a concomitant space instability, with the result that the horizontal stratification assumption is less valid than at other times. This may seem to contradict the requirement of "stable synoptic situation" imposed in classifying the A or B profiles; however, the judgment of stability is based on an over-all profile which is of necessity local to the weather sounding equipment. An exception to this limitation occurs when data are obtained by helicopter mounted refractometer, but here the data collecting time may introduce some uncertainties.

As an indication of the seasonal behavior of the diurnal cycle, it is instructive to compare α_Y's for various periods of the year. The trend is illustrated in Table II, where the 3-month groups have been chosen in such a way as to isolate the conditions in the period centered, more or less, on the winter solstice. During this time, surface heating in the hours before 0900 should be considerably less than for other times of the year.

These figures seem to fit the general weather picture very well. In all cases α_Y(A.M.) is higher than α_Y(P.M.), and the tendency is most striking for the November–January period. During August–October they are nearly the same, and both are quite high, probably because of occasional rains during this time. In the February–April period, α_Y for both morning and afternoon is fairly low, due perhaps to winds and consequent good mixing of the atmosphere. The minimum is reached for the May–July period, due to ground heating well before 0900 and the general dryness. A contributing factor may also be May winds, which are not unknown in this area.

The tendency for ϵ_{rms} to be high when the data have high α_Y is therefore probably related more to the instability of the meteorological situation near the ground than it is to a failure of the ray-tracing procedure when applied to extreme cases. Unfortunately, the data presently on hand do not include enough cases of high bending during times of supposed high stability to give any valid statistical weight either for or against the hypothesis. Nevertheless, the low figures for ϵ_{rms} at 1400 lead to a strong presumption that, during the other stable period, around 0200, it should also be low, even though bending at this time would be expected to be high.

TABLE II

Time Period		No. of Cases (A, B, C)	α_Y
August through October	A.M.	11	0.54
	P.M.	9	0.53
	Combined	20	0.53
November through January	A.M.	24	0.72
	P.M.	25	0.25
	Combined	49	0.53
February through April	A.M.	32	0.39
	P.M.	27	0.33
	Combined	59	0.36
May through July	A.M.	17	0.21
	P.M.	20	0.13
	Combined	37	0.17

Another point that deserves special comment is the very high α_Y for Class A (A.M.) cases, as contrasted with B and C. This arises because the classification A generally necessitates the inclusion of wiresonde data. The use of wiresonde is restricted to days on which winds are less than 10 knots; consequently, the atmosphere is not as likely to be well mixed at such times as it is otherwise, and a variety of profiles may occur, which have sharply stratified moisture layers, temperature inversions, etc. Class A (P.M.) cases, on the other hand, have the lowest α_Y of any of the groups because on clear, calm afternoons the morning inversion has generally disappeared, and the temperature distribution is near adiabatic.

In the scatter diagrams (Figs. 3 and 4), the main diagonal represents perfect agreement between observed and computed values, while the two unbroken lines on either side show the radar accuracy. The dotted lines show the standard deviation of all observed angles, and are intended merely as a rough guide in evaluating the over-all results.

Surface Refractive Index

In the course of this study, the following question has frequently arisen: might there not be an adequate angle correction procedure based only on a knowledge of surface refractive index? Such a procedure, as compared with ray-tracing from a complete profile, would greatly mitigate the amount of effort required in making corrections.

[3] J. P. Day and L. G. Trolese, "Propagation of short radio waves over desert terrain," PROC. IRE, vol. 38, pp. 165–175; February, 1950.

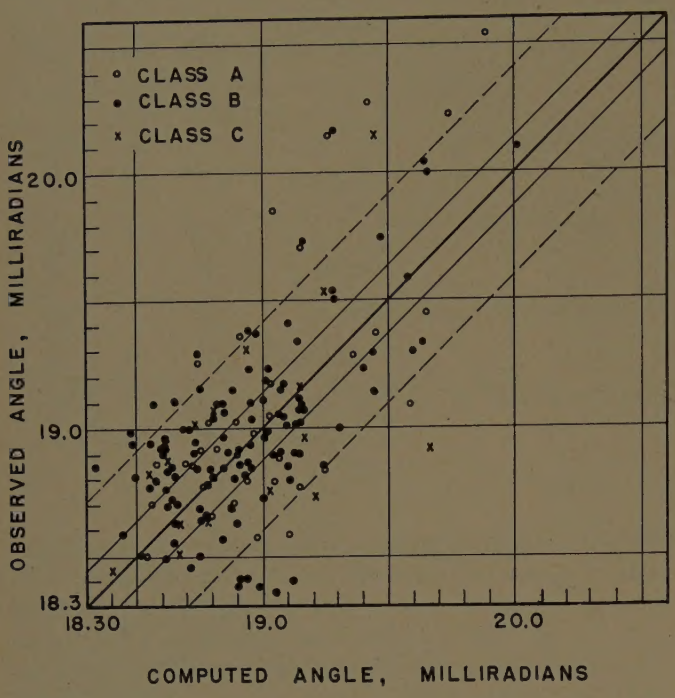

Fig. 3.

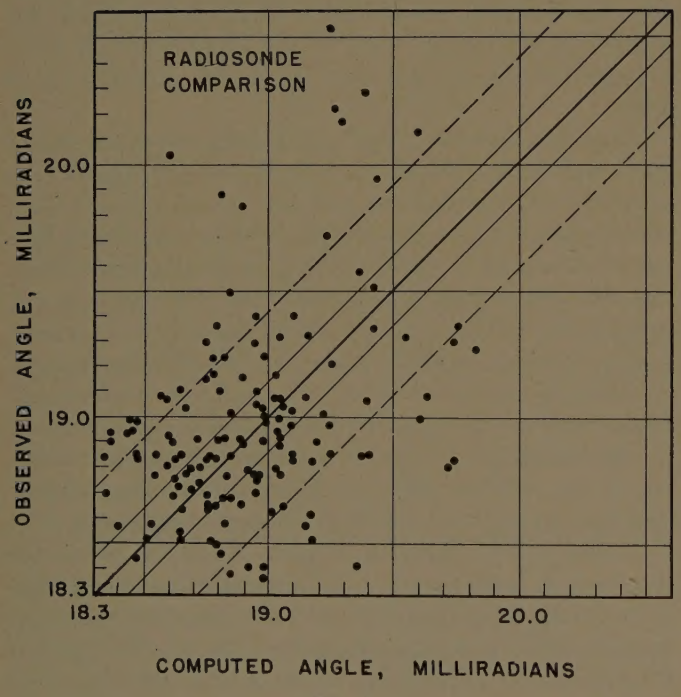

Fig. 4.

One such procedure that has been proposed[4] involves the assumption that a fair representation of weather conditions is given by a refractive index profile which is exponential between N_0 (ground value of N) and a fixed value $N_1 = 128$ N-units at 20,000 feet above the surface. Specifically, the profile is described by: $N = N_0 e^{-BY}$, where Y is height above surface and N the corresponding N-value. For given N_0, B is obtained by evaluating the expression at 20,000 feet. Above this height, an average profile is used.

Profiles made up in this way can be ray-traced to give a table of correction factors for the pertinent range of N_0. These factors are used in a simple formula which gives the angle correction for a given range and angle.

As is shown in Table III, the method gives corrections which, statistically, are a slight but probably not worthwhile improvement over those that would result from a fixed standard atmosphere. The average improvement is 7.5 per cent, or about 0.03 milliradian. Since the method does not involve a classification of the weather situation, the results are given when this method is applied to all the cases which were used in Classes A, B, and C. It is perhaps worth mentioning, however, that ϵ_{rms}/α_Y varies only slightly for different samples of data, provided the samples contain a reasonable number of readings.

TABLE III
CORRECTIONS BASED ON SURFACE REFRACTIVE INDEX ONLY

Time Group	Number	ϵ_{rms}	α_Y	ϵ_{rms}/α_Y
A.M.	84	0.450 milliradian	0.491 milliradian	0.916
P.M.	81	0.280 milliradian	0.294 milliradian	0.952
Combined	165	0.376 milliradian	0.406 milliradian	0.926

CONCLUSIONS

The following main conclusions are drawn.

1) The high accuracy of the radar used in this experiment allows a fairly definite conclusion as to the main source of the discrepancies between computed and observed elevation angles. The rms error for combined A, B, C data amounts to about 0.31 milliradian, and taking radar accuracy to be 0.14 milliradian, the error contribution from weather is evidently about 0.28 milliradian. This is of nearly the same magnitude as the total error.

If this weather contribution is assumed to include an rms error of about 0.13 milliradian arising from scintillations or other sudden, unpredictable changes, and if this is subtracted quadratically, then the remaining meteorological uncertainties are given by the figure 0.25 milliradian rms. This quantity should represent two main factors:

a) limitations in determining the true refractive index profile,
b) departures from the horizontal stratification picture.

2) In evaluating the extent to which bending can be predicted, it is apparent that when weather deviates considerably from the average condition, the probability of error in computing the bending is increased. This probability is minimized, however, when best quality meteorological information is used. The correlation be-

[4] K. E. Pearson, D. D. Kasparek, and L. N. Tarrant, "The Refraction Correction Developed for the AN/FPS-16 Radar at White Sands Missile Range," U. S. Army Signal Missile Support Agency, White Sands Missile Range, N. M., Tech. Memo. 577; November, 1958.

tween quality of weather data and the improvement gained over a standard atmosphere is direct and definite, both regarding Anderson, *et al.*,[1] and this paper.

3) The Class R data, consisting entirely of radiosonde profiles, give no reduction of error over that which would have resulted from using a standard atmosphere. This and the Class C results indicate quite strongly that radiosonde information alone, under the conditions of this test, is virtually worthless for ray-tracing purposes.

4) The corrections deduced from surface refractive index, by the method described in the previous section, gave an improvement of about 0.03 milliradian rms over the error which would have resulted from a standard atmosphere assumption. This is considered insignificant for most practical purposes.

5) In the WSMR area, particularly, the time of day and season of year constitute valuable information on a) what type of average profiles can be expected, and b) what type and degree of variation from these averages can be expected. Possibly this knowledge can be guided by surface refractive index and initial gradient readings taken near the radar site to obtain corrections rivaling those obtained by ray-tracing from complete Class A profiles.

The Flared Slot: A Moderately Directive Flush-Mounted Broad-Band Antenna*

J. W. EBERLE†, C. A. LEVIS†, SENIOR MEMBER, IRE, AND D. McCOY‡, MEMBER, IRE

***Summary*—The flared slot is a simply constructed antenna designed to be flush-mounted in a horizontal surface. Its pattern is a moderately directive pencil beam over a 4:1 frequency band, and its impedance bandwidth is essentially that of a coaxial line-to-ridged waveguide transition. Both vertically and horizontally polarized models are discussed.**

I. Introduction

ANTENNAS having a single, smooth beam of moderate directivity are finding increasing use in aircraft and airport installations in connection with homing or ground-directed approach systems. The Yagi arrays and horns commonly used to obtain such patterns are frequently inapplicable to high-performance aircraft or to airport installations where the only available locations often are flat surfaces, such as the underside of the fuselage, wings, or horizontal stabilizer, or the ground near or even in the runways. A class of traveling-wave antennas suitable for installation in such locations was briefly described by Stephenson and Walter [1]. The further development of one of these antennas, named a flared slot antenna, is discussed below. Its construction, far field patterns and impedance over a wide range of frequencies, bandwidth, and near-field structure are discussed. The effect of certain modifications which might be necessary in typical installations has also been investigated.

* Received by the PGAP, August 3, 1959; revised manuscript received, March 3, 1960. This work was performed at The Ohio State University, Columbus, and was sponsored by the Air Research and Development Command, Wright Air Development Center, Wright-Patterson Air Force Base, Ohio.

† Antenna Lab., Dept. of Elec. Engrg., The Ohio State University, Columbus, Ohio.

‡ General Electric Co., Syracuse, N. Y. Formerly at Antenna Lab., Dept. of Elec. Engrg., The Ohio State University, Columbus, Ohio.

II. Vertically Polarized Flared-Slot Antenna

A vertically polarized flared-slot antenna is pictured in Fig. 1, and the basic construction appears in Fig. 2.

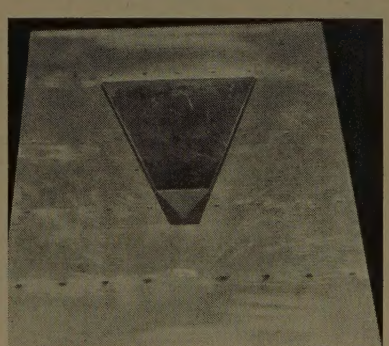

Fig. 1—Flared-slot antenna for vertical polarization.

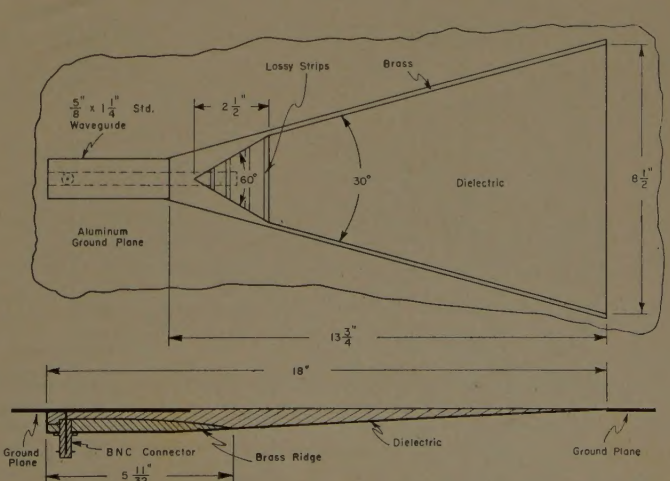

Fig. 2—Basic construction of vertically polarized antenna.

Energy entering at the coaxial feed is transferred through a ridged dielectric-filled waveguide section to the radiating aperture. The coax-to-waveguide transition was designed with the use of ridged-guide data by Cohn [2], [3] to give a wide-band transition to 50-ohm cable. The antenna itself is based on a traveling-wave design by C. H. Walter. It employs a phase velocity somewhat slower than that of free space and exhibits a clean endfire pattern over a 4:1 frequency band.

The impedance locus of the antenna is shown in Fig. 3 as measured on a Hewlett-Packard slotted coaxial section through UG 491 A/U and UG 201/U adaptors. The impedance bandwidth is limited by cutoff at the low-frequency end, and by the waveguide back plate at the high-frequency end, where it appears as an effective short-circuit at the feedpoint. The bandwidth for which the VSWR does not exceed a given value is plotted in Fig. 4.

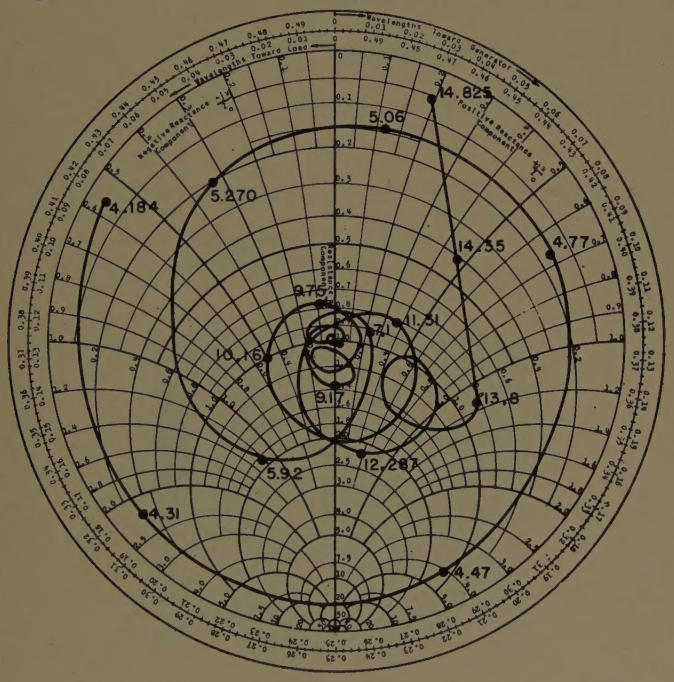

Fig. 3—VSWR vs wavelength (in cm) of vertically polarized antenna.

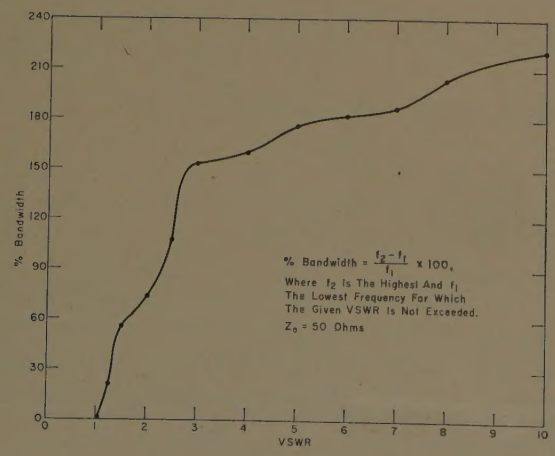

Fig. 4—Impedance bandwidth of vertically polarized antenna.

The far-field strength (voltage) patterns of the antenna are shown in Fig. 5, which pertains to the resin-filled model of Fig. 1, and in Fig. 6, which gives the patterns of an earlier paraffin-wax-filled model. The coordinates used appear in Fig. 7 (p. 464). The resin used was Stycast 35 and had a relative dielectric con-

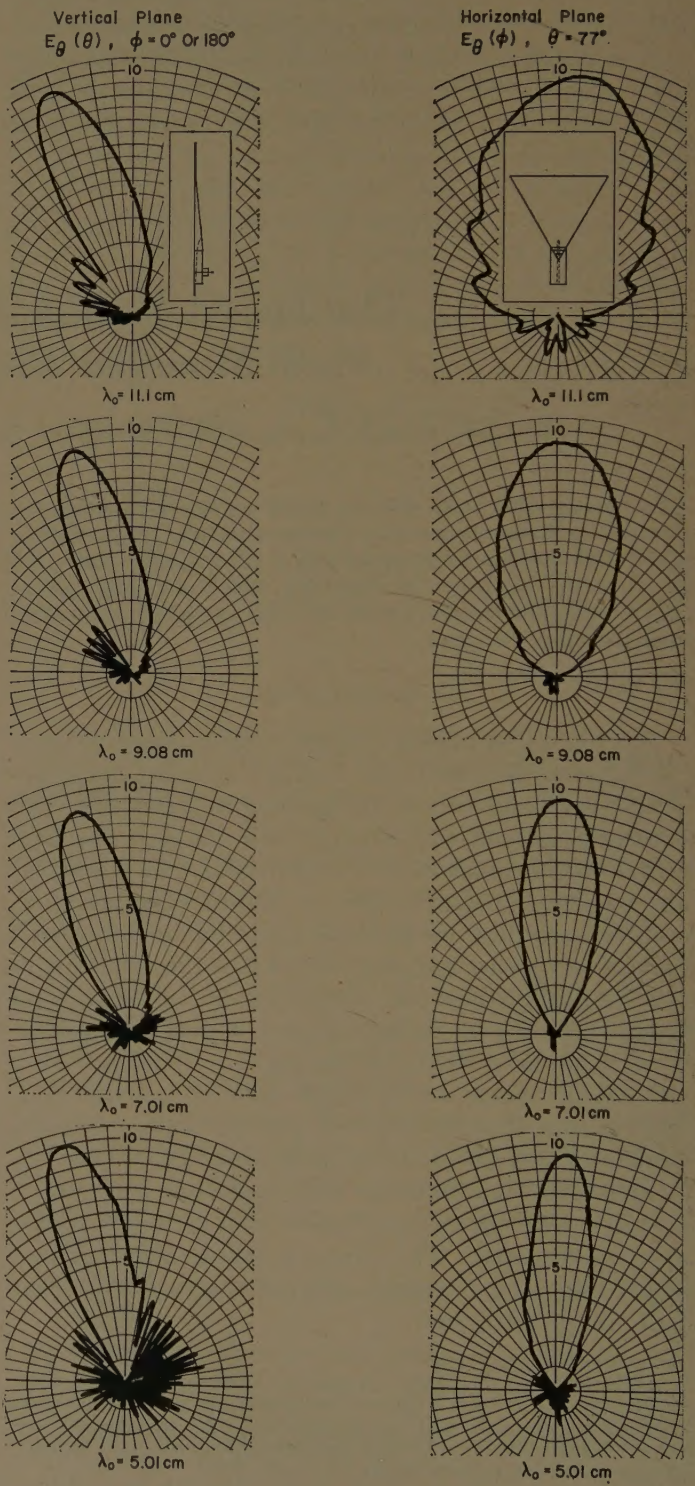

Fig. 5—Field-strength (voltage) patterns of the vertically polarized flared-slot antenna of Fig. 1.

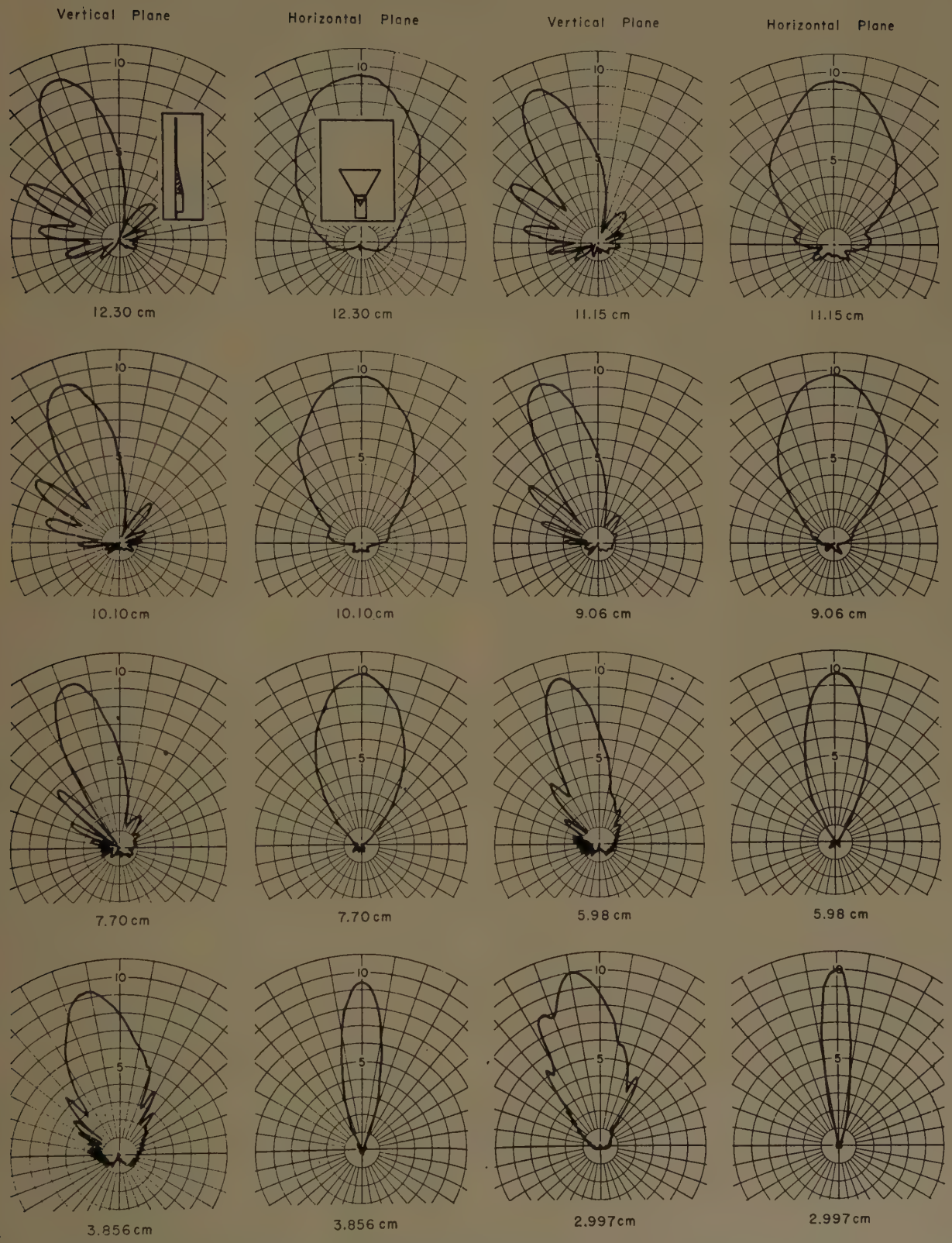

Fig. 6—Field-strength (voltage) patterns of a vertically polarized flared-slot prototype. Horizontal plane patterns at $\theta = 70°$. For coordinate system, see Fig. 7.

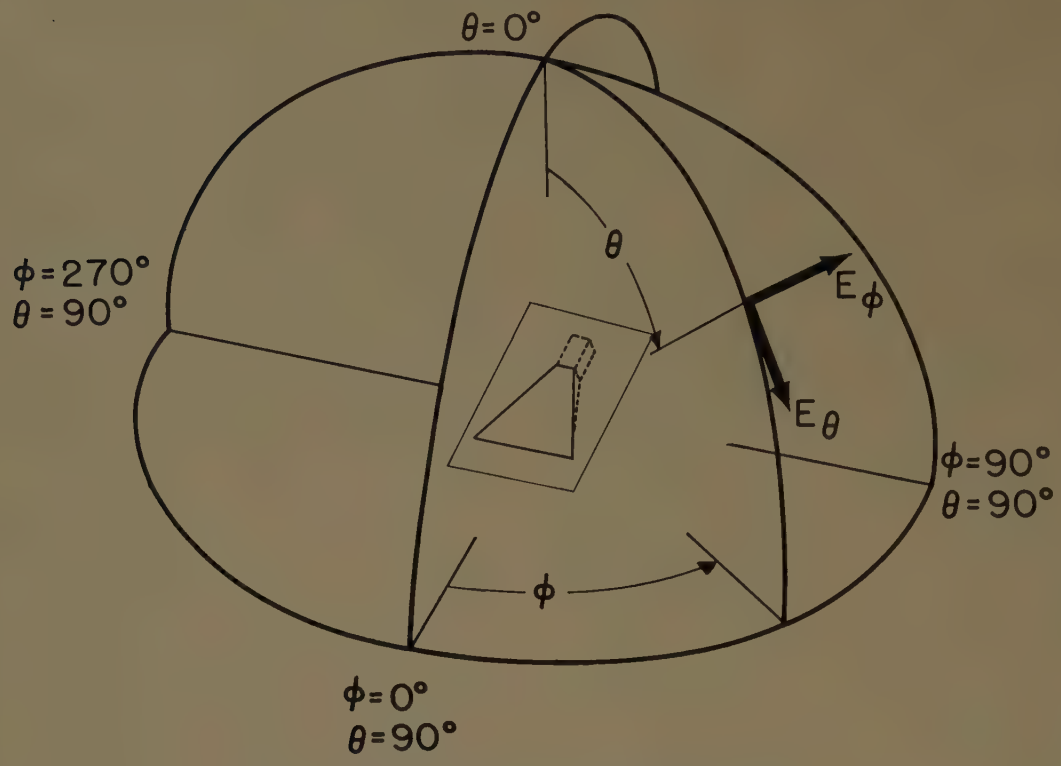

Fig. 7—Coordinate system for field-strength patterns.

stant of 2.58. The dielectric constant of paraffin is 2.25. The extremely wide range of endfire operation (over a 4:1 frequency band) is clearly evident in Figs. 5 and 6. The limitation at the high-frequency end is due to higher-order modes in the waveguide which are launched into the aperture and cause beam deterioration. At the low-frequency end, the discontinuity at the beginning of the aperture can cause spurious radiation. A "discontinuity minimizer" consisting of transverse Aquadag strips imbedded in the dielectric (Fig. 2) is an effective means of reducing this effect with some sacrifice of efficiency. Fig. 8 (p. 465), shows the effect of two different sizes of the discontinuity minimizer. The efficiency of this particular antenna has not been tested, but measurements on a paraffin-filled antenna without ridge feed showed an efficiency reduction from 80 per cent to to 55 per cent when the minimizer was used. For receiving applications this is not serious, since the directivity increases, so that gain is not affected adversely.

The structure of the antenna near field at midband ($\lambda_0 = 5.017$ cm) is shown in the phase and amplitude plots of Figs. 9 and 10, respectively. The quantity plotted is the electric field component tangential to the dielectric-air interface and parallel to its centerline at a distance of 0.005 cm from the interface. The orthogonal tangential component was lower by 25.1 db over the entire surface. The measurements were made with a phase-sensitive coherent detection system [4], [5] developed at this Laboratory. Contours are not plotted near the discontinuity minimizer because the probe was too large to resolve the rapid variations of the field in this region. No data were taken at the far edges of the antenna.

The polarization of the antenna far field is pure vertical; over the entire frequency band, the cross-polarized component is 15 db below the maximum of the desired component. This can easily be understood in terms of the measured near field. Referring to Fig. 11 (p. 466), the longitudinal electric field in the aperture is equivalent to a set of magnetic currents flowing in the surface at right angles to the indicated field lines. The equivalent magnetic currents are related to the electric far field as ordinary electric currents are to the magnetic field, and thus they produce the far field shown, which is vertically polarized.

III. Horizontally Polarized Flared-Slot Antenna

A horizontally polarized flared-slot antenna is shown in Fig. 12. The basic construction appears in Fig. 13, and a method of feeding is sketched in Fig. 14. The similarity of this antenna to the vertically polarized model is immediately apparent. The major differences are in the feed probe, which is parallel to the aperture for horizontal polarization, and the greater feed section and aperture depths required to propagate the resulting waveguide mode.

The direction of the electric field in the aperture is sketched in Fig. 15. The corresponding equivalent currents are perpendicular to the electric field and are also indicated in the figure, and the resulting electric far field

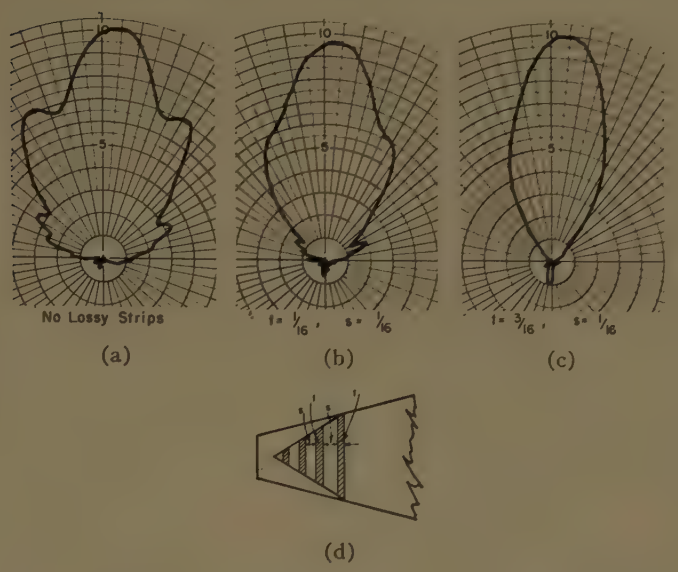

Fig. 8—Discontinuity minimizer effect on pattern of vertically polarized antenna. Dimensions are given in inches. The shaded strips represent Aquadag paint.

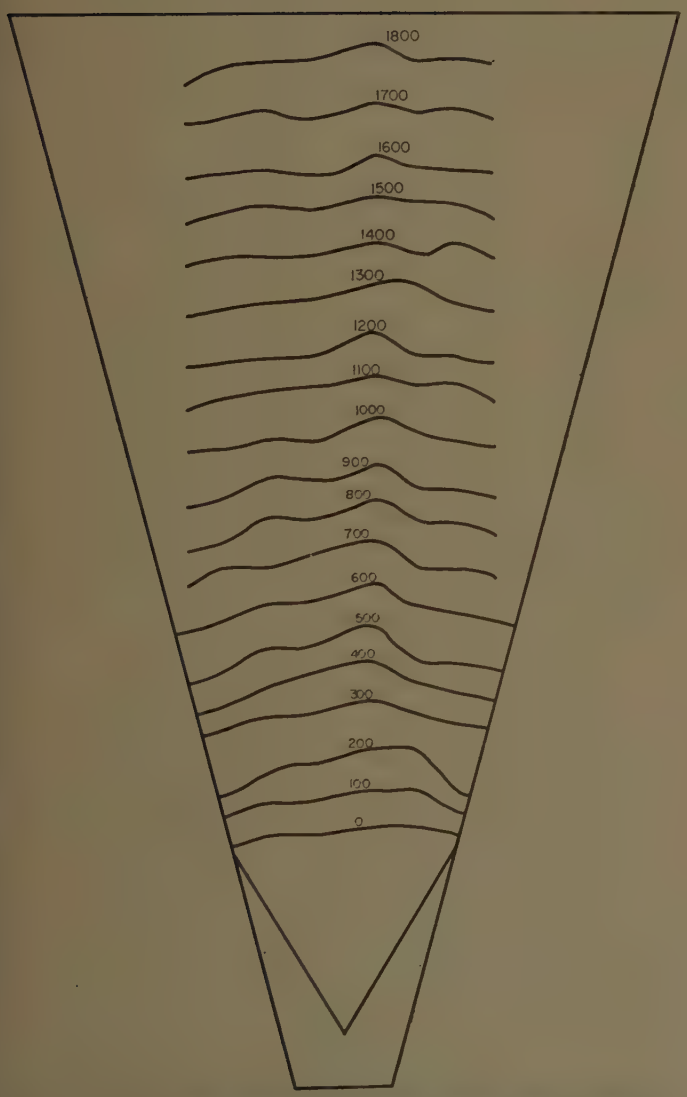

Fig. 9—Electric field phase contours 0.005 cm above the aperture of the vertically polarized antenna (Fig. 1). Component parallel to the line of symmetry. $\lambda_0 = 5.017$ cm.

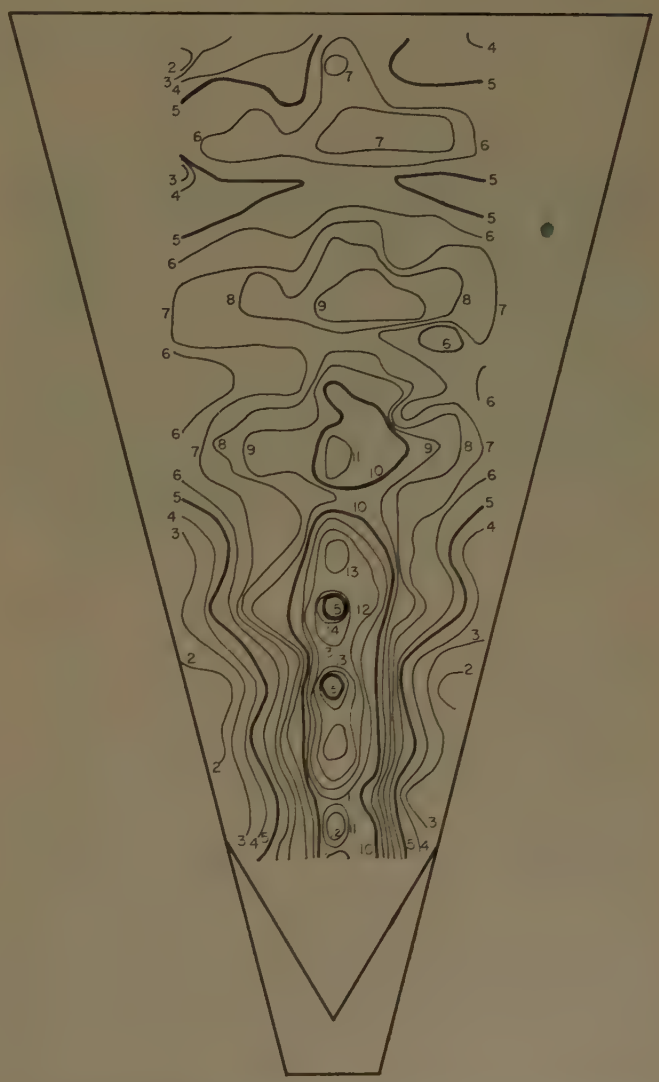

Fig. 10—Electric field-strength contours 0.005 cm above the aperture of the vertically polarized antenna (Fig. 1). Component parallel to the line of symmetry. $\lambda_0 = 5.017$ cm.

Fig. 11—Polarization relations of vertically polarized flared-slot antenna. Solid arrows denote electric field lines; dashed arrows, equivalent magnetic currents.

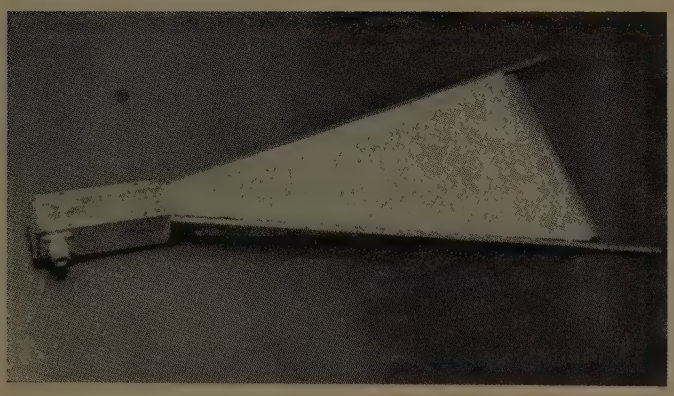

Fig. 12—Horizontally polarized flared-slot antenna.

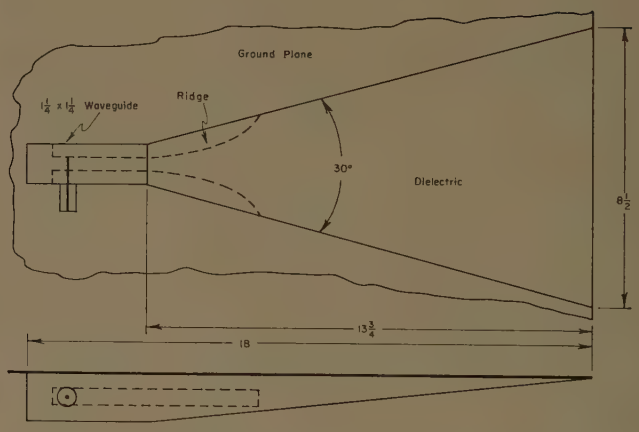

Fig. 13—Basic construction of horizontally polarized antenna.

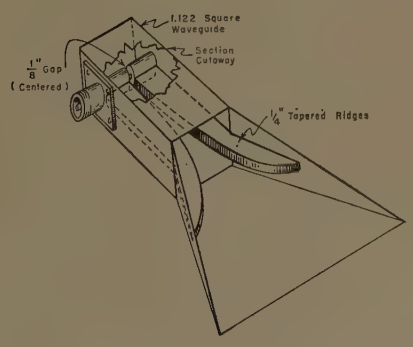

Fig. 14—Feed section of horizontally polarized flared-slot antenna.

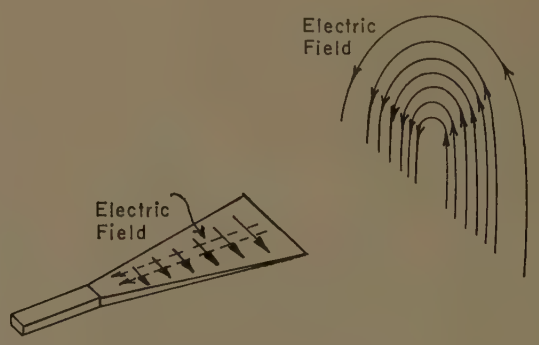

Fig. 15—Polarization relations of horizontally polarized antenna. Solid arrows represent electric field lines; dashed arrows represent equivalent magnetic currents.

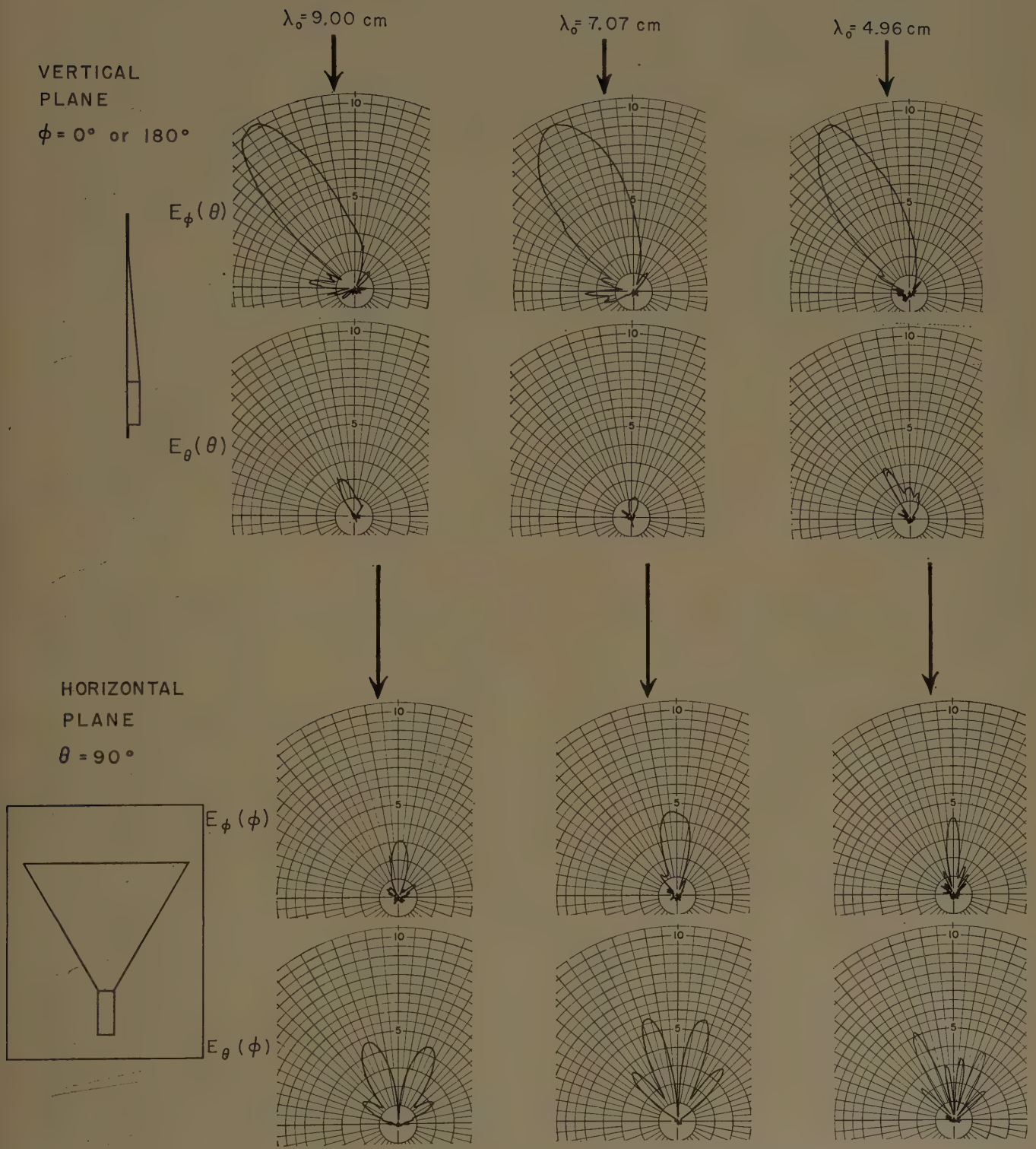

Fig. 16—Field-strength (voltage) patterns of horizontally polarized flared-slot antenna of Fig. 12. For coordinate system, see Fig. 7.

(*Fig. 16 cont'd on next page.*)

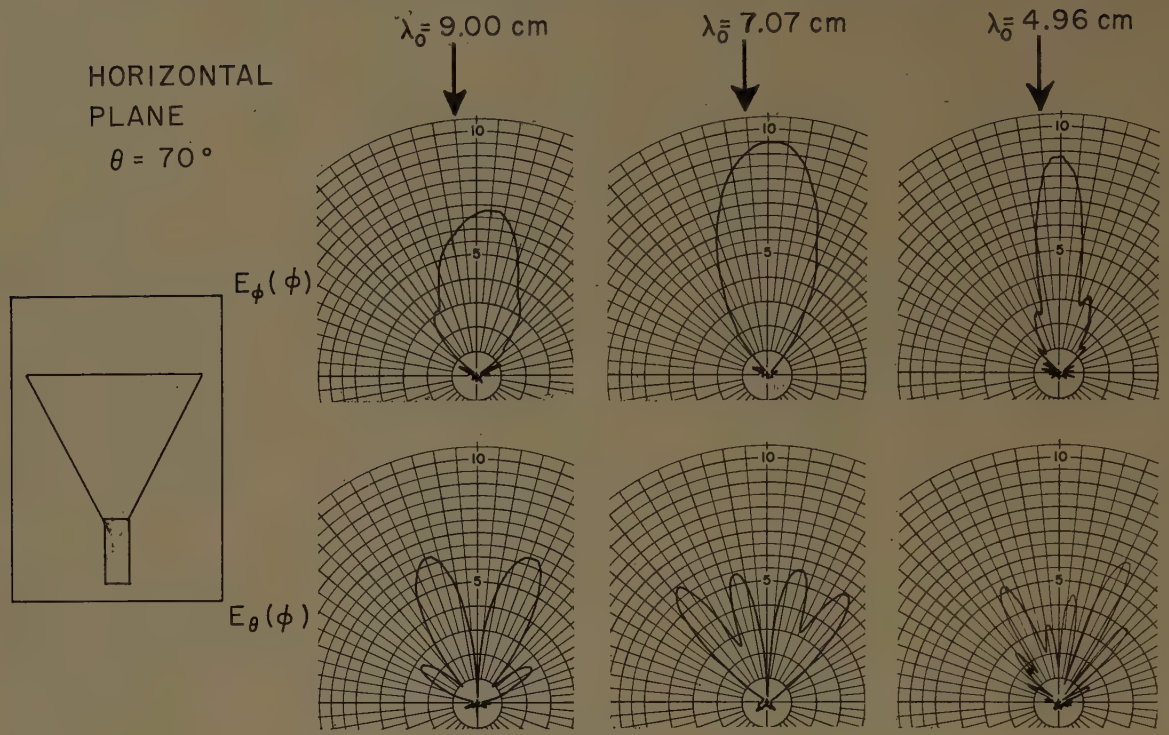

Fig. 16—(Continued.)

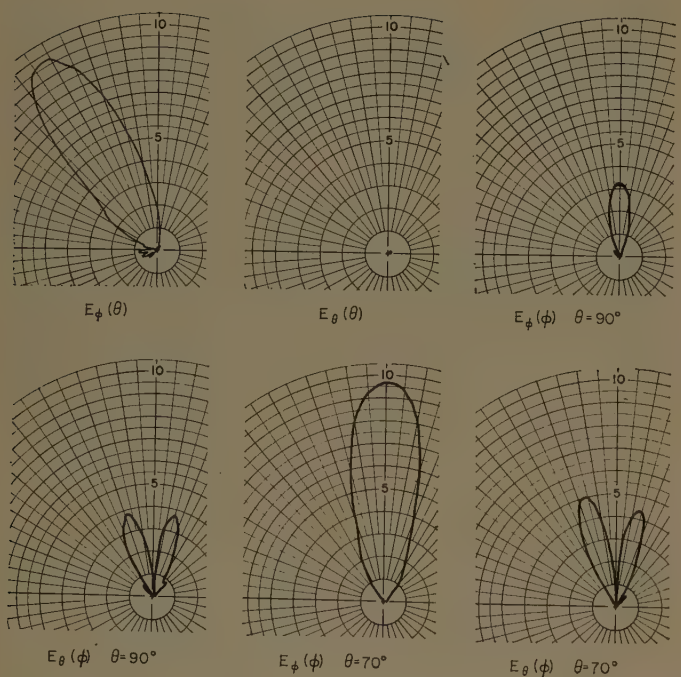

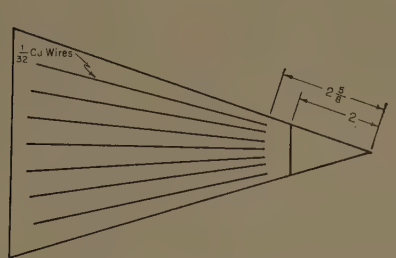

Fig. 17—Discontinuity minimizer effect on patterns of horizontally polarized antenna; compare with Fig. 16. $\lambda_0 = 7.07$ cm.

is shown. It is apparent that a substantial portion of the main beam is horizontally polarized, but there are two vertically polarized regions at the beam edges. These appear as distinct lobes in most of the horizontal-plane patterns.

The far-field patterns of the antenna of Fig. 12 are shown in Fig. 16. The dielectric is paraffin wax, and no discontinuity minimizer was used. If a discontinuity minimizer were to be employed to extend the antenna bandwidth, its lossy strips should run longitudinally, since this is the direction of the unwanted electric field component. The effect of such a discontinuity minimizer is shown in Fig. 17.

The horizontally polarized model received less development effort than the vertically polarized version. All models employed paraffin wax as dielectric, and no attempt was made to broadband the impedance characteristics.

IV. Bibliography

[1] B. T. Stevenson and C. H. Walter, "Endfire slot antennas," IRE Trans. on Antennas and Propagation, vol. AP-3, pp. 81–86; April, 1955.
[2] S. B. Cohn, "Properties of ridge waveguide," Proc. IRE, vol. 35, pp. 783–788; August, 1947.
[3] S. B. Cohn, "Design of simple broad band waveguide to coaxial line junctions," Proc. IRE, vol. 35, pp. 920–926; September, 1947.
[4] J. H. Richmond, "Measurement of time-quadrature components of microwave signals," IRE Trans. on Microwave Theory and Technique, vol. MTT-3, pp. 13–15; April, 1955.
[5] D. McCoy, "Near Field Measurements of Slot Antennas," Antenna Lab., The Ohio State University Research Foundation, Rept. No. 667-15; August 15, 1956. (Prepared under Contract AF 33(616)-3353, Air Research and Development Command, Wright Air Development Center, Wright-Patterson Air Force Base, Ohio.)

Mathematical and Experimental Studies of a Wide-Band Vertically Polarized Antenna*

P. FOLDES†, MEMBER, IRE

Summary—**Theory and experimental results are presented for an omnidirectional, vertically polarized antenna. One of the developed models has 7 db gain, VSWR <1.7, and 50 kw power handling capacity in a 2:1 frequency band. The new antenna is simple in construction and has a single coaxial feed point.**

Introduction

In recent years considerable effort was exerted in developing very wide frequency banded antenna systems. The definition of "wide-band" was continuously extended and at present this term usually refers to a band which has an end frequency ratio of about 1.5:1 or more.

In the present paper, an antenna type which belongs to this group will be discussed. It will be shown that a circularly symmetrical, vertically polarized antenna system can be obtained by means of a coaxial feed horn and a circularly symmetrical reflector. The antenna has omnidirectional pattern in the horizontal plane and highly directive or shaped beam in the vertical plane. The feed system has a coaxial input, with a very low VSWR. The antenna system does not contain any resonant element and therefore its impedance characteristics remain practically constant in a very wide frequency band. At the same time, the reflector configuration assures that the pattern changes only slightly in a 2:1 frequency band. The novel antenna structure can be related to a discone-type antenna.[1] However, its feed system can be considered as an improvement because of the mechanically favorable arrangement. The system is particularly useful for very-high-power application in the UHF band. Theoretical explanations will be given for the feed system and experimental verification for the performance of the new antenna.

General Description of Operation

The basic electrical arrangement of the proposed antenna is shown in Fig. 1. This represents the principal parts of the antenna, namely:

1) a rigid coaxial transmission line, propagating the TEM mode;
2) a toroidal transition section, which inverts the inner and outer conductors of the coaxial line 1);
3) a coaxial horn section, which feeds the circular aperture with a TEM mode;
4) an iris, to cancel the aperture reflection of the horn in a wide band; and

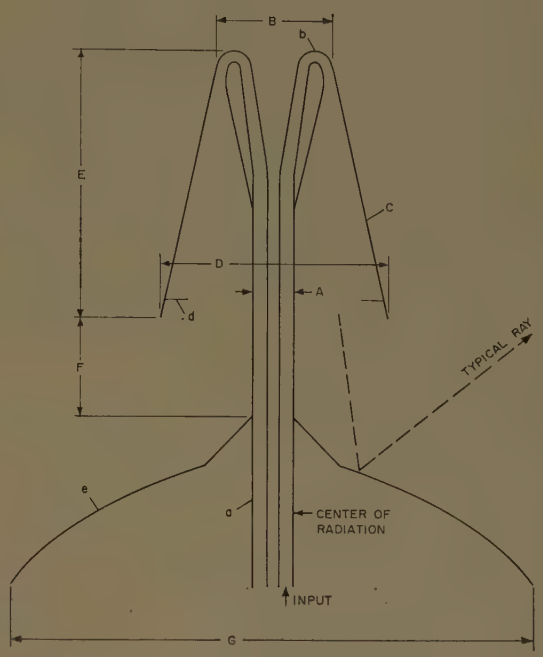

Fig. 1—Electrical schematic of UHF antenna for vertical polarization.

5) a reflector, having particular curvature for radiation of energy into space.

The operation of this antenna can be summarized as follows: the antenna consists of two main parts, the feed system and the reflector. The feed system is basically a transition between the small cross section of the coaxial line and the considerably larger cross section of the coaxial horn aperture. The reflector transforms the primary spherical wave, radiated by the horn, into the far field distribution.

Fig. 1 indicates some of the details which are necessary in order to obtain the desired operation. A tapered coaxial transmission line section serves at the input of the antenna. This line section transforms the characteristic impedance of the 50-ohm feed line to a smaller value. This lower impedance is necessary to minimize the dimensions of the toroidal line section. For low impedance lines, the diameter of the outer conductor does not differ much from that of the inner. Therefore, the decrease of impedance must be accompanied by an over-all increase in the diameters to minimize losses.

The toroidal section 2) can be designed for constant characteristic impedance. This is achieved by varying the distance between the two conductors along the direction of propagation. At the same time, the radius of curvature of this section must be kept large compared

* Received by the PGAP, December 1, 1959; revised manuscript received, March 18, 1960.
† RCA Victor Co., Ltd., Montreal, Quebec, Can.
[1] J. J. Nail, "Designing discone antennas," *Electronics*, vol. 26, pp. 167–169; August, 1953.

to the difference in radii of the conductors. Optimum dimensions will result if the ratio of the distance between the conductors to the radius of curvature remains constant. This constant ratio will result in a "quasi-toroidal" transmission line having a spiral cross section through the axis of the conductors. The toroidal line is terminated by a coaxial horn 3). This section must provide a matched termination in the required frequency band and, at the same time, it must illuminate the reflector in a specific way. The impedance characteristic of this horn is principally determined by its length and the angle between the inner and outer conductors. Moreover, the radiation direction of the horn depends on this angle and the size of the aperture. Therefore, the radiation pattern of the horn can be controlled by these parameters in a relatively wide range. It should be realized that the cone angle, which is determined by a line bisecting the vertex angle of the horn, not only shapes the curvature of the phase front emerging from the horn, but also has some effect on the possibility of higher modes being propagated. Such higher modes might result in cross polarized components and asymmetries in the far field. Therefore, the possibility of these modes being propagated should be eliminated by maintaining the cone angle at a small value.

The near field of the coaxial horn is reflected by the reflector 5). This reflector can have quite general characteristics. Namely, it can be made as a "reflecting lens," which results in specified amplitude and phase characteristics in the outgoing wave. In the following, detailed experimental data will be presented only for the case when the reflector is a wire mesh surface.

Geometry of the Feed System

From the preceding paragraph, it follows that a point source is required for illuminating the reflector. This point source can be a coaxial horn, where a wide-frequency-band operation is assured. This horn should have a certain aperture size for the required pattern function, while the input of the antenna should be a standard size coaxial transmission line. Thus, a transformer section is required between this aperture and the input line. For mechanical reasons, it is convenient to feed the antenna at the bottom, so this transformer section should also invert the direction of propagation.

The characteristic impedance at the input of the antenna is

$$Z_0 = 60 \ln \frac{b_0}{a_0} \quad \text{ohm.} \tag{1}$$

In the first section of this transition, this impedance is transformed to a smaller value,

$$Z_1 = 60 \ln \frac{b_1}{a_1} \quad \text{ohm,} \tag{2}$$

where b_0, b_1 and a_0, a_1 are the diameters of the outer and inner conductors at the beginning and at the end of this section. The attenuation per unit length within this section is

$$\alpha_0 = T \frac{\frac{1}{a} + \frac{1}{b}}{\ln \frac{b}{a}} = T \frac{1}{b} \frac{\tau + 1}{\ln \tau}, \tag{3}$$

where T is a constant which depends on frequency and material, and a and b are the diameters of the conductors at a particular cross section and $\tau = b/a$. The design criterion for this section is a constant loss in any cross section. Thus,

$$\frac{1}{b} \frac{\tau + 1}{\ln \tau} = \frac{\alpha}{T} = \text{const.} \tag{4}$$

The length of this section can be about 1.5 of the maximum wavelengths, if a conical taper is used, and somewhat less if a Tchebycheff-type stepped transformer is used.[2]

A toroidal transmission line can follow the input transformer. The geometry of this line section can be analyzed by a simplified theory, assuming that two lossless conducting strips are arranged parallel to each other (see Fig. 2). Let their width be A, their separation B, and their length extend to infinity. If $B \ll A$, the effect of the edges is negligible and a pure TEM mode can be propagated between the strips. The phase constant will be equal to that for free space, $\beta = 2\pi/\lambda$. Under these conditions, the transverse field components E_x and H_y will exist as indicated in Fig. 2(a). This transmission line has an inductivity[3] $L = \mu(B/A)$ and a capacity $C = \epsilon(A/B)$ per unit length. Now let us bend this strip line around an axis which is parallel to the width A or the y-direction [(see Fig. 2(b)]. If the two strips run along a circular arc, the field components for these portions may be expressed in cylindrical coordinates. For such a system of coordinates, the E_x component becomes an E_ρ component, with the H_y designation remaining unchanged. However, boundary conditions necessitate

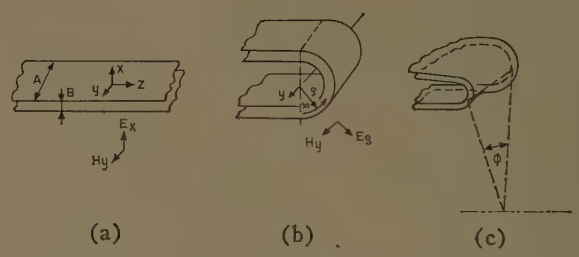

Fig. 2—Generation of the toroidal line. (a) Strip line. (b) Cylindrical line. (c) Toroidal line.

[2] S. B. Cohn, "Optimum design of stepped transmission line transformers," IRE Trans. on Microwave Theory and Techniques, vol. MTT-3, pp. 16–21; April, 1955.

[3] S. A. Schelkunoff, "Electromagnetic Waves," D. Van Nostrand Co., Inc., New York, N. Y., p. 324; 1943.

the existence of an E_ϕ component. For $\rho \gg A$, this component will be very small and hence the new mode will be very similar to the previous TEM mode. For the cylindrical part of the arrangement the inductance L' and capacitance C' per radian are, respectively,

$$L' = \frac{\mu(\rho_2^2 - \rho_1^2)}{2A} = \frac{\mu \Delta \rho}{A} \quad \text{and} \tag{5}$$

$$C' = \frac{\epsilon A}{\ln \frac{\rho_2}{\rho_1}} \tag{6}$$

where $\Delta = \rho_2 - \rho_1$ and $\rho = (\rho_1 + \rho_2)/2$, and ρ_1 and ρ_2 are the radii of curvature of the strips. Let us assume now that the line will be bent around the original z-axis too. In this way, a toroidal system is obtained and Fig. 2(c) shows a small section of it. The last shaping of the lines does not introduce any new field component, but the width A of the strips must now be measured along the new arc, which is now a full circle. If the radius of this second forming operation is large relative to the separation Δ between the two conducting surfaces, the characteristic impedance can be calculated from the L' and C' values defined above. At an angle of ϕ (see Fig. 2), the value of A can be computed as

$$A = 2\pi[r_K + \rho(1 - \cos \phi)], \tag{7}$$

where

$$r_K = \frac{b - \Delta_0}{2},$$

and Δ_0 is the conductor distance at the input of the toroidal line.

Thus the value of the characteristic impedance and the phase constant for the toroidal section can be written

$$K = \left[\frac{L'}{C'}\right]^{1/2} = \frac{60\Delta}{r_K + \rho(1 - \cos \phi)} \left[\frac{\rho}{\Delta} \ln \frac{\rho_2}{\rho_1}\right]^{1/2}$$

$$\cong \frac{60\Delta}{r_K + \rho(1 - \cos \phi)} \left[1 + \frac{\Delta^2}{24\rho^2}\right]$$

$$\cong \frac{60\Delta}{r_K + \rho(1 - \cos \phi)} \tag{8}$$

$$\beta_\phi = \omega[L'C']^{1/2} = \beta \left[\frac{\Delta \rho}{\ln \frac{\rho_2}{\rho_1}}\right]$$

$$\cong \beta\rho\left(1 + \frac{\Delta^2}{24\rho^2}\right) \cong \beta\rho. \tag{9}$$

The characteristic impedance at the input of this section is

$$K_0 = \frac{60\Delta_0}{r_K} = \frac{120\Delta_0}{b - \Delta_0}. \tag{10}$$

The design objective for this toroidal section is to maintain a constant characteristic impedance $K = K_0$ throughout the length of this section. This means

$$\frac{120\Delta_0}{b - \Delta_0} = \frac{120\Delta}{b - \Delta_0 + 2\rho(1 - \cos \phi)} \tag{11}$$

from which

$$\Delta = \Delta_0\left[1 + \frac{2\rho}{b - \Delta_0}(1 - \cos \phi)\right]. \tag{12}$$

From (4), it is seen that

$$b = \frac{\tau + 1}{\ln \tau} \frac{T}{\alpha} \tag{13}$$

and

$$\Delta_0 = \frac{b - a}{2} = \frac{b\left[1 - \frac{a}{b}\right]}{2} = \frac{\tau^2 - 1}{\tau \ln \tau} \frac{T}{2\alpha}. \tag{14}$$

The equation for Δ becomes

$$\Delta = \frac{\tau^2 - 1}{\tau \ln \tau}\left[1 + \frac{2\rho(1 - \cos \phi)}{\frac{\tau + 1}{\ln \tau}\frac{T}{\alpha} - \frac{\tau^2 - 1}{\tau \ln \tau}\frac{T}{2\alpha}}\right]. \tag{15}$$

Eq. (15) gives the values of the separation Δ in terms of the angle ϕ. In this equation there are two parameters, ρ and τ. The radius must increase in proportion to the separation Δ, which in turn must be kept small if small over-all size is desired.

If $\rho = 5\Delta$, then (15) becomes

$$\Delta = \frac{E_0}{1 - E_0F_0}, \tag{16}$$

in which

$$E_0 = \frac{\tau^2 - 1}{\tau \ln \tau}, \qquad F_0 = \frac{10(1 - \cos \phi)}{\frac{T}{\alpha}\frac{\tau - 0.5}{\tau - 1}}, \tag{17}$$

and in this case

$$\rho = 5\frac{E_0}{1 - E_0F_0}. \tag{18}$$

Fig. 3 exhibits the typical dimensions of a feed system, calculated in accordance with the above equations for the 225–400-mc frequency band.

The size of the mouth of the horn was determined from the aperture distribution required for the antenna system. (The remaining dimensions were calculated from the input VSWR and power handling capacity requirements.)

An inspection of Fig. 1 suggests that the antenna system contains several reflection sources from the input VSWR standpoint. The possible sources are:

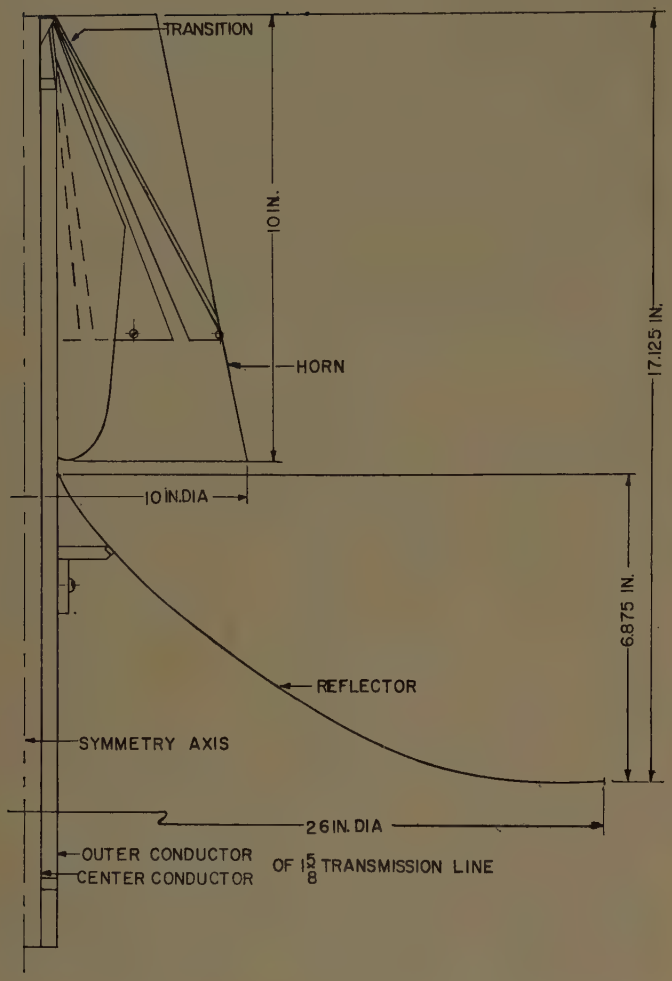

Fig. 3—Layout of small-scale experimental antenna.

1) the central part of the reflector,
2) the aperture of the horn,
3) the end of the toroidal line,
4) the input of the toroidal line, and
5) the input of the impedance transformer.

The larger part of these reflections can be calculated in a straight forward way and will not be discussed here. However, the results of these calculations show that the individual reflections are less than a few per cent and a very low input VSWR can be obtained in a 2:1 frequency band. Some experimental data will be presented in the following paragraph.

Experimental Results

Though the possible use of the above discussed feed system and reflector structures is quite wide, experimental data will only be given for one particular application. In this case a medium gain (6~8 db) antenna was required, with slight beam shaping in the vertical plane.

Two small-scale models were constructed for the 2.0–3.8 kmc frequency band. Fig. 4(a) and 4(b) show the two models. The model in Fig. 4(a) is a smaller gain antenna and was built mainly for pattern measurements. Therefore, it does not contain the toroidal line section. However, the input VSWR data of this model are characteristic for the reflection of the horn aperture and reflector and were less than 1.32 in the whole frequency band. At the same time, the gain of this model was in the order of 6 db (see curve *A* on Fig. 8), and the cross polarized (horizontal) field component was at least 14 db less than the vertically polarized component.

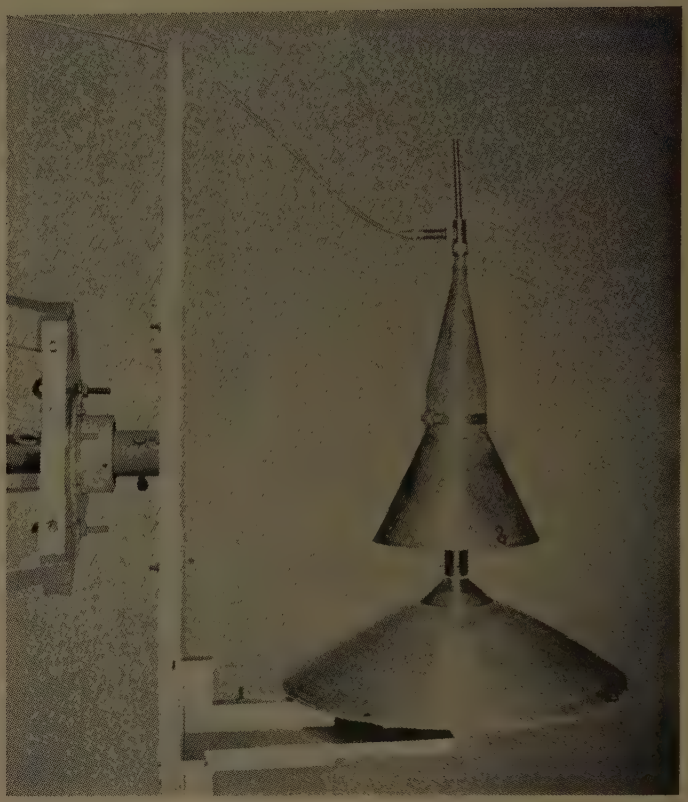

(a)

(b)

Fig. 4.

The model represented in Fig. 4(b) is closer to the final form of the antenna, therefore more details will be given about the characteristics of this antenna.

It was experienced that the inverting transition in the feed horn was a rather critical component of the system.

This transition affects the impedance behavior of the antenna to a significant degree and, moreover, has a great influence on the appearance of higher-order modes and any such higher modes will disturb the gain characteristic of the antenna. During these experiments it was found, moreover, that a rather simple transition yielded a VSWR of 1.7 or better, together with the design objective for the gain of 7 db.

If the coaxial horn has a throat impedance equal to the characteristic impedance of the input line, a match will result. This condition is more easily obtained towards the lower-frequency end of the band. As the frequency is increased, the energy stored in the joint becomes larger and hence any junction effect will become more pronounced. This junction effect can be decreased be keeping the characteristic impedance at the junction between input line and horn at a low value.

Based on this consideration, an impedance of 25 ohms was chosen for the input of the coaxial horn. Calculations have shown that a four-step Tchebycheff transformer is capable of achieving an almost perfect match between the 25 ohms and the 50 ohms impedance of the feed line.

The four steps are necessitated by the wide frequency band to be covered. During the experiments, however, it was found that a single quarter-wave transformer already gives an impedance match within the specified limits (VSWR <1.8). The actual transformer was built by inserting a Teflon spacer 0.9 inch long at the cross section of the junction, giving a section of 35 ohms, one quarter-wave long in the middle of the frequency band.

Physically, the reflector was constructed from 64 rods formed to the proper (nearly parabolic) shape. Only half of these rods extended the full length of the cross section; the other half was used to fill in the spacing between the full-length ones at the greater radii. Such a reflector properly built can reasonably be assumed to support a surface wave besides reflecting an incident wave. Thus, such a reflector can be the source of a complex radiation. The upper portion will act more as a reflector, radiating a broadside pattern, with the lower part supporting a traveling wave, *i.e.*, radiating as an endfire antenna.

The existence of a separate guided and reflected wave can be proved relatively easily by varying the distance between the reflector and the horn. If the separation is small, then practically no reflected wave can occur and the energy is propagated along the gradually increasing center conductor of the coaxial horn. The direction of the radiation maximum encloses a very small angle with a line which is tangent to the end of the reflector. This radiation can be considered as an endfire radiation generated by the guided wave along the reflector. The angle of maximum radiation decreases with the size of the reflector.[4]

If the separation between the horn and dish is large, the latter can be considered as a pure reflector, and the radiation maximum can be determined approximately by means of geometrical optics. In this case the angle of maximum radiation is independent from the size of the reflector and is determined by the relative position of the focal point of the reflector and the radiation center of the horn. In the intermediate range, both radiations exist and depending on the energies content and phase relationship of the two modes, various pattern shapes can be generated.

Fig. 5 shows some measured patterns as a function of the horn reflector separation. Curve *A* shows a typical guided (or endfire) beam while *B* represents a reflected

[4] E. M. T. Jones, "An annular corrugated-surface antenna," Proc. IRE, vol. 40, pp. 721–725; June, 1952.

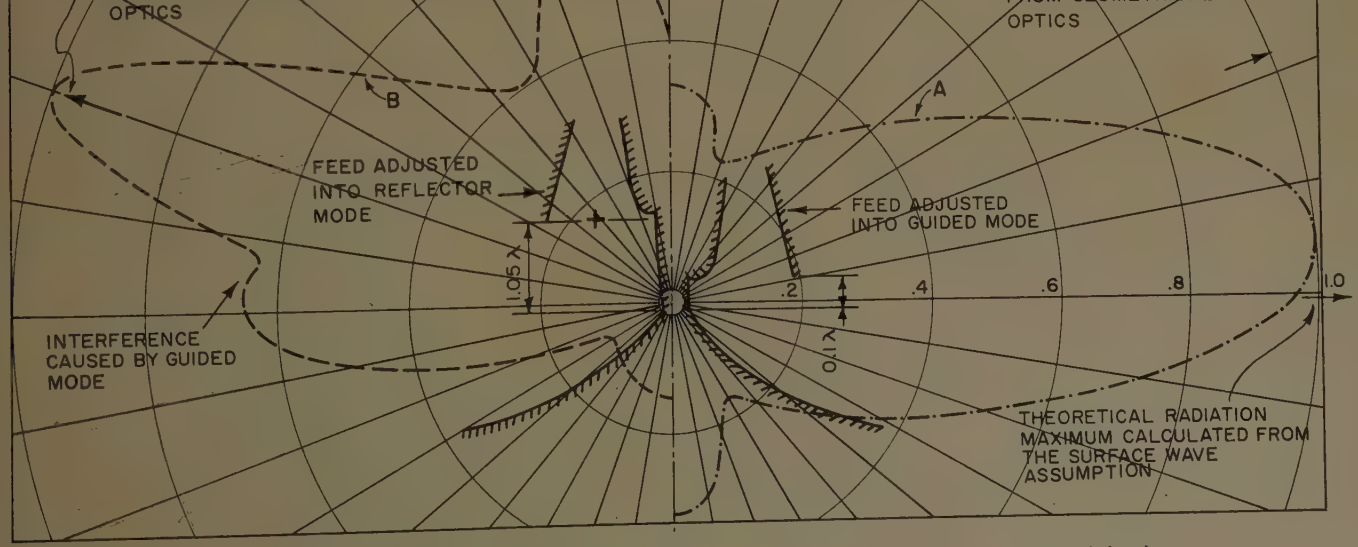

Fig. 5—The existence of guided and reflected wave in the antenna system (experimental data).

(or broadside) pattern, with the same surface wave effect. Further details were published by the author in another paper.[5]

Within the dimensions of this experimental model, the "broadside" part of the reflector can be estimated to extend over approximately two wavelengths with the "endfire" section being of about the same dimension when considered for the lower end of the frequency band. Simultaneously, the beam emanating from the horn is rather wide at the lower frequencies, thus illuminating the outer "endfire" portion relatively well. In case of both parts of the reflector radiating about equal power, the over-all beamwidth of this system will be about 30 per cent smaller than that of a broadside system alone. No particular attention was given in the design of the model antenna to this surface wave. However, the 3-db beamwidth of 22–24° obtained at the low frequencies clearly indicates the presence of such a surface or traveling wave. As the frequency is increased, the horn radiates a narrower beam, decreasing the illumination of that part of the reflector from which the end fire radiation originates. Moreover, the phase relation between the reflected wave and the surface wave on the reflector is disturbed, resulting in a very constant gain over a wide frequency range (see Fig. 8).

The separation of the rods forming the reflector is widest between the full-length rods just inside the half length rods and at the outer edge. At the highest frequency this separation is about one-third of a wavelength. While under these conditions some of the incident energy most likely will not be reflected, this arrangement can be considered to be very simple structurally and so represent a smaller wind load.

Two of the more important dimensions could be varied in the model. These were the spacing y between the horn and the reflector and the length x of the gap in the inverting transition. Within the time available, it was not possible to determine the exact optima for these dimensions, but the dimensions given in Fig. 3 are thought to be very close to these optimum values. In the course of the experiments, the pattern in the vertical plane was found to be little affected by variation of the horn-reflector spacing from 0.5 to 1.5 inches.

The other dimension variable in the model, the length x of the gap in the transition, was found to be quite critical with reference to good impedance matching.

Fig. 6(a) to 6(h) shows the measured vertical patterns for the model *B* antenna. Fig. 7 summarizes these patterns with respect to 3-db beamwidth and the direction of the main beam. The following information can be extracted from these figures.

1) The direction of the main beam varies from about 19° above the horizon to approximately 1°, with an average of close to 10°. The design value was

[5] P. Foldes and S. Komlos, "Theoretical and experimental study of wide band paraboloid antenna with central reflector feed," *RCA Rev.*, vol. 21, pp. 94–116; March, 1960.

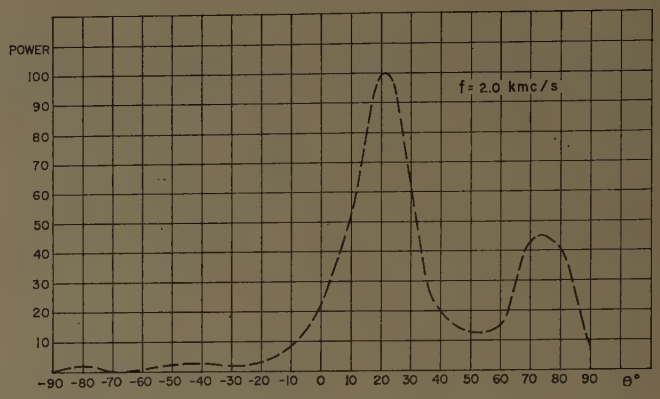

(a)

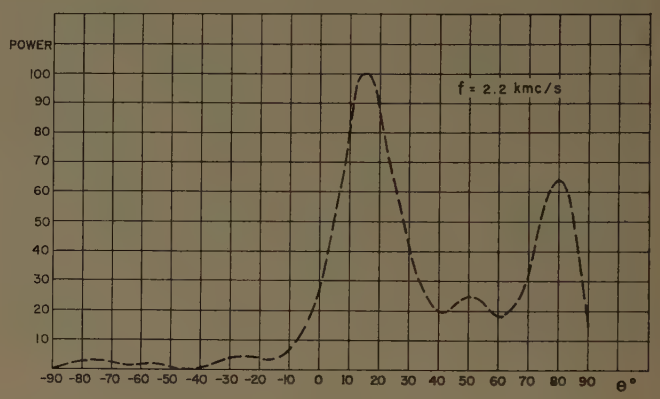

(b)

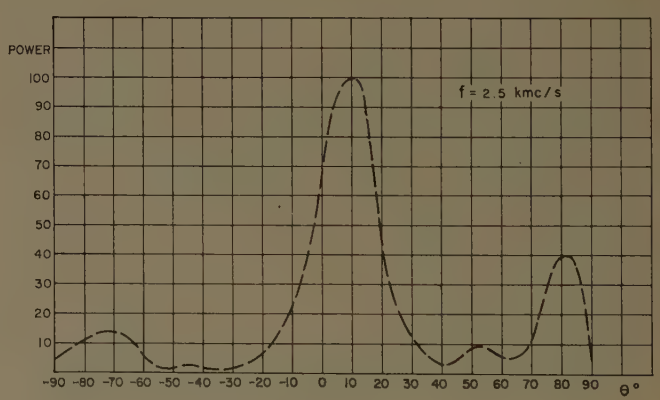

(c)

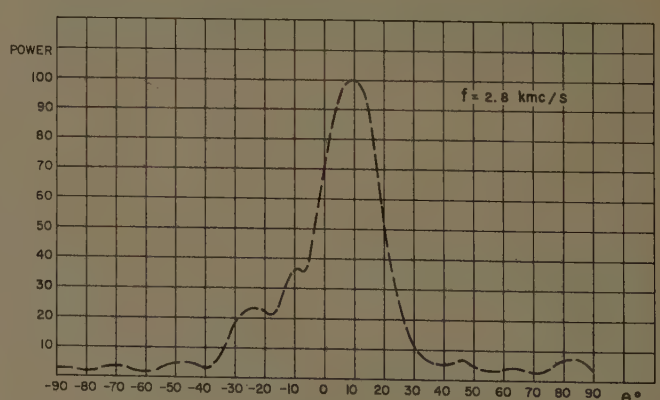

(d)

Fig. 6—Vertical patterns.

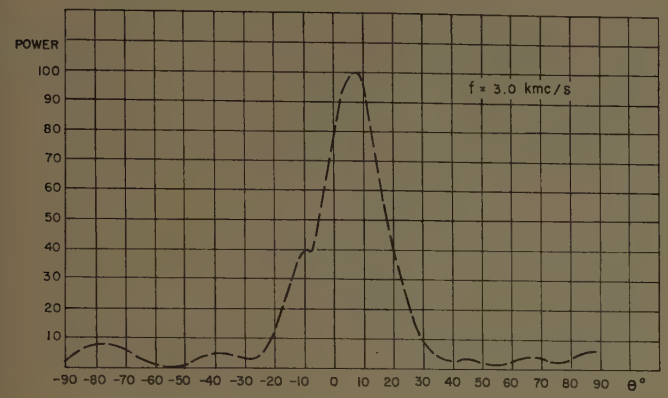

(e)

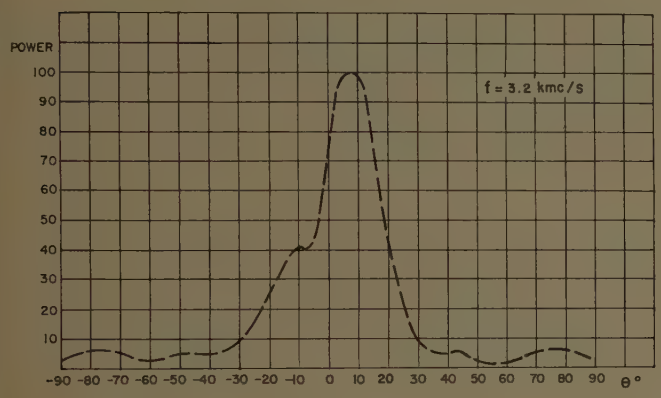

(f)

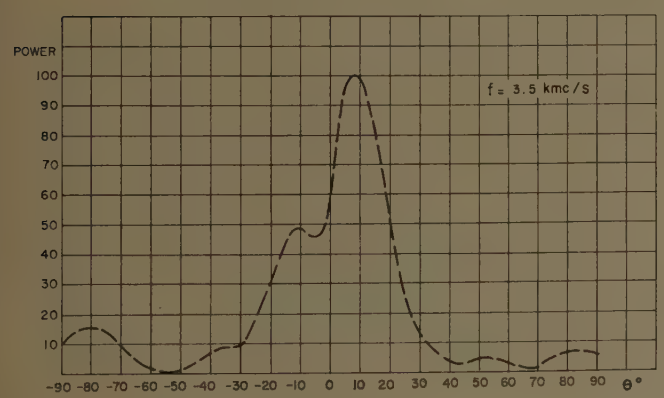

(g)

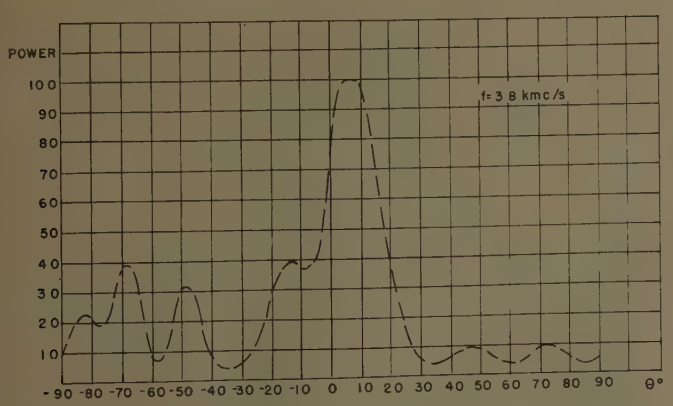

(h)

Fig. 6—cont'd.

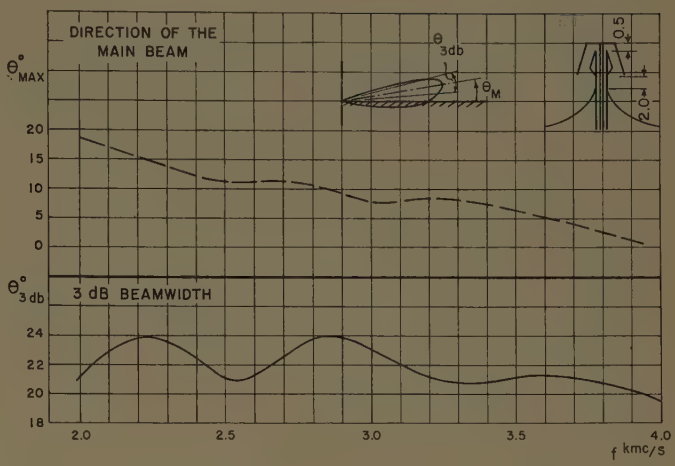

Fig. 7.

5° and a somewhat smaller variation had been anticipated. The average can be adjusted simply by increasing the distance y, but a somewhat steeper reflector shape will be necessary to reduce the variation in the beam tilt.

2) The 3-db beamwidth shows some fluctuations with frequency, but these are fairly small. Most likely these fluctuations came from spurious propagation (higher-order modes) and from some interference between reflected and surface waves. Improving the symmetry of the system mechanically will reduce the possibility for higher mode propagation, and the interference problem can be minimized by refining the design of the horn and the reflector.

3) The high angle radiation from 70° to 90° is relatively large at the low-frequency end of the band. This is the result of the shape of this particular reflector. With increasing frequency, the radiation from the horn becomes more concentrated towards the parabolic section of the reflector and the high angle radiation decreases. In the center of the band, the radiation is basically in a single beam and at the high-frequency end, the radiation through the reflector becomes greater and results in a relatively high field over the range $-70°$ to $-90°$. Giving the reflector a closer meshed design will decrease this radiation. The sidelobe levels at $\pm 90°$ are high; however, the energy content in these lobes is small in relation to the main beam in the case of omnidirectional radiation, and are tolerable in many practical cases.

The gain of this experimental model was determined from the pattern measurements by method of integration and the result is shown in Fig. 8 by curve *B*.

While the 3-db beamwidth varied slightly, the gain remains almost constant with frequency. This is considered to be due to the high and low angle radiation properties discussed before. Fig. 8 shows that the gain of this model ranges from 6.7 to 7.1 db, with 7 db being the design objective.

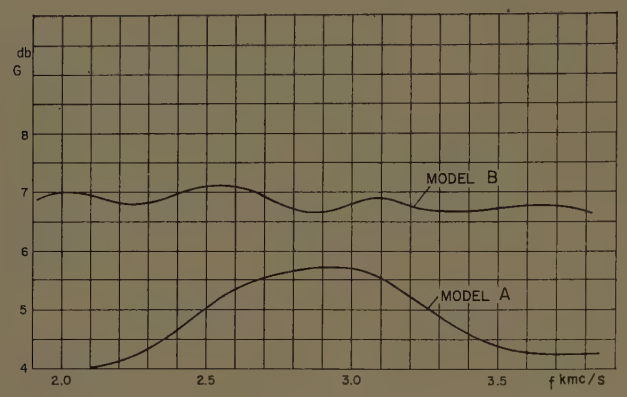

Fig. 8—Gain above isotropic radiator.

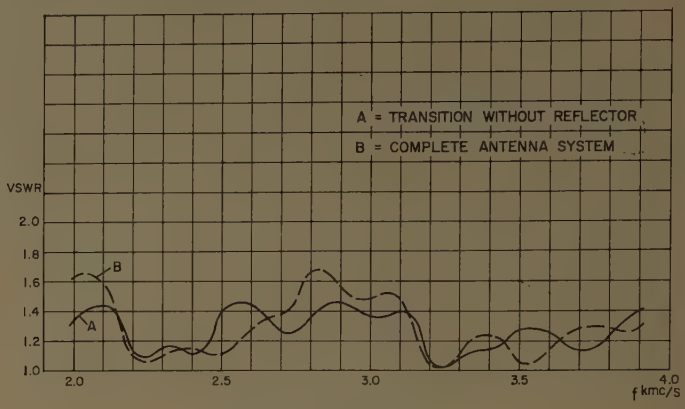

Fig. 9—Input VSWR.

The VSWR behavior of the antenna is depicted in Fig. 9. Curve *A* gives the performance of the system with the reflector removed. This curve, therefore, is a close indication of the VSWR characteristic of the inversion transition.

Curve *B* is a plot of the VSWR of the complete system. The addition of the reflector results in a slight increase only. Maxima VSWR values without and with the reflector are 1.45 and 1.68. From this it appears that the transition is the important and limiting part with respect to impedance characteristic.

Comparison of VSWR and gain curve reveals an interesting correspondence. The relatively high VSWR at about 2.1 and 2.8 kmc is related to a relatively large 3-db beamwidth and corresponding low gain. This indicates the existence of higher-order spurious modes at these frequencies, resulting in higher reflections and improper illumination of the reflector.

Conclusions

The given simple methods of calculations are satisfactory as a design basis of the new antenna. The measured experimental data show that the developed system is useful for middle gain, high-power UHF applications. On the other hand, it should be noted that the given experimental results are not the optimum and merely indicate the usefulness of the principle.

Maximally Flat and Quasi-Smooth Sector Beams*

A. KSIENSKI†

Summary—**Methods for the synthesis of sector beams are presented and illustrated with examples. First a perfectly smooth and square beam, the equivalent of the maximally flat transfer function of network theory, is discussed and synthesized. It is then shown that realization of such beams by means of relatively short arrays is feasible when a certain amount of oscillation is permitted. The resulting beam approximates the maximally flat one in an almost equal ripple fashion, the amplitude of the ripple depending on the length of the array and the desired slope of the main beam.**

* Received by the PGAP, December 8, 1959; revised manuscript received, March 1, 1960. The research reported in this paper has been sponsored by the Electronics Research Directorate of the Air Force Cambridge Research Center, Air Research and Development Command, Bedford, Mass, under Contract No. AF19(604)-3508.

† Microwave Res. Lab., Hughes Aircraft Co., Culver City, Calif.

I. Introduction

CERTAIN antenna applications require sector beams of constant signal level over a certain range of the observation angle Θ. Beyond that range, the signal level is supposed to decay as fast as possible and stay at a very low level for the rest of the observation range. The smoothness of the beam top is required for certain reconnaissance and search operations where the errors introduced by oscillating patterns cannot be corrected by the system. Also, certain low-noise high-precision antenna applications require beams of this type. The permitted deviations from the desired signal levels are too small to permit either a Fourier or a Woodward type synthesis. What is presently desired is a

flat topped beam, similar to the "Butterworth" or "maximally flat" transfer function in network theory. This paper describes methods for the synthesis of such beams. First, the network and the array problems will be compared, and it will be shown why the same technique cannot be applied to both.

The Equivalent Problem in Network Theory

The expression for the maximally flat transfer function in network theory is given by

$$f(\omega) = \frac{1}{1 + \omega^{2n}} \qquad 0 \leq \omega \leq \infty \tag{1}$$

where ω is the frequency variable.[1] In this function, depicted in Fig. 1, the first $(2n-1)$ derivatives vanish at the origin which produces the flat top effect for $\omega < 1$, while the high power of ω in the denominator causes the fast decay of the function for $\omega > 1$.

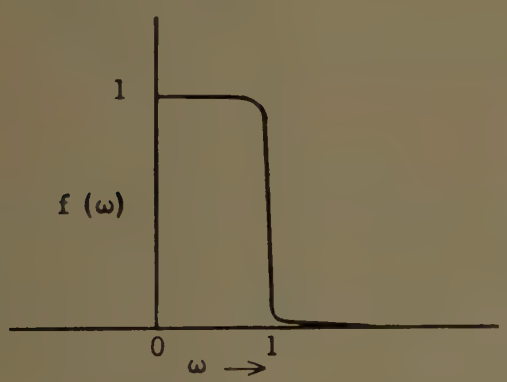

Fig. 1—Maximally flat transfer function.

Let us now examine the antenna pattern expression representing a half-wavelength[2] spaced array of $2N+1$ elements. For a pattern symmetric with respect to the origin, the expression is

$$F(u) = \sum_{0}^{N} a_n \cos n\pi u \tag{2}$$

where $u = \sin\theta$. When (2) is compared with the general expression representing a network function,

$$f(\omega) = \frac{\sum_{0}^{N} a_n \omega^n}{\sum_{0}^{M} b_n \omega^n} \qquad 0 \leq \omega \leq \infty, \tag{3}$$

it is clear that the most important advantage of (3) is that it contains poles, which may be used to produce fast changes of the function at desired points and produce zeros for $\omega \to \infty$. This results in the high attenuation of $f(\omega)$ for $\omega > 1$ and contributes to the squareness of the Butterworth function.

Since in the antenna array case there are no attenuation factors corresponding to poles, one is forced to divide the available parameters between the origin and the end of the visible range. An examination of (2) will show that there are $N+1$ parameters, and they can be divided in any desired proportion between the two end points ($u=0$ and $u=1$). The present goal is to obtain a pattern that has a flat-topped beam which attenuates smoothly to zero at the highest possible rate for the given number of elements in the array. This will be considered as the equivalent for antenna arrays of the "maximally flat" function.

II. Maximally Flat Beams

General Discussion

The necessary constraints may be imposed directly on (2), and the resulting a_n computed. Such a solution would involve a matrix inversion, which may be quite cumbersome. What is more important, it is difficult to evaluate the behavior of a trigonometric polynomial for incremental values of θ or to evaluate other functional properties. Ordinary polynomials can be handled more easily since their properties are simpler in many respects and can be directly evaluated. Therefore the trigonometric polynomial will be converted into a simple polynomial form and the various operations and evaluations will be carried out in that form. In the last step, however, the polynomial is reconverted to a trigonometric form to avoid slow convergence. As will be shown later, a polynomial of a very high order is required to obtain a satisfactory square beam. However, when the polynomial is transformed into its trigonometric representation, it is found that the series is so highly convergent that only the first few terms are significant.

Using this technique, rewriting (2) in powers of $\cos \pi u$, and substituting $x = \cos \pi u$ gives[3]

$$F(x) = \sum_{0}^{N} A_n x^n \qquad \begin{matrix} -1 \leq x \leq +1 \\ 1 \geq u \geq 0 \\ \frac{\pi}{2} \geq \theta \geq 0. \end{matrix} \tag{4}$$

Since the derivative behavior of the pattern is of interest, the following expression will be discussed:

$$F'(x) = \sum_{0}^{N-1} B_n x^n. \tag{5}$$

$F(x)$ will then be obtained by integrating the desired $F'(x)$.

[1] S. Butterworth, "On the theory of filter amplifiers," *Experimental Wireless*, vol. 7, pp. 536–541; October, 1930.

[2] The inter-element spacing may be varied with well known results. See S. Silver, "Microwave antenna theory and design," M. I. T., Rad. Lab. Ser., McGraw-Hill Book Co., Inc., New York, N. Y., vol. 12, p. 261; 1949.

[3] In the present discussion an array of an odd number of elements is assumed. The even number case is discussed in Section IV.

Since the derivatives of the pattern are to vanish at the end points only, zeros of appropriate orders are placed there to obtain a desired beamwidth. Thus the general expression for the pattern derivative is given by

$$F'(x) = (x + 1)^{\alpha}(x - 1)^{\beta}, \tag{6}$$

where $\alpha+\beta=N-1$, and where the ratio of α/β is chosen to produce a given beamwidth.

The choice of a particular beamwidth, $\pm 30°$, will simplify calculations and aid in the determination of the characteristics of such beams. Most of the details worked out for this example will apply to other beamwidths.

Beams of $\pm 30°$

If the zeros of the derivative are equally divided between the origin and the end of the visible range, a 30° beamwidth is obtained.[4] This can be seen from (6); letting $\alpha=\beta=m$ yields

$$F'(x) = (x^2 - 1)^m, \tag{7}$$

which is symmetric with respect to the origin. Thus the angle θ corresponding to the value $x=0$ represents the beamwidth. To make sure that the desired pattern is obtained, the proper sign must be attached to make $F'(x)$ non-negative for $|x| \leq 1$. Thus the correct expression is given by

$$F'(x) = (1 - x^2)^m. \tag{8}$$

$F(x)$ is then given by

$$F(x) = \int_0^x (1 - x^2)^m dx + A_0, \tag{9}$$

where A_0 is reserved to adjust the level of $F(x)$ so that

$$F(-1) = 0 \qquad \left(\theta = \pm \frac{\pi}{2}\right). \tag{10}$$

Example

Let us compute the excitation distribution and the pattern for $N=7$ which corresponds to $m=3$. Applying (9) and (10) we obtain, after converting to cos $n\pi u$ and expanding,

$$F(u) = 0.457 + 0.547 \cos \pi u - 0.109 \cos 3\pi u + 0.0215 \cos 5\pi u - 0.002 \cos 7\pi u. \tag{11}$$

This pattern is plotted in Fig. 2 and compared to a Fourier approximation of the same desired sector beam of $\pm 30°$ width. In both methods the same number of elements was used. Note the smoothness of the maximally flat beam and the perfect agreement with the desired pattern for the first $\pm 15°$. This, however, is obtained at the expense of beam slope.

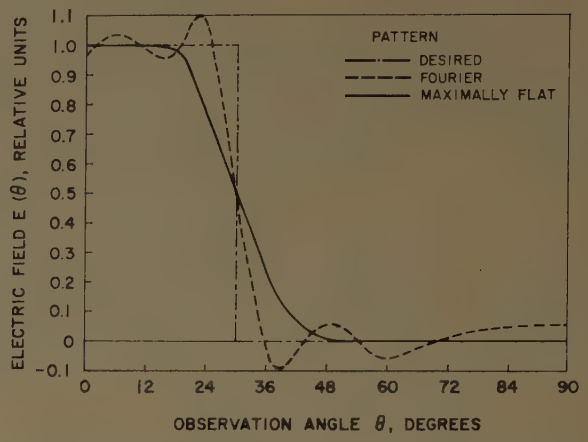

Fig. 2—Sector beam produced by a 7-wavelength array.

The slope at the transition from the main beam to the sidelobe region and its interaction with the flatness requirements will now be discussed. The slope[5] at the transition point $x=0$ may be specified by choosing an appropriate value for c in

$$F'(x) = c(1 - x^2)^m, \tag{12}$$

and the desired flatness may be specified in terms of maximum allowable value of $F'(x)$ for $|x|$ larger than some desired value. This will determine m, that is, the length of the array. If the specification is given in terms of allowable deviation of the main beam from the constant signal level, the following approximation may be used to simplify computation. The behavior of $F'(x)$ in the vicinity of $x=+1$ is affected primarily by the mth-order zero at $x=+1$ and may therefore be approximated by

$$g'(x) = a^m c x^m \qquad 1 < a < 2, \tag{13}$$

where the center of coordinates was shifted to $x=1$, and where the effect of the zeros at $x=-1$ is represented by a^m. For an allowable deviation Δ, we obtain

$$g(x) = \int_0^{1/2} c a^m x^m dx \leq \Delta. \tag{14}$$

For $a=2$ the upper limit for m is obtained,

$$m \leq \frac{c}{2\Delta} - 1. \tag{15}$$

Now, a specification which is most likely to appear is the desired interval in x over which the beam has to decay, say to 10 per cent of its value. This is the equivalent of the decay time in networks. For this purpose, the follow-

[4] Beamwidth is defined as the angular distance between the points of maximum beam slope which in this discussion are equivalent to 6-db points.

[5] The actual slope with respect to θ, the observation angle, is given by

$$\frac{dF}{d\theta} = F'(x)\pi \sin(\pi u) \cos \theta.$$

ing simple approximation may be used. Since the change considered is for small values of x,

$$(1 - x^2)^m \simeq e^{-mx^2} \quad \text{for} \quad x \ll 1. \tag{16}$$

Hence, given the value of x_0 for which the beam should decay to 10 per cent of its initial value, or should reach 90 per cent of its final value, the following relation may be employed:

$$\frac{\int_0^\infty e^{-mx^2}dx - \int_0^{x_0} e^{-mx^2}dx}{\int_0^\infty e^{-mx^2}dx} = 0.1. \tag{17}$$

Substituting (to convert to the standard form of the error function)

$$x = \frac{t}{\sqrt{m}}, \tag{18}$$

and normalizing results in

$$\frac{2}{\sqrt{\pi}}\int_0^{x_0\sqrt{m}} e^{-t^2}dt = \frac{a}{b} = 0.9, \tag{19}$$

where a/b represents the fraction of the final value to be reached. Assuming that $x_0 = 0.1$, inserting this value into (19), and using error function tables[6] results in $m = 134.5$. Thus, given a desired "rise time" to any fraction of the final value, the required value of m can be computed.

Beams of Arbitrary Width

Maximally flat beams of varying width will now be derived and their characteristics evaluated. It will be shown that the beams closely approach a square shape for increasing array lengths.

An appropriate change is made in the ratio of the constants α and β appearing in (6), so that the beamwidth may be varied without introducing oscillations. The transition point, which is defined as the point of maximum slope, moves from $x = 0$ to the point at which $F''(x)$ vanishes. Changing the exponent notation from (α, β) to $(n, \alpha n)$ results in

$$F''(x) = 0 = [(1 - x)^n(1 + x)^{\alpha n}]', \tag{20}$$

where

$$n + \alpha n = N - 1.$$

The solution of (20) yields

$$x = \frac{\alpha - 1}{\alpha + 1}. \tag{21}$$

[6] L. J. Comrie, "Chamber's Six Figure Mathematical Tables," D. Van Nostrand Co., Inc., New York, N. Y., vol. 2, p. 518; 1949.

Thus when α is adjusted from zero to a large value, the beamwidth changes from a very wide and flat beam to a narrow main beam which is flat in the sidelobe region. The first beam is obtained by letting $\alpha = 0$; all parameters are used to produce zeros of the derivative at the origin which yields

$$F'(x) = (1 - x)^{N-1}. \tag{22}$$

This form may be useful where an approximation to an omnidirectional pattern is needed. The second beam is obtained when α is large and is given by

$$F'(x) = (1 + x)^{N-1}. \tag{23}$$

This is better known as the binomial pattern, which is obtained when all parameters are used to produce zeros at the end of the visible range, and it has the property of being the narrowest possible beam having no sidelobes.

An additional means of beamwidth variation is to vary interelement spacing. Thus, if no scanning is expected, one may contract the main beam up to the point where secondary beams begin to appear. On the other hand one may widen the beam as much as desired, subject only to the minimum practical interelement spacing.

Transition Slope and Beam Flatness as a Function of Array Length

The beam height must be normalized to unity at the origin so that the true shape of the beam in terms of maximum slope will be discernible, as well as the slope variation throughout the pattern.

The point of maximum slope is given by (21). The slope at that point is

$$F'\left(\frac{\alpha - 1}{\alpha + 1}\right) = \left[\left(\frac{2}{\alpha + 1}\right)^{\alpha+1}\alpha^\alpha\right]^n. \tag{24}$$

In order to normalize the above expression, the beam height is computed,

$$H(\alpha, n) = \int_{-1}^{+1} (1 + x)^n(1 - x)^{\alpha n}dx$$

$$= 2^{(\alpha+1)n+1}B(n + 1, \alpha n + 1) \tag{25}$$

where B is the Beta function. Since αn is an integer, factorials may be used, and

$$H(\alpha, n) = \frac{2^{n(\alpha+1)+1}}{(\alpha + 1)n + 1}\,\frac{n!(\alpha n)!}{[(\alpha + 1)n]!}. \tag{26}$$

The resultant expression for maximum slope is given by

$$\frac{F'\left(\frac{\alpha - 1}{\alpha + 1}\right)}{H(\alpha, n)} = \frac{[(\alpha + 1)n + 1]}{2(\alpha + 1)^{n(\alpha+1)}}\,\frac{[(\alpha + 1)n]!}{n!(\alpha n)!}\,\alpha^{n\alpha}. \tag{27}$$

As n and αn increase, Stirling's formula for the factorial may be used, yielding

$$\frac{F'\left(\frac{\alpha-1}{\alpha+1}\right)}{H(\alpha, n)} = \frac{1}{2}\sqrt{\frac{\alpha+1}{\alpha}}\,\frac{(\alpha+1)n+1}{\sqrt{2\pi n}}. \quad (28)$$

This indicates that the slope is proportional to $\sqrt{n}$ for fixed α. Then, as a function of α, it again grows for both small α, where the denominator takes over, and for larger α where the numerator contributes to the growth. For all points other than the break point, $(\alpha-1/\alpha+1)$, the slope tends to zero, and the rate of decay is proportional to the power of n.

Let Δ denote the increment from the point of maximum slope. It can be shown that

$$\log\frac{F'\left(\frac{\alpha-1}{\alpha+1}+\Delta\right)}{H(\alpha, n)} \simeq n\left[\log\left(1-\frac{\alpha+1}{2}\Delta\right) + \alpha\log\left(1+\frac{\alpha+1}{2\alpha}\Delta\right)\right], \quad (29)$$

plus terms not containing the factor n. Assuming that Δ is a small increment and keeping the terms up to Δ^3 yields the approximation

$$\log F'\left(\frac{\alpha-1}{\alpha+1}+\Delta\right) \simeq n\left\{-\frac{\Delta^2}{2}\left[\left(\frac{\alpha+1}{2\alpha}\right)^2 + \alpha\left(\frac{\alpha+1}{2\alpha}\right)^2\right]\right\}, \quad (30)$$

which is negative for all positive values of α. Hence,

$$\lim_{n\to\infty} F'\left(\frac{\alpha-1}{\alpha+1}+\Delta\right) \to 0. \quad (31)$$

From (28) and (30), it is seen that the beams converge to a rectangular shape as the array length increases, and that this holds for any beamwidth.

Since most of the detailed analysis presented for the $\pm 30°$ beam can easily be extended to beams having other widths, no further elaboration is necessary.

III. Quasi-Smooth Sector Beams

In Section II the mathematical model was developed for maximally flat beams. Exact realization of the patterns considered would require very long arrays for a fairly square sector beam. This is the price that must be paid for a perfectly smooth beam. However, in practice a perfectly smooth beam cannot be distinguished from a beam whose oscillations are of an amplitude which cannot be detected by the measuring apparatus. Hence, the absolutely smooth pattern may be replaced with a relatively smooth pattern having oscillations sufficiently small in amplitude. This is precisely where the conversion back into the trigonometric form is most important. The rapid convergence of the trigonometric series permits omission of a large part of its terms, and the synthesis technique is consequently economical in number of elements.

A more appropriate formula is first developed for obtaining the excitation coefficients. Eq. (9) can be rewritten as

$$F(\phi) = \int_0^{\cos\phi} (1-t^2)^n dt = \sum_{k=1}^{N} a_k \cos k\phi \qquad (k \text{ odd}), \quad (32)$$

where A_0 was dropped and a beam of $\pm 30°$ is again used as an example.

Taking a derivative with respect to ϕ under the integral sign, expanding in terms of $\sin\phi$, and integrating, one obtains the following series:[7]

$$F(\phi) = \frac{(2n+1)!}{n!(n+1)!}\cos\phi - \frac{1}{3}\frac{(2n+1)!}{(n-1)!(n+2)!}\cos 3\phi + \cdots + \frac{(-1)^n}{2n+1}\cos(2n+1)\phi. \quad (33)$$

Since the absolute values of the coefficients are of little importance, only the relative magnitude is required, and this relationship is given by

$$\frac{a_{r-1}}{a_r} = \frac{2(n-r)+1}{2(n-r)+3}\,\frac{r}{2n-r+2}. \quad (34)$$

Thus the first coefficient, that of $\cos\phi$, is assumed to be unity, and the others are obtained by means of (34). Also, from the same equation, an upper bound can be obtained for the error involved in truncating the series after a given term. For example, when $r=2n/3$,

$$\frac{a_{r-1}}{a_r} = \frac{2\left(\frac{n}{3}\right)+1}{2\left(\frac{n}{3}\right)+3}\,\frac{\frac{2}{3}n}{\frac{4}{3}n+2} < \frac{1}{2}. \quad (35)$$

Thus all terms following $a_{2n/3}$ will be multiplied by factors smaller than one half. This implies that a geometric series whose common ratio is $q=\frac{1}{2}$ has terms larger than the series under consideration, and thus can be used as an upper bound for convergence and error estimates.

[7] For details, see A. Ksienski, "Maximally-Flat and Quasi-Smooth Beams," Hughes Aircraft Co., Culver City, Calif., Scientific Rept. No. 3508/2, p. 19; 1959.

Example

Consider $n=50$ and compute the first ten coefficients.[8] The resulting expression is given by

$$\begin{aligned} F(u) = {} & A_0 + \cos \pi u - 0.321 \cos 3\pi u + 0.178 \cos 5\pi u \\ & - 0.113 \cos 7\pi u + 0.075 \cos 9\pi u \\ & - 0.050 \cos 11\pi u + 0.034 \cos 13\pi u \\ & - 0.022 \cos 15\pi u + 0.014 \cos 17\pi u \\ & - 0.009 \cos 19\pi u. \end{aligned} \tag{36}$$

When (36) is plotted as shown in Fig. 3, it is seen that the actual error or oscillation amplitude is equal to the omitted term 0.006 rather than 0.016, as the estimate would indicate. The reason for that is the alternating nature of the series, which decreases the significance of the omitted portion. Also note that, because of dominance of the first omitted term over the following ones, the pattern has an almost equal ripple characteristic.

The above discussion was concerned with $\pm 30°$ beams, but the results indicate the behavior for other beamwidths. The main difference is in the computation of the excitation coefficients. Using the expression corresponding to (32), and converting to $\cos \phi$, we obtain

$$F(\phi) = \int_{\pi/2}^{\cos \phi} (1+t)^n (1-t)^{\alpha n} dt, \tag{37}$$

which, upon substituting $2\theta = \phi$, yields

$$\begin{aligned} F'(\theta) &= 2^{(\alpha+1)n+1} \sin^{2\alpha n+1} \theta \cos^{2n+1} \theta \\ &= \sum_{k=2}^{2N} b_k \sin k\theta \qquad (k \text{ even}). \end{aligned} \tag{38}$$

The coefficients b_n may be obtained either by expansion or by Fourier sine inversion

$$b_k = A \int_{-\pi}^{\pi} \sin^{2\alpha n+1} \theta \cos^{2n+1} \theta \sin k\theta d\theta, \tag{39}$$

where A is a constant common to all coefficients. The resulting series is integrated as before, after ϕ is substituted for 2ϕ in (38).

IV. Synthesis by Means of Arrays of an Even Number of Elements

A symmetric pattern produced by an array of $2N$ elements spaced a half wavelength apart is given by

$$F(u) = \sum_{1}^{N} a_n \cos \left[\frac{(2n-1)\pi u}{2} \right]. \tag{40}$$

This may be transformed into a polynomial given by

$$F(x) = \sum_{1}^{N} A_n x^{2n-1}, \tag{41}$$

[8] A_0 is chosen as to make $F(u)$ vanish at $u=1$.

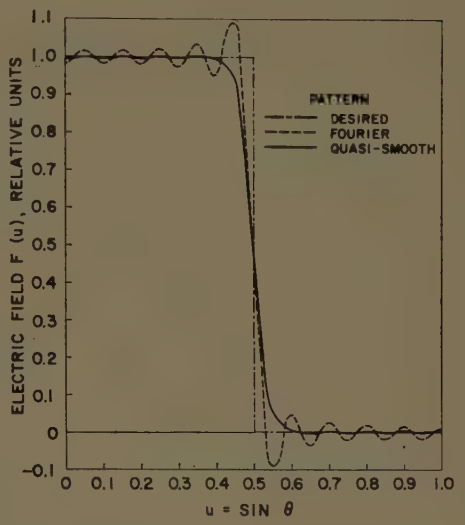

Fig. 3—Quasi-smooth sector beam produced by a 19-wavelength array (21 elements).

where $x=\cos(\pi u/2)$. Taking the derivative of the above expression, we obtain

$$F'(x) = \sum_{1}^{N} B_n x^{2n-2}. \tag{42}$$

To obtain a maximally flat beam the zeros have to be placed at $x=1$, and $x=0$ corresponding to $u=0$ and $u=\pm 1$. The expression, therefore, for the derivative is given by

$$F'(x) = cx^{2\alpha}(1-x^2)^{\beta}, \tag{43}$$

where $\alpha+\beta=N-1$, as in the previous case of an odd number of elements. The reason that (43) is given in even powers is, of course, to conform to (42), which contains only even powers. This formulation does not distort the pattern in any way, since all the zeros of the derivative appear at the correct points, namely at $x=0$, 1. The zero at $x=-1$ corresponds to $u=2$, which expresses the behavior of the pattern in the invisible range where similar beams are formed above and below the u axis. The details of analysis are parallel to the ones concerning arrays of odd number of elements and, therefore, will not be discussed further.

V. Sector Beams Derived from Optimum Patterns

The synthesis method presented in this section has the advantage of extreme simplicity and practicality. It is obtained almost directly from a Tchebycheff pattern, or similar pencil beam patterns, and can draw on a large backlog of information and tabulated data available for these patterns. It can thus be very useful for the antenna engineer as a source of readily accessible design information or as a means of estimating the performance of an array without elaborate computation.

The synthesis procedure is based on the reduction of

a desired pattern into a combination of simpler pattern functions of forms that are either easier to synthesize or that may have been already synthesized and optimized.[9] This procedure may involve differential and integral operators, operating on elementary pattern functions to produce the desired shaped beam. Thus, all operations are carried out in the $u=\sin\theta$ domain until the final results are obtained. Then the corresponding operations are carried out on the excitation distributions; this procedure is permissible since the distributions are themselves connected by a linear operator to the patterns, namely a Fourier transform. In many cases the required operations may be rather simple, as for example the Woodward synthesis, which involved only the addition of elementary patterns. Another simple operation is the integration or differentiation of an elementary pattern of any Tchebycheff or $\sin x/x$ form that may yield a desired pattern.

In the present case of a sector beam, the derivative with respect to $u=\sin\theta$ yields two delta functions displaced from each other and of opposite sign (see Fig. 4). Now the required operation is quite clear; two pencil beams of Tchebycheff, Taylor, or other appropriate nature are directed to $\pm u_0$, respectively, and subtracted from each other. The resultant pattern is then integrated, yielding the desired approximation to a sector beam.

The excitation distribution is derived by means of the corresponding operations carried out on the original pencil beam distributions, as will be demonstrated in the following example. The patterns obtained by such operations will, of course, not be of optimum nature themselves, even if derived from optimized beams. However, as the results indicate they are of very satisfactory form, the errors can be easily estimated, and, what is rather important, very few calculations are necessary.

To provide a fair comparison, the sector beam synthesized here will be, by means of an array of the same number of elements, as in Section III. Let $T(u)$ represent the appropriate Tchebycheff pattern given by[10]

$$T(u) = \sum_{n=0}^{N} A_n \cos n\pi u. \tag{44}$$

If u_0 represents the desired beamwidth of the sector beam, the pencil beam combination will be

$$F'(u) = \sum_{n=0}^{N} A_n \cos n\pi(u-u_0) - \sum_{n=0}^{N} A_n \cos n\pi(u+u_0)$$
$$= \sum_{n=0}^{N} A_n \sin(n\pi u_0)\sin n\pi u, \tag{45}$$

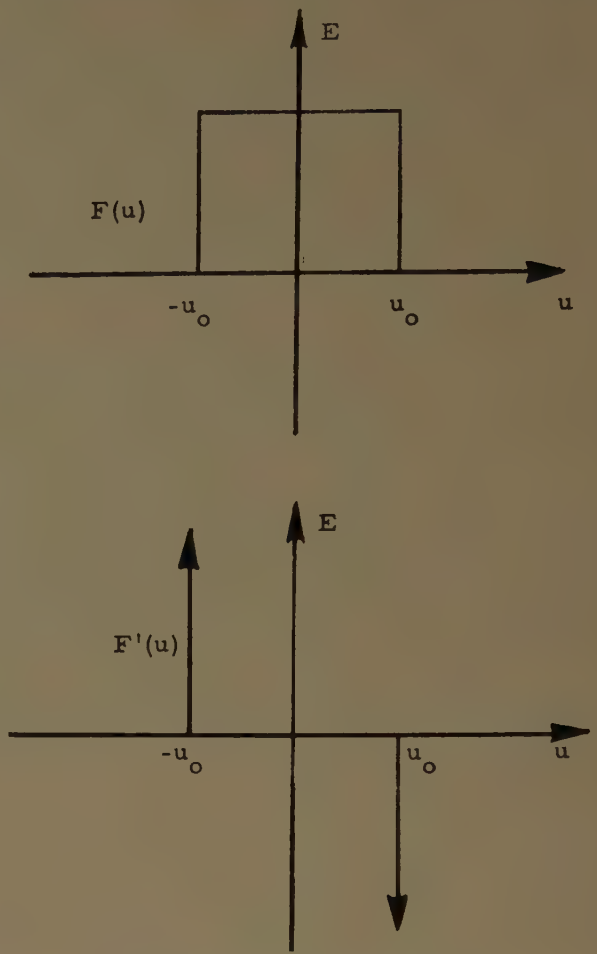

Fig. 4—A sector beam and its derivative.

from which we obtain the desired pattern

$$F(u) = \sum_{n=0}^{N} \frac{A_n}{n} \sin(n\pi u_0)\cos n\pi u, \tag{46}$$

where the A_n are the original excitation coefficients of the Tchebycheff pattern.[11] For the case of $u_0=\frac{1}{2}$ we obtain

$$F(u) = A_0 + \sum_{n=1}^{N} \frac{A_n}{n}(-1)^{\frac{n-1}{2}} \cos n\pi u \quad (n \text{ odd}), \tag{47}$$

in which A_0 is chosen to make $F(u)$ vanish at $u=1$. Introducing the proper coefficients obtained from a 38-element, 40-db Tchebycheff, we obtain

$$F(u) = A_0 + \cos\pi u - 0.319\cos 3\pi u + 0.176\cos 5\pi u$$
$$- 0.116\cos 7\pi u + 0.071\cos 9\pi u$$
$$- 0.046\cos 11\pi u + 0.029\cos 13\pi u$$
$$- 0.017\cos 15\pi u + 0.009\cos 17\pi u$$
$$- 0.008\cos 19\pi u. \tag{48}$$

[9] O. R. Price and R. F. Hyneman have independently conceived a similar idea which they applied to the synthesis of a monopulse pattern. See "Distribution Functions for Monopulse Antenna Difference Patterns," Hughes Res. Lab., Malibu, Calif., Res. Rept. No. 143.

[10] This expression assumes an odd number of elements; however, for an even number of elements, the procedure is identical.

[11] L. B. Brown and G. A. Sharp, "Tchebycheff Antenna Distribution, Beamwidth, and Gain Tables," Naval Ordanance Lab., Corona, Calif., NAVORD Rept. No. 4629; 1958.

A comparison of (36) shows the closeness of the two results. $F(u)$ is plotted in Fig. 5, which shows that we have an equal ripple for almost the whole range of u, indicating that the pattern is close to the optimum "rise time" for a given oscillation amplitude.

We shall now investigate the relation between the main beam to sidelobe ratio of the derived sector beam and the corresponding ratio of the original pencil beam. Since the sector beam represents the area under the pencil beam, the sidelobe level is not directly related to the sidelobe peak values of the original pattern, but rather to the area under those lobes. Thus in the region where the oscillation of the Tchebycheff pattern is rapid the resulting sidelobes are smaller, and when the oscillations are relatively slow, the sidelobe level will increase. When we have the summation of two (or more) beams, the oscillation rates will be different in the two beams for the same value of u, and the resulting sidelobes will oscillate at a higher rate and with higher amplitudes. This increased rate will tend to reduce the integrated sidelobe level from the value which would have resulted if the sum of the peaks carried over directly. The sidelobe level can be computed in approximate fashion by the use of the ideal space factor[12] $\cos(\pi\sqrt{u^2-A^2})$ as the pencil beam, and the resulting ratio is multiplied by a factor of 2 to compensate for the increase in sidelobe level due to sidelobe combinations and of course for the fact that the distribution is not ideal. Since the area of the slowest sidelobe is of interest, one may assume that $u \gg A$ and the sidelobe area is given by

$$A_{s.l.} = \int_{-\pi/2}^{\pi/2} \cos \pi\sqrt{u^2 - A^2}\, du \cdot \int_{-\pi/2}^{\pi/2} \cos \pi u du = \frac{2}{\pi} \cdot \tag{49}$$

The area under the main beam represents the height of the sector beam and is given by

$$A_{m.b.} \simeq \int_{-A}^{A} \cos \pi\sqrt{u^2 - A^2}\, du. \tag{50}$$

Substituting

$$u = A \sin \phi,$$

we obtain

$$A_{m.b.} = A \int_{-\pi/2}^{\pi/2} \cos(i\pi A \cos\phi) \cos\phi d\phi = A\pi\Omega_1(\pi i A), \tag{51}$$

[12] T. T. Taylor, "Design of line source antennas for narrow beamwidth and low sidelobes," IRE Trans. on Antennas and Propagation, vol. AP-3, pp. 16–28; January, 1955. Note that in this paper $u = 2a/\lambda \cos\theta$, where $2a$ is the aperture width. Although the space factor refers to a continuous aperture, it may be used for a discrete array with negligible error.

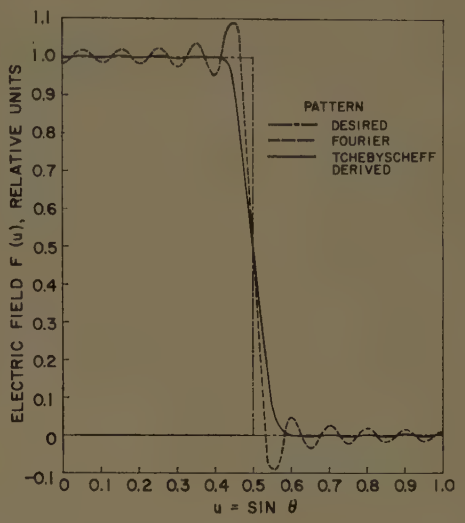

Fig. 5—Tcheybcheff-derived sector beam produced by a 19-wavelength array (21 elements).

where $\Omega_n(Z)$ is the Lommel-Weber function of nth order. If a table of these functions is not readily available, the following series expansion may be used:[13]

$$\frac{\pi}{2}\Omega_1(\pi i A) = \left[1 + \frac{A^2\pi^2}{2^2 - 1} + \frac{A^4\pi^4}{(2^2 - 1)(4^2 - 1)} + \frac{A^6\pi^6}{(2^2 - 1)(4^2 - 1)(6^2 - 1)} + \cdots\right]. \tag{52}$$

This series converges quite rapidly. Applying these results to our example where a 40-db sidelobe ratio was considered, the value of A is given by 5.3, and the corresponding value for (52) is 50.37. The main beam to sidelobe ratio is

$$\frac{A_{m.b.}}{A_{s.l.}} = \frac{A\pi\Omega_1(i\pi A)}{2/\pi} = 266. \tag{53}$$

The actual sidelobe level is at a ratio of 1:158 to the main beam, which indicates that the sidelobes have not added directly; direct addition would have resulted in a ratio of 1:133. Thus, the sidelobe level has been reduced somewhat. Actually the sidelobe level may be further reduced by a slight alteration of the shift angle u_0, which determines the way in which the sidelobes of the pencil beams combine. This is particularly effective in arrays of a small number of elements where most of the sidelobes are spaced fairly uniformly and, by a proper shift, the sidelobes of the two patterns may be made to cancel each other almost completely.

The following relations between the Tchebycheff and sector beams may be used. Given a desired "rise time" for the sector beam, a Tchebycheff beam of the cor

[13] E. Jahnke and F. Ernde, "Tables of Functions," Dover Publications, New York, N. Y., p. 211; 1945.

responding beamwidth is chosen. Thus, for example, if the sector beam is to reach to within 10 per cent of its final value within an interval θ, this interval is chosen as the beamwidth for the "parent" Tchebycheff and where the beamwidth is presently defined as between 10-db points. One can easily estimate the area under the pencil beam to determine what portion of it constitutes 90 per cent, or any other percentage specified, and thus obtain the appropriate interval θ defining the beamwidth. Once the beamwidth is determined, the array length is obtained from the permitted oscillation amplitude or sidelobe ratio.

VI. Synthesis by Means of Modified Fourier Techniques

In order to provide a more complete exposition of synthesis methods applicable to sector beam synthesis, alternative methods will be briefly reviewed. If one desires only to eliminate or reduce the ripple contained in a Fourier synthesized sector beam, there are several methods which will accomplish that task. These methods apply a taper to the Fourier coefficients, and thus insure a smooth convergence to the desired pattern. The Fejer summation technique[14] applies a linear taper given by

$$A'_n = \frac{N - n + 1}{N} A_n \qquad (n \geq 1), \tag{54}$$

where A_n is the nth Fourier coefficient, and the A'_n is the modified one, and where the series has $N+1$ terms. The results of such a taper are shown in Fig. 6 and compared to the sector beam synthesized earlier. It is seen that the ripples completely disappeared. However, the beam shape suffered substantially. One may apply a more sophisticated taper or summation scheme, called the "Cesaro m" summation, in which the weighting factor is given by

$$\frac{(N-1)!(N-n+m)!}{(N-n)!(N+m-1)!}. \tag{55}$$

By varying m between zero and unity, various tapers between the original Fourier ($m=0$) to the Fejer ($m=1$) can be obtained, thus trading between the ripple content and beam squareness. The disadvantage in the above techniques is that one has no way of predicting the oscillation amplitude for a given taper or the resulting beam steepness; thus, the method involves a trial and error procedure to obtain the desired beam shape.

[14] E. A. Guillemin, "Mathematics of Circuit Analysis," John Wiley and Sons, Inc., New York, N. Y., p. 496; 1949.

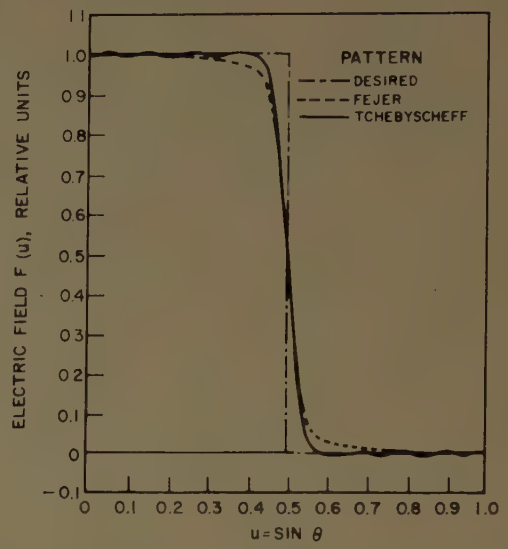

Fig. 6—Comparison between a Fejer and Tchebycheff derived sector beam.

VII. Conclusions

We have shown how a radiation pattern equivalent in nature to the maximally flat transfer function of network theory can be synthesized. This implies that the sector beam synthesized approaches a square beam without any oscillation (or sidelobes) occurring throughout the whole range of the observation variable. The "squareness" of the beam, *i.e.*, its flatness and rate of cutoff, is related to the length of the array, and will approach the perfect shape as closely as desired for increasing array lengths. Since the array lengths required for perfectly smooth beams of reasonable flatness and cutoff rate are rather large, and since perfect smoothness is undetectable, a more practical approach is considered. It is shown that the series representing the excitation coefficients converges so rapidly that only the first few terms are needed to obtain the desired beam with almost negligible oscillations, and only a relatively short array is then required. Because of the nature of the series, the first neglected term approximates the oscillation level.

The last part of the paper presents an alternative synthesis technique for obtaining, in a rather simple fashion, a sector beam of desired oscillation level and cutoff rate. This technique uses pencil beams as "parent" patterns, from which the sector beam is derived by integration. The sidelobe level of the resulting beam is indirectly related to the original pattern and is, in fact, somewhat reduced. The main advantage of the method is that most of the tabulated data relating to Tchebycheff and Taylor patterns can be almost directly applied, and the results approach an equal ripple approximation.

A Geometrical Optics Method of Pattern Synthesis for Linear Arrays*

HOWARD E. SHANKS†

Summary—**A unique phase expression is given which allows synthesis of a wide variety of shaped radiation patterns for a linear array. The accompanying amplitude distribution is found by a stationary phase evaluation of the radiation integral and is shown to be functionally related to the desired radiation pattern. Because of the optical type of approximation (stationary phase) used to evaluate the radiation integral, the method is most applicable to antennas with large size-to-wavelength ratios.**

Introduction

THE problem of pattern synthesis from array type antennas has received considerable attention for a number of years. Dolph[1] and Taylor,[2] among others, have contributed greatly to the understanding of directive pattern synthesis from linear arrays. In addition, the work of Woodward[3] and Dunbar[4] has established methods by which patterns with shaped characteristics can be synthesized. Although this body of information has many applications, situations arise for which these methods are either not physically realizable or not of optimum utility.

This paper describes a technique for shaped beam synthesis which, although related to that outlined by Dunbar,[4] is applicable to a variety of practical antenna configurations. Both schemes utilize a stationary phase evaluation of the radiation integral and are therefore equivalent from the standpoint of ultimate accuracy. The present theory differs from Dunbar's in that a judicious choice of the phase distribution is made and the amplitude excitation is adjusted to produce a desired radiation pattern. Moreover, once the range of synthesis is fixed, the phase expression remains unchanged for any type of pattern; the pattern under this condition is controlled only by the amplitude distribution. The required phase distribution is a simply varying function, and hence the present method may be of considerable value as an alternate technique or as the preferred technique in special situations.

* Received by the PGAP, October 16, 1959; revised manuscript received, February 22, 1960. This work was supported by the USAF under Contract No. AF19(604)-3508 with the Air Force Cambridge Reserve Center. Similar material has been published as Scientific Rept. 3508/1 on this contract.

† American Systems, Inc., Inglewood, Calif. This work was performed while the author was with the Hughes Aircraft Co., Culver City, Calif.

[1] C. L. Dolph, "A current distribution for broadside arrays which optimizes the relationship between beamwidth and sidelobe level," PROC. IRE, vol. 34, pp. 335–348; June, 1946.

[2] T. T. Taylor, "Design of Line Sources for Narrow Beamwidth and Low Sidelobes," Hughes Aircraft Co., Culver City, Calif., Tech. Memo. No. 316; July 31, 1953.

[3] P. M. Woodward, "A method of calculating the field over a plane aperture required to produce a given polar diagram," *J. IEE*, vol. 93, 1946.

[4] A. S. Dunbar, "On the theory of beam shaping," *J. Appl. Phys.*, vol. 23, pp. 847–853; August, 1952.

Theory

It is common in the analysis of many types of arrays (particularly arrays of closely spaced elements) to approximate the array excitation by a continuous distribution. This is assumed in the present theory and results in little loss of generality since most practical arrays with discrete distributions approximate the continuous case rather well. The array orientation and geometry to be used in the analysis are illustrated in Fig. 1.

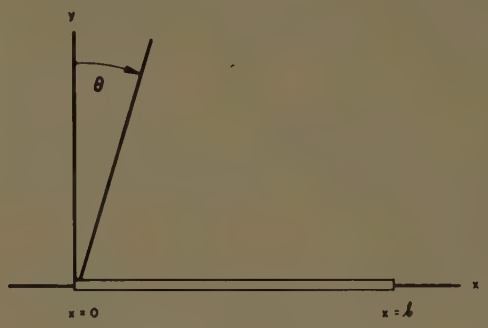

Fig. 1—Linear array geometry.

The integral representation for the radiation pattern from such a line source is given by

$$g(\theta) = A(\theta) \int_0^l \psi(x) e^{j\Phi(x)} e^{jkx \sin\theta} dx \qquad (1)$$

where $A(\theta)$ is a factor related to the polarization of the array, and $\psi(x)$ and $\Phi(x)$ are the amplitude and phase distributions, respectively. The element factor is not essential to the synthesis procedure and may be eliminated by redefining $f(\theta) = g(\theta)/A(\theta)$. Under this condition (1) becomes

$$f(\theta) = \int_0^l \psi(x) e^{j\Phi(x)} e^{jkx \sin\theta} dx. \qquad (2)$$

This expression can be considered the basic equation for synthesis from line sources of either the discrete or continuous variety. The synthesis problem is then one of determining $\psi(x)$ and $\Phi(x)$ so as to produce a prescribed pattern $f(\theta)$.

Because of the problems inherent in synthesizing a given pattern over the entire real spatial domain, it is common to specify a restricted angular domain as the region of interest. For definiteness, it will be assumed here that the pattern is specified in the range $\theta_0 \leq \theta \leq \theta_m$. As a result, the procedure will allow synthesis of a given pattern only within this range and will provide no control outside of this region.

A unique phase expression utilizing this angular range, which is the key to the entire synthesis procedure, may be written:

$$\Phi(x) = \frac{kl}{\theta_m - \theta_0} \cos\left[\frac{\theta_m - \theta_0}{l} x + \theta_0\right]. \quad (3)$$

It should be noted that this expression is a function only of the array length in wavelengths and the angular range. For the present, this relation is presented without justification. However, a plausible derivation based on intuitive considerations is given in the Appendix. Its utility will become apparent in the stationary phase evaluation of the radiation integral.

When (3) is substituted into (2), the radiation integral becomes

$$f(\theta) = \int_0^l \psi(x) \exp jk\left\{\frac{l}{\theta_m - \theta_0} \cos\left[\frac{\theta_m - \theta_0}{l} x + \theta_0\right] + x \sin\theta\right\} dx. \quad (4)$$

Considerable simplification is realized when the array length is normalized to unity by letting $\eta = x/l$. Eq. (4) then becomes

$$f(\theta) = \int_0^1 \psi(\eta) \exp jkl\left\{\frac{\cos\left[(\theta_m - \theta_0)\eta + \theta_0\right]}{(\theta_m - \theta_0)} + \eta \sin\theta\right\} d\eta. \quad (5)$$

The general synthesis result is obtained when the integral of (5) is evaluated by stationary phase methods. The stationary phase method of integral evaluation is outlined by

$$\int_{\alpha-\epsilon}^{\alpha+\epsilon} h(x) e^{j\beta u(x)} dx = \left[\frac{2\pi}{\beta u''(\alpha)}\right]^{1/2} h(\alpha) \exp j\left[\beta u(\alpha) + \frac{\pi}{4}\right] + \mathcal{O}\left(\frac{1}{\beta}\right) \quad (6)$$

where $u'(\alpha) = 0$; that is, α is the value of x for which the phase is stationary. When the first term in this expansion is used to approximate the integral, an error of the order of $1/\beta$ is made. This approximation, then, becomes better as the value of β increases. In the present formulation [see (5)] β corresponds to kl, the array length in wavelengths. The consequences of this error in terms of the array length will be mentioned later.

Applying (6) to (5) results in the integrated radiation pattern,

$$f(\theta) = l\sqrt{\frac{2\pi}{kl}}\, \psi\left(\frac{\theta - \theta_0}{\theta_m - \theta_0}\right) \sec^{1/2}\theta \cdot \exp jkl\left[\frac{\cos\theta}{\theta_m - \theta_0} + \frac{\theta - \theta_0}{\theta_m - \theta_0} \sin\theta\right], \quad (7)$$

where the stationary phase point η_s is given by

$$\eta_s = \frac{\theta - \theta_0}{\theta_m - \theta_0}.$$

Since, in most practical antennas, only the magnitude of the field is of interest, the phase term is unimportant and may be neglected. In addition, the proportionality constants are not essential and can be neglected without redefining $f(\theta)$. Under these conditions,

$$|f(\theta)| = \psi\left(\frac{\theta - \theta_0}{\theta_m - \theta_0}\right) \sec^{1/2}\theta. \quad (8)$$

Close examination of (8) reveals that if the argument of ψ is chosen as a special function of η, namely

$$\psi(\eta) = \psi[(\theta_m - \theta_0)\eta + \theta_0], \quad (9)$$

then (8) reduces to

$$|f(\theta)| = \psi(\theta) \sec^{1/2}\theta.$$

This relation may be solved to obtain the required amplitude distribution ψ in terms of the pattern $f(\theta)$. When this is done,

$$\psi(\theta) = |f(\theta)| \cos^{1/2}\theta. \quad (10)$$

With the result from (10), the complete aperture excitation necessary to synthesize a desired pattern $f(\theta)$ is given by

$$f[(\theta_m - \theta_0)\eta + \theta_0] \cos^{1/2}[(\theta_m - \theta_0)\eta + \theta_0] \cdot \exp j\frac{kl}{\theta_m - \theta_0} \cos[(\theta_m - \theta_0)\eta + \theta_0]. \quad (11)$$

It should be noted that once the length of the array (kl) and the range $\theta_0 \leq \theta \leq \theta_m$ are fixed, the pattern is controlled only through the amplitude distribution. As mentioned earlier, the stationary phase evaluation of the integral leading to (11) involves an approximation based on neglecting a term of the order of $1/kl$. The accuracy of the synthesis procedure can thus be expected to increase as the array length (kl) increases. This fact is verified in the following section where several patterns are computed exactly, using the synthesized distributions.

Numerical Computations and Patterns

The accuracy and utility of the present technique are best illustrated by graphical comparisons of the desired and synthesized radiation patterns. This is accomplished by an exact numerical evaluation of the radiation integral using the distribution obtained by the synthesis procedure. This calculation has been carried out for a cosecant-squared pattern and a sector type pattern using various values of the synthesis parameters kl, θ_m, and θ_0. As an example of the calculation, consider a sector pattern which is to be uniform over the range $-45° \leq \theta \leq 45°$ for an array with $kl = 100$. The

radiation integral under this condition is

$$f(\theta) = \int_0^1 \cos^{1/2}\left[\frac{\pi\eta}{2} - \frac{\pi}{4}\right] \exp j\frac{200}{\pi} \cos\left[\frac{\pi\eta}{2} - \frac{\pi}{4}\right] \cdot \exp\left[j100\eta \sin\theta\right] d\eta,$$

which is readily integrated by numerical methods. Table I is a compilation of the patterns calculated with the values of the parameters used in each case.

TABLE I

Desired Pattern	kl	θ_0	θ_m
Sector	100	−45°	45°
Sector	1000	−45°	45°
csc²	100	10°	90°
csc²	1000	10°	90°
csc²	100	10°	80°
csc²	1000	10°	80°
csc²	100	10°	70°
csc²	1000	10°	70°

These computed patterns have been graphed and are displayed along with the desired patterns in Figs. 2–5. The results for the sector beam pattern shown in Fig. 2 deserve special mention. For $kl=1000$ an extremely close approximation to the desired form is realized, and the marked increase in accuracy for kl increasing from 100 to 1000 is evident.

The cosecant-squared results of Figs. 3–5 demonstrate the increase in accuracy with increasing array length and also provide an indication of the effect of angular range on the procedure. The closest approximation to the desired csc² pattern is obtained for the largest range ($10° \leq \theta \leq 90°$). This might have been expected from consideration of the synthesized distribution as the range approaches zero ($\theta_m - \theta_0 \to 0$). In this limit a uniform distribution is obtained, giving a pattern with many peaks and nulls.

Comparison With Other Synthesis Procedures

It is of interest to compare the present technique with conventional synthesis methods, in particular those of Dunbar[4] and Woodward.[3] One way of accomplishing this comparison is by computation of the exact radiation pattern from a distribution obtained from these synthesis methods; this is done for Dunbar's method. In addition, it will be shown mathematically that the inherent accuracies of all methods are similar. In the first case it will suffice to show that the present distribution is in fact mathematically compatible with Dunbar's. For comparison with Woodward's technique, it will be demonstrated that both methods are exact in the limit of array length increasing to infinity.

The basic equations of Dunbar's synthesis in the present notation are

$$\frac{d\Phi(\eta)}{d\eta} = kl \sin\left[\theta(\eta)\right] \tag{12}$$

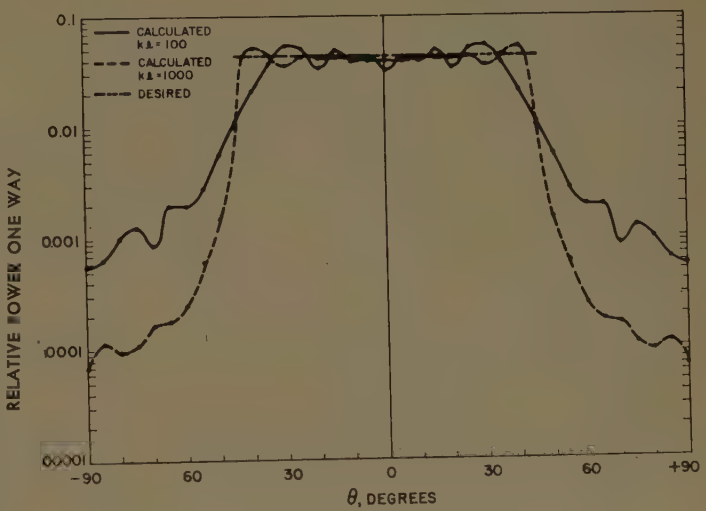

Fig. 2—Desired and calculated sector beam patterns; $\theta_0 = -45°$, $\theta_m = 45°$.

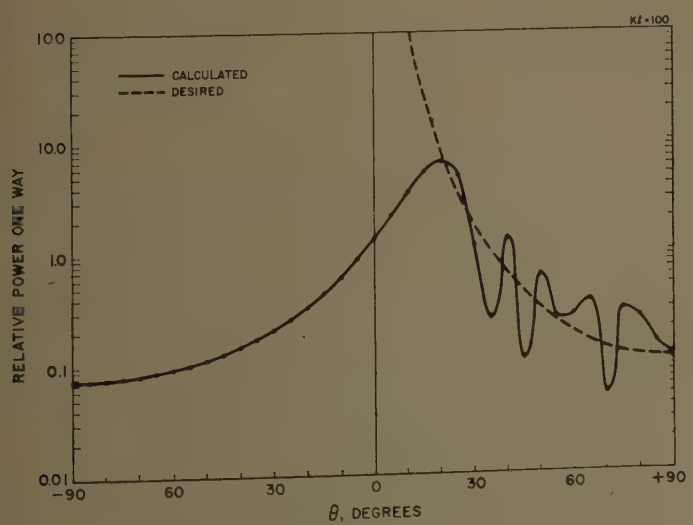

(a)

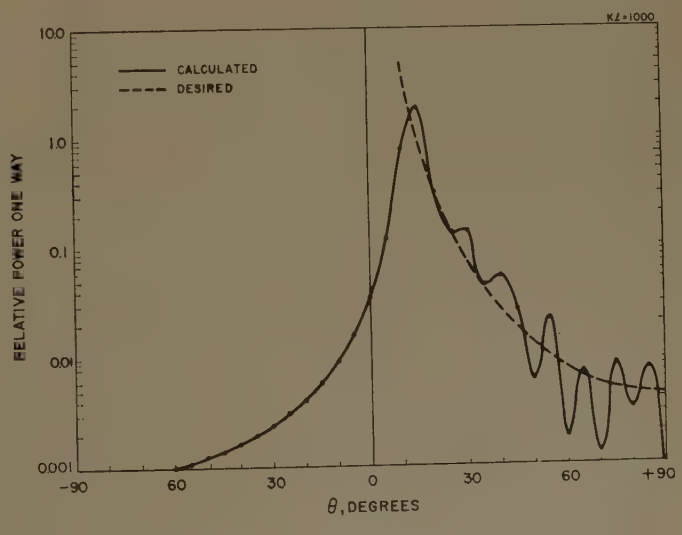

(b)

Fig. 3—Desired and calculated csc² patterns; $\theta_0 = 10°$, $\theta_m = 90°$.

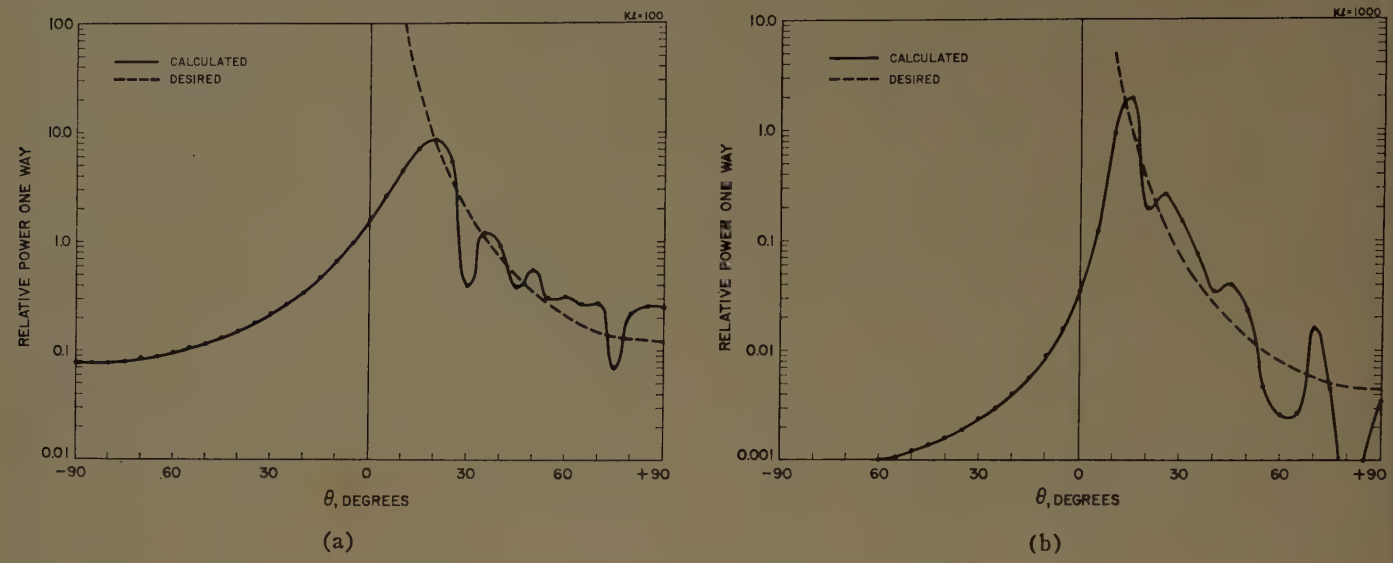

Fig. 4—Desired and calculated csc² patterns; $\theta_0 = 10°$, $\theta_m = 80°$.

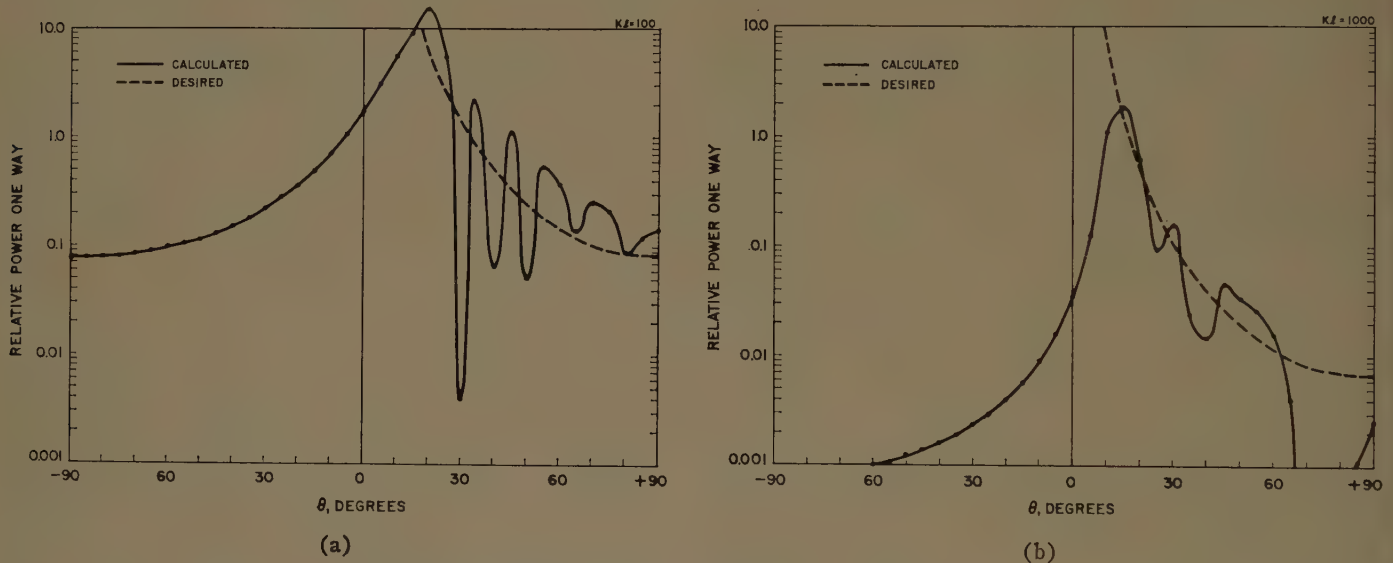

Fig. 5—Desired and calculated csc² patterns; $\theta_0 = 10°$, $\theta_m = 70°$.

and

$$\cos\theta[f(\theta)]^2 d\theta = \psi^2(\eta)d\eta \tag{13}$$

where (12) is the differential equation for the phase distribution and (13) is an equation which must be solved to find $\theta(\eta)$. If the amplitude distribution obtained in this paper, (11), is substituted into (13), there results

$$\cos\theta f^2(\theta)d\theta = \cos[(\theta_m - \theta_0)\eta + \theta_0] f^2[(\theta_m - \theta_0)\eta + \theta_0]d\eta. \tag{14}$$

Noting that the functional form of both sides of this equation are identical, we can immediately conclude that

$$\theta(\eta) = (\theta_m - \theta_0)\eta + \theta_0.$$

Substituting this result into (12) and integrating gives

$$\Phi(\eta) = \frac{kl}{\theta_m - \theta_0}\cos[(\theta_m - \theta_0)\eta + \theta_0]. \tag{15}$$

This result is identical with the phase in (11) and verifies that the present results are completely compatible with the procedure of Dunbar.

In Dunbar's paper an example of his synthesis technique is presented. For this example the desired pattern was $|f(\theta)|^2 = \csc^2\theta\cos\theta$ for the range $10° \leq \theta \leq 50°$. The array length chosen in this case corresponded to $kl = 130$. This same pattern with identical parameters was synthesized using the present theory and the exact radiation pattern was calculated by numerical methods. Both Dunbar's result and the present data are displayed in Fig. 6.

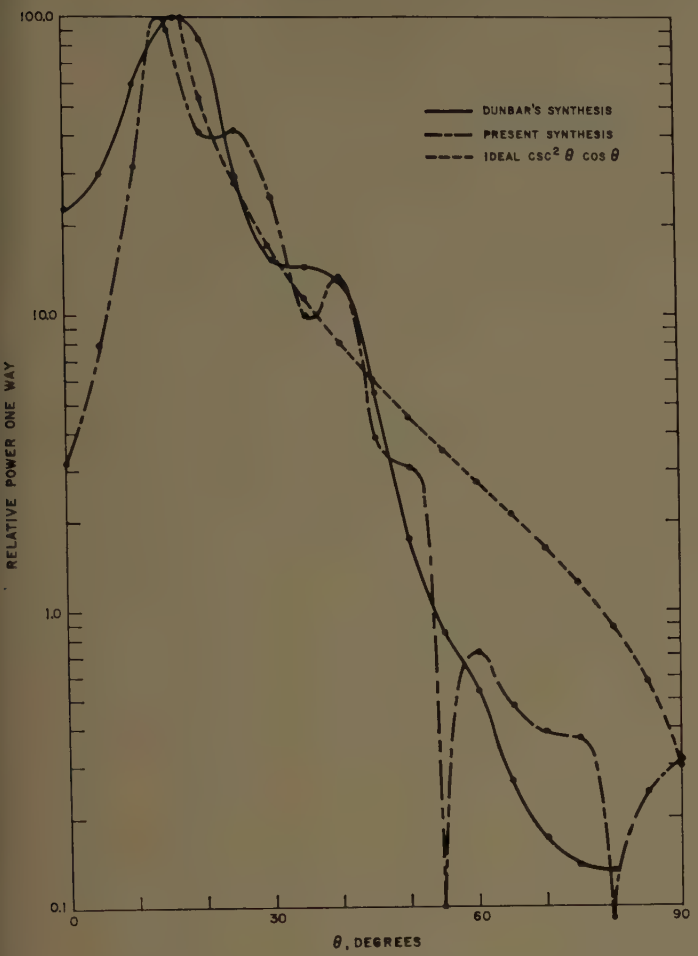

Fig. 6—Comparison of computed patterns by two synthesis methods; $kl=130$, $\theta_0=10°$, $\theta_m=50°$.

From these data both methods can be seen to provide an adequate approximation to the ideal pattern. Depending on the error criterion which is chosen as a measure of the accuracy of the approximation, one result may fare better than the other. As a result a definitive statement cannot be made as to the relative utility of the procedures. However, in a particular application one method may provide a better approximation than the other and may also be more readily realizable with a practical antenna.

The method of Woodward is based on the expansion of a desired shaped beam pattern $f(\theta)$ in a series of the following form,

$$g(\theta) = \sum_{n=-N/2}^{n=N/2} A_n \frac{\sin kl[\sin\theta - \sin\theta_n]}{\sin\theta - \sin\theta_n}, \qquad (16)$$

where the θ_n are taken in increments of pattern beamwidth between the first nulls. By this procedure the A_n are directly related to the desired pattern by

$$A_n = f(\theta_n).$$

This procedure obviously involves an approximation which can be shown to be more accurate as the array length increases. In the limit of infinite length, θ_n becomes a continuous variable α and the summation becomes an integral. That is,

$$\lim_{kl\to\infty} g(\theta) = \lim_{kl\to\infty} \int_{\alpha_0}^{\alpha_m} f(\alpha) \frac{\sin kl[\sin\theta - \sin\alpha]}{\sin\theta - \sin\alpha} d\alpha. \qquad (17)$$

But,

$$\lim_{kl\to\infty} \frac{\sin kl[\sin\theta - \sin\alpha]}{\sin\theta - \sin\alpha} = \delta(\theta - \alpha)$$

so that

$$\lim_{kl\to\infty} g(\theta) = \int_{\alpha_0}^{\alpha_m} f(\alpha)\delta(\theta - \alpha)d\alpha = f(\theta). \qquad (18)$$

Thus, Woodward's method is exact in the limit of infinite array length.

Although the above work demonstrates the equivalence of Woodward's method and the present technique in the limit of infinite length, this in itself is not enough. To show complete correlation between the inherent accuracies of the two methods, it would be necessary to demonstrate that both approximations approach this limit in the same way, namely $\mathcal{O}(1/kl)$. It has not been possible to show this, and it is doubtful that this is true. It is entirely possible that Woodward's method converges to the limit faster, implying a more accurate approximation for finite length arrays. Nevertheless, for finite but large arrays ($kl \simeq 1000$), the difficulties in working with Woodward's technique may not be worth the additional accuracy obtained.

Conclusions

A relatively simple and straightforward synthesis technique has been demonstrated which may find application in certain antenna problems. The technique should find particular application for extremely large antennas requiring shaped beam characteristics. In addition, the fixed phase nature of the synthesized phase distribution suggests applications to variable pattern antennas; the possibility of amplitude "scanning" is an important special case of this class of applications.

Because of the approximate nature of this method, in a critical application an exact calculation of the radiation pattern should be made to determine whether the result is compatible with design specifications. However, for arrays with ($kl \simeq 1000$) the results should be well within the specifications for any practical shaped beam design.

Appendix

In the body of this paper the phase distribution which is the key to the entire synthesis procedure is written without justification. Although the fact that this expression is usable is sufficient justification, a heuristic derivation is of interest.

This derivation is based on the following reasoning. Let the phase distribution along the array be such that the energy from two points at x and $x+dx$ on the array add in phase in the far-field direction (θ) associated with the position x. Mathematically this condition is expressed by

$$d\Phi(x) = -kdx \sin [\theta(x)] \tag{19}$$

where $\Phi(x)$ is the phase distribution and $\theta(x)$ explicitly denotes that the far field point must be a function of the position along the array. This relation can be taken as the simplest functional form, namely linear. We then obtain

$$\theta(x) = \frac{(\theta_m - \theta_0)}{l} x + \theta_0. \tag{20}$$

Substituting (20) into (19) results in

$$\frac{d\Phi(x)}{dx} = -k \sin \left[\frac{\theta_m - \theta_0}{l} x + \theta_0 \right] \tag{21}$$

which may be readily integrated to give

$$\Phi(x) = \frac{kl}{\theta_m - \theta_0} \cos \left[\frac{\theta_m - \theta_0}{l} x + \theta_0 \right]. \tag{22}$$

This result is identical to that used in the radiation integral earlier.

Implicit in the above formulation is the assumption that the energy radiated from the region dx at x will contribute to the far field only in a small vicinity around the direction $\theta(x)$. Obviously this is not true since the element pattern of an element dx is essentially omnidirectional. However, if the array becomes very long, the elements dx can be considered to have finite length. The element pattern can then be reasonably directive and will confine the energy mainly in the desired far-field direction. In the mathematical derivation this effect occurs by virtue of the increasing accuracy of the stationary phase method with larger kl.

Gain Limitations of Large Antennas*

ROBERT C. HANSEN†

Summary—**Arrays of many elements and continuous aperture antennas are very often designed using Taylor's "approximate" space factor which is optimum in resolution, *i.e.*, it offers minimum beamwidth for a given sidelobe ratio. This space factor has a number of equal level sidelobes followed by tapered lobes, the latter being necessary to make the aperture function physically realizable. For conventional antennas, these designs offer gain which, while not that of a uniform aperture, is quite satisfactory. Very long (or large) antennas with their narrow beamwidths, however, may exhibit a severe gain degradation due to large energy contained in the sidelobes. Thus the sidelobe behavior must be carefully controlled to realize the full gain available. Data are presented for the gain variation of various Taylor equal sidelobe designs, and of the modified sin x/x one-parameter family as a function of aperture length.**

I. Introduction

In recent years, considerable effort has been expended towards the design and realization of antennas optimum in the sense of having the narrowest beamwidth, hence best resolution, for a given sidelobe level. The Dolph-Tchebycheff array distribution has been shown to be optimum in this sense [1]–[3]. To recapitulate, the Dolph design provides that all sidelobes be of equal magnitude; this has the effect of narrowing the main beam compared to that of a pattern with tapered sidelobes where the largest is of the same amplitude as the Dolph case. The Dolph design is accomplished through forcing a correspondence between a Tchebycheff polynomial and the array polynomial. These aperture distributions are widely used and considerable literature exists to aid designers. These include the extensive tables [4] of Brown and Scharp and approximate formulas [5]. In the limit as the number of elements becomes very large, and the element spacing very small, the Dolph-Tchebycheff distribution becomes a Taylor "ideal" continuous distribution [6]. These distributions, which also have the equal sidelobe and optimum resolution characteristics, are widely used for the design of continuous line sources and apertures, and for arrays where the number of elements is large and the consequent Dolph-Tchebycheff computations tedious. Excellent tables of these aperture functions by

* Received by the PGAP, January 25, 1960; revised manuscript received, March 18, 1960.

† Space Technology Labs., Inc., Los Angeles, Calif. Formerly at Hughes Aircraft Co., Culver City, Calif.

Spellmire are also available [7]. The aforementioned references are primarily concerned with line source or rectangular aperture-type antennas; similar developments have been pursued by Taylor for circular arrays and circular apertures [8], [9]. For most antennas, the optimum beamwidth design offers a satisfactory gain value. However, in recent times, advanced system requirements have necessitated the realization of larger and larger antenna gains with construction of correspondingly larger and larger antennas. Thus, the question of optimum gain again needs to be investigated.

It has been suggested by H. Wheeler that the optimum beamwidth antennas do not provide optimum gain, especially where the antenna dimensions are large in wavelengths.[1] It is easy to see physically where a gain limit might occur. Take, for example, a long Dolph array or Taylor line source with fixed sidelobe ratio. The gain (strictly speaking, the directivity gain) is defined as the quotient of peak intensity (which we will keep fixed) to the total radiated power. The latter is the sum of the main beam power and the sidelobe power. For modest length antennas, the main beam power predominates, and as the beamwidth is narrowed (by increasing the length, of course), the radiated power decreases and the gain increases. However, the sidelobe power is essentially constant, since the sidelobe level is fixed, and all sidelobes have nearly the same shape. When the beamwidth becomes very narrow, the main beam power becomes small compared with the sidelobe power, and as the latter is nearly constant, so, therefore, is the gain. To remove this gain limitation, one must obviously taper the far-out sidelobe envelope. It is the purpose of this paper to investigate the effect upon gain of various tapers for some of the widely used aperture illumination functions. Similar reasoning shows that the gain cannot exceed the average sidelobe level. If 60-db gain is required, the average sidelobe level must be below −60 db. Ruze and others have pointed out that aperture errors affect the sidelobe structure strongly, and this represents another gain limitation.

II. Optimum Gain

The term "optimum gain" is used here in a very special sense. If no restrictions are placed on the aperture illumination function, infinite gain is, of course, possible [10], although this fact has not always been appreciated [11]. Bouwkamp and de Bruijn demonstrated that arbitrarily large directivity can be obtained for a line source, and Riblet [12] extended this demonstration to a two-dimensional distribution. The arbitrarily large gain is produced by an interference process in which large phase changes and large currents are used to produce a low value of effective radiating current.[2] This well-known phenomenon is called supergain and is generally avoided because it involves large energy storage and thereby high losses, and because of high sensitivity to excitation errors [14]. Tucker has pointed out that supergain designs are also undesirable because of their adverse signal-to-noise performance [15]. Thus, in practice, it is necessary to place some limit on the amount of supergain to be allowed. This limit can be an upper bound on the supergain ratio, which is the ratio of total power (reactive and radiated) to radiated power [6], or it can be a restriction on the allowable total phase change over the aperture, or a restriction upon the maximum slope of the aperture function. Determining the illumination function which yields maximum gain subject to one of these constraints represents an exceedingly formidable Euler-Lagrange problem, even for the simplest case of a line source. This problem has been solved by Proctor.[3] There are synthesis techniques where the gain is maximized subject to a different constraint, such as constant ohmic loss [16]. However, these do not appear to relate directly to limiting the amount of supergain. A different approach has been taken by Solymar [17] and Harrington [18]. Solymar determines the maximum gain for a specified supergain ratio and number of harmonics of the distribution function; Harrington relates the gain to the number of spherical harmonics used in expanding the pattern, and heuristically relates this to physical size.

Because of the extreme difficulty of these synthesis problems and because of the practical limitations of utilizing supergain, almost all aperture antennas are designed with a constant phase over the aperture. (For beam directions other than broadside, the constant phase is of course replaced by the linear phase corresponding to the desired beam direction.) Thus, in this paper, only constant phase distributions will be considered and "optimum gain" will be used in this context. It is readily demonstrated [19] by use of the Schwartz inequality that the constant amplitude (usually termed uniform amplitude) distribution has the largest gain of all constant phase designs.[4] However, the 13-db sidelobe ratio obtainable with the uniform illumination is often unsatisfactory for both radar and communications purposes. Thus, this paper will consider the variation of gain with length for two types of often used distributions:

1) tapered envelope distributions which afford greater sidelobe ratios, and
2) "approximate" Taylor distributions in which the far-out sidelobe envelope is tapered, but close-in sidelobes are of nearly equal amplitude.

III. Uniform Illumination

Gain factors will be given for the array or line source pattern only; the element pattern will be assumed to

[1] Private correspondence.

[2] For an array with a fixed number of elements, a maximum gain does exist. This problem has been solved for a small number of elements by Pritchard; see reference [13].

[3] E. K. Proctor, manuscript to be published.

[4] G. C. McCormack [20] shows that for an end-fed line source with ohmic losses, the uniform distribution must be modified to obtain optimum gain.

be isotropic. Because the gain of a long (of length L) uniform line source is $2L/\lambda$, it is convenient to normalize the gain, and to consider $\lambda G/2L$. For a square aperture antenna (again not including the element factor), the gain is found from

$$G_{\text{square}} = \pi G_{\text{line}}^2. \tag{1}$$

For a uniform line source, the normalized gain is readily written as

$$\frac{\lambda G}{2L} = \frac{1}{\int_{-L/\lambda}^{L/\lambda} \frac{\sin^2 \pi u}{\pi^2 u^2} du}$$

$$= \frac{\pi/2}{Si(KL) + (\cos KL - 1)/KL}, \tag{2}$$

where the normalized variable $u = L/\lambda \sin \theta$, $K = 2\pi/\lambda$, and $\mathrm{Si}(x)$ is the conventional sine integral.

The gain function is plotted in Fig. 1. For small KL, the normalized gain is greater than unity because the absolute gain G must equal unity for $KL = 0$ in accordance with the assumption of an isotropic element factor. This is just observable in Fig. 1 for $KL = 10$. The curve also contains imperceptible oscillations.

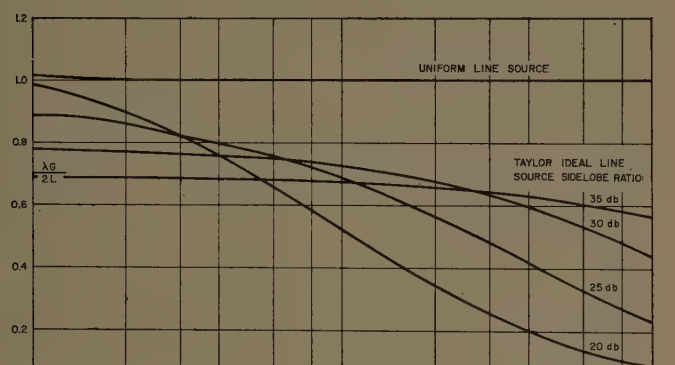

Fig. 1—Normalized gain vs length for uniform and ideal space factors.

IV. Taylor "Ideal" Space Factor

A continuous source equivalent to the Dolph-Tchebycheff array design is the Taylor "Ideal" aperture distribution and space factor [6]. The space factor has equal level sidelobes and is given by

$$P(u) = \cos^2(\pi\sqrt{u^2 - A^2}), \tag{3}$$

where the voltage sidelobe ratio η is related to the parameter A by $\eta = \cosh \pi A$. The aperture distribution corresponding to (3) is given as an infinite sum by Taylor, and has delta function singularities at each end. Thus the "ideal" distribution can only be approximated in any physical situation.

The "ideal" space factor gain is given by

$$G = P_{\max} \Big/ \int_0^{\pi/2} P(u) \cos\theta d\theta. \tag{4}$$

In order to evaluate the integral, it is separated into two at the change from cos to cosh, at $u_1 = A$. Call θ_1 the angle related to u_1, and let $\theta_1 = \pi/2 - \Delta$, where for long antennas Δ is small so that $\Delta \simeq \lambda A/L$. So the integral is

$$I_1 + I_2 = \int_0^{\pi/2-\Delta} \cos^2 \sqrt{\pi^2 u^2 - \pi^2 A^2} \cos\theta d\theta$$

$$+ \int_{\pi/2-\Delta}^{\pi/2} \cosh^2 \sqrt{\pi^2 A^2 - \pi^2 u^2} \cos\theta d\theta. \tag{5}$$

The second integral is evaluated by numerical fitting, using a sixth-degree polynomial with economized (Tchebycheff) coefficients. Error should be <2 per cent for sidelobe ratios between 20 and 40 db.

$$I_2 = \frac{2}{KL} \int_0^{\pi A} \cosh^2 \sqrt{\pi^2 A^2 - u^2}\, du = \frac{2\pi A \eta^2 .482}{KL}. \tag{6}$$

For I_1, approximate the integrand by $\cos^2 \pi u$ and integrate from 0 to $\pi/2$. This is equivalent to adding an extra fraction of sidelobe in the main beam position. For long antennas with many sidelobes and narrow main beams, this approximation is good.

$$I_1 \simeq \frac{\lambda}{L} \int_0^{L/\lambda} \cos^2 \pi u du = \frac{1}{2} + \frac{\sin KL}{2KL}. \tag{7}$$

Thus

$$\frac{\lambda G}{2L} = \frac{2\pi\eta^2}{KL + \sin KL + 1.93\pi A \eta^2}. \tag{8}$$

Fig. 1 depicts these gains for design sidelobe ratios of 20, 25, 30, and 35 db. The abscissa is L/λ, the line source length in wavelengths. As expected, it can be observed that the normalized gain falls off with increasing length; thus the gain does not increase linearly with length for long lengths and narrow beamwidths. For example, with 25-db sidelobes and $L = 100\ \lambda$, gain is down to 138 from 178. This would correspond to a line source gain of 21.4 db, or a square source gain of 47.8 db. Of more interest, however, are the "approximate" Taylor designs, which do not have singularities in the illumination function.

V. Taylor "Approximate" Space Factor

Taylor showed that there is a relation between the far-out sidelobe envelope and the behavior of the aperture distribution at the line source ends. To eliminate the infinite values of end excitation, the space factor must have a tapered far-out sidelobe envelope. The "approximate" design contains (nearly) equal sidelobes out to a transition point N, beyond which the envelope tapers down [6]. Thus the "ideal" pattern is approximated arbitrarily closely. Fig. 2 gives three examples of illumi-

nation function; as N becomes large, the end peaks tend toward a Delta function, giving the "ideal" distribution. The space factor is given as a continued product over the zeros; only the sidelobe integral I_1 of (5) is markedly different. This is now

$$I_1 = \int_0^{\pi/2-\Delta} \prod_{n=1}^{N-1} \left(1 - \frac{u^2}{\sigma^2 a_n^2}\right)^2 \cdot \prod_{n=N}^{M} \left(1 - \frac{u^2}{n^2}\right)^2 \cos\theta d\theta, \tag{9}$$

where $a_n^2 = A^2 + (n - \frac{1}{2})^2$ and σ is a main beam dilation factor close to unity produced by the shifting of zeros for $M > N$ to produce the taper (see Fig. 3). For $M \leq N$, the envelope is nearly constant; for $n \gg N$, it is sin X/X. In the region n near N, both envelopes are modified to join together. The integral over the sidelobes is evaluated by approximating each lobe by a sinusoid. Then the integral from u_1 to u_N is closely

$$\text{area} \simeq \frac{\lambda}{2L} \sum_{n=1}^{N-1} (u_{n+1} - u_n) \simeq \left[\frac{N-1}{2} - \frac{A^2\pi^2}{24}\right]\frac{\lambda}{L}, \tag{10}$$

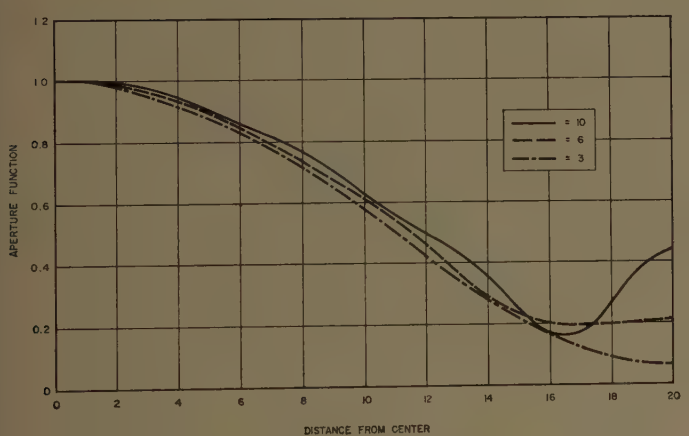

Fig. 2—Aperture distributions for 25-db sidelobe level for several N.

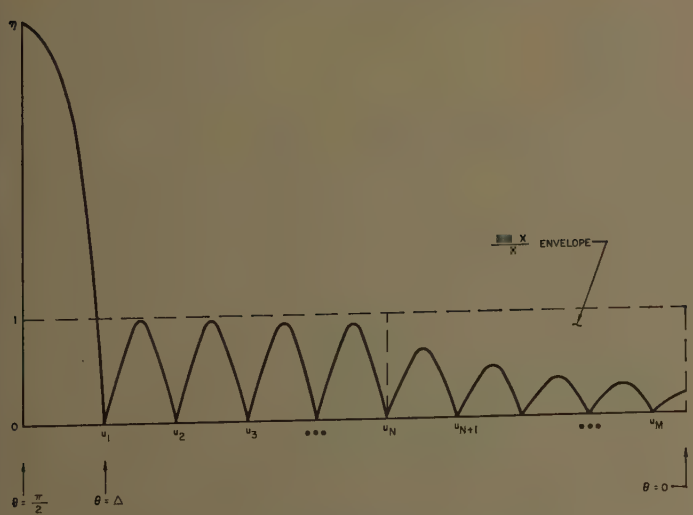

Fig. 3—Sketch of "approximate" space factor.

since

$$u_{n+1} - u_n \simeq 1 - \frac{A^2}{2n^2}. \tag{11}$$

The error in this approximation has not been evaluated, but is thought to be small. For the tapered sidelobes, the peaks are at $u = n - \frac{1}{2}$ with amplitude $2/\pi(2n-1)$. In this case, $u_{n+1} - u_n = 1$, and the integral from u_N to u_M is

$$\text{area} \simeq \frac{\lambda}{2L} \sum_{n=N}^{M} \frac{4(u_{n+1} - u_n)}{\pi^2(2n-1)^2} \simeq \frac{(M-N)\lambda}{2\pi^2 M(N+1)L}. \tag{12}$$

Now, neglecting the last partial lobe, $u_M = L/\lambda$, so the value of I_1 becomes

$$I_1 \simeq \frac{\lambda}{2L}\left[N - 1 - \frac{\pi^2 A^2}{12}\right] + \frac{\lambda\left(1 - \frac{\lambda N}{L}\right)}{2\pi^2 L(N+1)}. \tag{13}$$

The expression for normalized gain then becomes

$$\frac{\lambda G}{2L} = \frac{2\pi\eta^2}{1.93\pi A\eta^2 + 2\pi\left(N - 1 - \frac{\pi^2 A^2}{12}\right) + \frac{2\left(1 - \frac{\lambda N}{L}\right)}{\pi(N+1)}}. \tag{14}$$

Because $2/\pi N \ll 1.93\ \pi A\eta^2$, and because $\pi^2/6 \ll 1.93\eta^2$, result (14) can be simplified with small loss in accuracy to

$$\frac{\lambda G}{2L} = \frac{2\eta^2}{1.93A\eta^2 + 2(N-1)}. \tag{15}$$

If the sidelobe "break point" N remains fixed as L increases, the normalized gain is constant; that is, the gain increases directly with L as desired. A more practical design, however, would allow N to increase with L to efficiently use the aperture in producing a narrow main beam. Two cases have been computed, for $N = M/2$ and $N = M/4$. Each of these cases will exhibit a decrease of normalized gain for long lengths of line source. Figs. 4 and 5 display this for the two cases and for the 20-, 25-, 30-, and 35-db sidelobe levels.

As an example of the use of these data, suppose a line source of length $L/\lambda = 100$ is desired, with 25-db sidelobes. For a choice of $N = M/2$, or half of the sidelobes equal level and half tapered, the normalized gain is 0.8 compared to 0.91 for short line sources. The 0.8 value gives a line source gain of 22 db or a square source gain of 49 db. For $N = M/4$, or three-fourths of the lobes tapered, the normalized gain is 0.85.

Eq. (15) indicates that for a fixed length antenna, gain is maximized by using a minimum value of N. This is incorrect, as (15) does not include the beamwidth dilation factor [6] σ which is

$$\sigma = \frac{N}{\sqrt{A^2 + (N - \frac{1}{2})^2}}. \tag{16}$$

As N is decreased, the sidelobe integral decreases, thereby increasing gain. However for small N, σ is no longer approximately unity, and as N is decreased to this range, the main beam integral increases, thereby decreasing gain. Taylor [6] has given the values of N for maximum gain for the limiting case of infinite length. Examination of (14) shows that only the last term of the denominator contains the length, and if $N>3, L/\lambda>4$, this term will be less than one per cent of the preceding term. Thus for any practical length, Taylor's results are applicable. Similar results can be obtained by including σ^2 in the first term of the denominator of (14), and locating the maximum value of N. Because both main and sidelobe integrals change only slightly for small values of N, the approximation that sidelobes are of unit height out to N, whereas these actually decrease, produces a shift in maximum calculated from (14). Table I gives the values of N which give maximum gain for a fixed length of source. Values of normalized gain may be compared with the uniform source ($L=10\ \lambda$), where sidelobe ratio is 13.2 db, gain 1.01, and beamwidth 5.04°.

For short line sources with a few sidelobes, the approximations made in obtaining the gain are sufficient to indicate a value of gain for the 20-db Taylor case higher than uniform; this is, of course, not valid. Good accuracy is obtained for $L>20\ \lambda$.

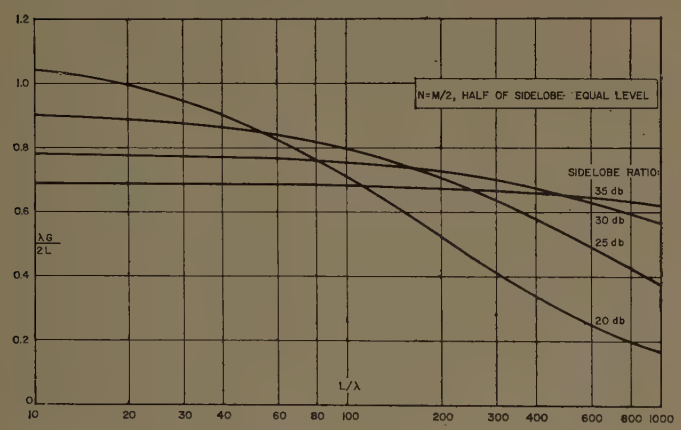

Fig. 4—Normalized gain vs length for Taylor approximate space factor.

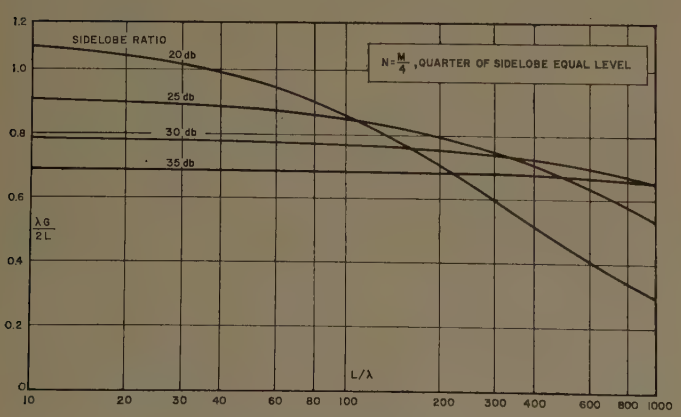

Fig. 5—Normalized gain vs length for Taylor approximate space factor.

VI. Taylor One-Parameter Space Factors

A family of tapered sidelobe distributions has been derived by Taylor [21]. These are of the modified sin X/X type. The space factor (pattern) is given by

$$P(u) = \frac{\sin \pi\sqrt{u^2 - B^2}}{\pi\sqrt{u^2 - B^2}}. \tag{17}$$

The sidelobe ratio η is 4.6 sinh $\pi B/\pi B$; the aperture function is

$$F(p) = J_0(jB\sqrt{\pi^2 - p^2}), \tag{18}$$

where $J_0(jx)$ is the Bessel function for imaginary argument.

These distributions offer the designer patterns with tapered sidelobe envelopes and with sidelobe ratios greater than the 13.2 db obtained for the uniform case. Because of the taper, the normalized gain is nearly constant, and the asymptotic value for large L may be used. This is [21]

$$\frac{\lambda G}{2L} = \frac{2 \sinh^2 \pi B}{\pi B \bar{I}_0(2\pi B)}, \tag{19}$$

where $\bar{I}_0(x) = \int_0^x I_0(\xi)d\xi$; see Rothman.[5] Values of normalized gain and beamwidth per wavelength of source length are in Table II. These sources have a highly tapered illumination function, and may be used where a sacrifice of gain and beamwidth can be tolerated in order to obtain rapidly decreasing sidelobes, *e.g.*, low-noise antenna designs.

TABLE I

Transition Points for Maximum Gain

Sidelobe Ratio	N_{max} (Taylor)	N_{max} Eq. (14)	Maximum $\lambda G/2L$	Beamwidth per Inverse Wavelength (4 per cent Dilation)
20 db	6	9	0.97	53.2°
25 db	12*	18*	0.90	58.2°
30 db	—	36*	0.75	63.1°
35 db	—	64*	0.67	67.5°

* Very broad maxima.

TABLE II

Taylor One-Parameter Sources

Sidelobe Ratio	$G/2L$	Beamwidth per Inverse Wavelength
20 db	0.933	58.6°
25 db	0.863	63.9°
30 db	0.801	68.8°
35 db	0.751	73.2°

[5] M. Rothman, "Table of $\bar{I}_0(x)$ for 0(.1) 20(1) 25," *Quart. J. Mech. and Appl. Math.*, vol. 2, pt. 2, pp. 212–217; 1949.

The "ideal" space factor, where all sidelobes are equal and the one-parameter family can be considered as special cases of a two-parameter family, developed by Bickmore and Chu [22]. This two-parameter space factor is

$$F(u) = \frac{J_\gamma(\pi\sqrt{u^2 - C^2})}{[\pi\sqrt{u^2 - C^2}]^\gamma}, \qquad (20)$$

where γ is real. C is related to the sidelobe ratio and $u = L/\lambda \sin\theta$. The second parameter is γ. When $\gamma = -\frac{1}{2}$, (20) reduces to Taylor's "ideal" space factor $\cos(\pi\sqrt{u^2 - C^2})$, whereas for $\gamma = +\frac{1}{2}$ we get the modified one-parameter family $\sin(\pi\sqrt{u^2 - C^2})/\pi\sqrt{u^2 - C^2}$. Intermediate values of γ yield different sidelobe envelope tapers. This versatile family of space factors allows insight into the interrelationship between sidelobe taper, beamwidth, and zeros of the aperture function.

VII. Conclusions

The widely used Taylor "approximate" line source designs must be carefully used for dimensions very large in wavelengths. At the same time, this approximate space factor yields the best compromise between gain and resolution. It is possible, using the curves given, to choose the sidelobe break point so as to realize nearly all of the gain available from a stipulated sidelobe ratio and yet maintain close to the optimum beamwidth.

Acknowledgment

Curve fitting was performed by Mrs. Helen Arens; calculations were performed by Mary Brady.

Bibliography

[1] C. L. Dolph, "A current distribution for broadside arrays which optimizes the relationship between beamwidth and sidelobe level," Proc. IRE, vol. 34, pp. 335–348; June, 1946.
[2] H. J. Riblet, "Note on Dolph," Proc. IRE, vol. 35, pp. 489–492; May, 1947.
[3] R. L. Pritchard, "Optimum directivity patterns for linear point arrays," *J. Acoust. Soc. Am.*, vol. 25, pp. 879–891; September, 1953.
[4] L. B. Brown and G. A. Sharp, "Tschebyscheff Antenna Distribution, Beamwidth, and Gain Tables," Naval Ordnance Lab., Corona, Calif., NOLC Rept. No. 383; February, 1958.
[5] G. J. van der Maas, "A simplified calculation for Dolph-Tchebycheff arrays," *J. Appl. Phys.*, vol. 25, pp. 121–124; January, 1954.
[6] T. T. Taylor, "Design of line-source antennas for narrow beamwidth and low sidelobes," IRE Trans. on Antennas and Propagation, vol. AP-3, pp. 16–28; January, 1955.
[7] R. J. Spellmire, "Tables of Taylor Aperture Distributions," Microwave Lab., Hughes Aircraft Co., Culver City, Calif., Rept. No. TM 581; October, 1958.
[8] T. T. Taylor, "Design of Circular Apertures for Narrow Beamwidth and Low Sidelobes," Microwave Lab., Hughes Aircraft Co., Culver City, Calif., Rept. No. TM372; August, 1954.
[9] R. C. Hansen, "Tables of Taylor Distributions for Circular Aperture Antennas," Microwave Lab., Hughes Aircraft Co., Culver City, Calif., Rept. No. TM587; February, 1959.
[10] C. J. Bouwkamp and N. G. de Bruijn, "The problem of optimum antenna current distribution," *Philips Res. Repts.*, vol. 1, pp. 135–158; 1946.
[11] L. La Paz and G. A. Miller, "Optimum current distribution on vertical antennas," Proc. IRE, vol. 31, pp. 214–231; May, 1943.
[12] H. J. Riblet, "Note on the maximum directivity of an antenna," Proc. IRE, vol. 36, pp. 620–623; May, 1948.
[13] R. L. Pritchard, "Maximum directivity index of a linear point array," *J. Acoust. Soc. Am.*, vol. 26, pp. 1034–1039; November, 1954.
[14] E. C. Jordan, "Electromagnetic Waves and Radiating Systems," Prentice-Hall, Inc., New York, N. Y., p. 445; 1950.
[15] D. G. Tucker, "Signal/noise performance of super-directive arrays," *Acustica*, vol. 8, pp. 112–116; 1958.
[16] J. L. Yen, "On the synthesis of line-sources and infinite strip-sources," IRE Trans. on Antennas and Propagation, vol. AP-5, pp. 40–46; January, 1957.
[17] L. Solymar, "Maximum gain of a line source antenna if the distribution function is a finite Fourier series," IRE Trans. on Antennas and Propagation, vol. AP-6, pp. 215–219; July, 1958.
[18] R. F. Harrington, "On the gain and beamwidth of directional antennas," IRE Trans. on Antennas and Propagation, vol. AP-6, pp. 219–225; July, 1958.
[19] S. Silver, "Microwave Antenna Theory and Design," M.I.T. Rad. Lab. Series, McGraw-Hill Book Co., Inc., p. 177; 1949.
[20] G. C. McCormick, "The optimum aperture function in a long array," IRE Trans. on Antennas and Propagation, vol. AP-5, pp. 144–145; January, 1957.
[21] T. T. Taylor, "One Parameter Family of Line Sources Producing Modified Sin $\pi u/\pi u$ Patterns," Microwave Lab., Hughes Aircraft Co., Culver City, Calif., Rept. No. TM 324; September, 1953.
[22] R. W. Bickmore and R. J. Spellmire, "A Two-Parameter Family of Line Sources," Microwave Lab., Hughes Aircraft Co., Culver City, Calif., Rept. No. TM 594; October, 1956.

Some Equivalences Between Equally and Unequally Spaced Arrays*

SHELDON S. SANDLER†

Summary—**General analytical expressions are presented for unequally spaced arrays. These relations allow for the analysis of the nonuniformly spaced array in terms of its equivalent uniformly spaced array. The inherent broad-band qualities of the nonuniformly spaced array are discussed. Some equivalence is made between the amplitude and spatial variation in the uniformly and nonuniformly spaced array. The general synthesis problem is discussed. An array with monotonically increasing interelement spacings is presented as an example of the theory.**

Introduction

IN GENERAL, a linear array with uniformly spaced elements produces a radiation pattern which has several major maxima of equal height (grating lobes). This reproduction of the principal maxima prevents operation over a broad frequency range. A solution to the problem of reducing the minor principal maxima has been proposed involving a linear array with nonuniformly spaced elements.[1] This type of radiator will be referred to as a nonuniformly spaced array.

A general discussion of nonuniformly spaced arrays has been given by Unz.[2] The classical expansions were performed on the far zone pattern. The complexity of this formulation limits its practical application. It is believed that the present analysis offers some advantage in understanding problems associated with nonuniformly spaced arrays. Furthermore, some important properties of nonuniformly spaced arrays may be readily demonstrated and should find usefulness in normal array applications. For example, there is an equivalence between the variation of the individual element distances from the array center and amplitude tapering of a uniformly spaced array.

As an introduction to the theory of nonuniformly spaced arrays consider the uniformly spaced array shown in Fig. 1. The far zone field for this array may be found by summing up the contributions due to the individual radiators. With no loss of generality, the analysis may be restricted to the case of N isotropic elements driven in identical time phase. For this case the radiation field is directly proportional to the uniformly spaced array factor given by

$$A(\Phi) = 1 + 2 \sum_{m=1}^{(N-1)/2} \cos 2\pi m d \cos \Phi, \qquad (1)$$

where

d = element spacing in fractions of a wavelength,
N = total number of elements.

It is easily seen from (1) that the array factor is periodic since it repeats when the argument changes by an angle of π radians. The usual method of reducing (*i.e.*, to zero) the level of the secondary maxima is to restrict the spacing. However, the secondary maxima may not be reduced when the element spacing exceeds a half wavelength. For example, an array with two-wavelength spacing will have its second principal maxima at $\Phi = \pi/3$ repeated at $\Phi = 0$.

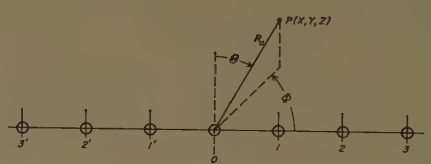

Fig. 1—Uniform array.

Nonuniformly Spaced Arrays

A useful physical picture of the nonuniformly spaced array is concerned with the concept of spatial frequency. Spatial frequency is a measure of the variation of each element contribution with far field angle. With this definition, the lowest array frequency may be associated with the center element, the next highest with the $m = 1$ term in (1), etc. The concept of spatial frequency may be visualized by considering two sources separated by a distance d. The radiation pattern for the two sources will have an increasing number of visible lobes as d is increased. The linear array consists of a large number of such couplets since the center element serves as a reference. With respect to the center element, the uniformly spaced array is seen to contain a spectrum of frequencies which are integral harmonics of the fundamental frequency determined by the first element position. In this case, each spectral component is located at the physical element position, and the locations are uniformly distributed over the length of the array.

* Received by the PGAP, February 5, 1960; revised manuscript received, March 25, 1960. This work was supported in part by Rome Air Development Center, Rome, N. Y., under Contract No. AF 30(602)-1776.

† Electronic Communications, Inc., Timonium, Md.

[1] D. D. King, R. F. Packard, and R. K. Thomas, "Broadband Steerable Linear Arrays," Electronic Communications, Inc., Timonium, Md., prepared for AFCRC, Contract No. AF 19(604)-5234; October 7, 1959.

[2] H. Unz, "Linear Arrays with Arbitrarily Distributed Elements," Electronics Res. Lab., University of California, Berkeley, Ser. No. 60, Issue No. 168; November 2, 1956.

Consider the nonuniformly spaced array factor given by

$$A(\Phi) = 1 + 2 \sum_{m=1}^{M} \cos (2\pi d_m \cos \Phi), \tag{2}$$

where

d_m = distance from the mth element to the center of the array in fractions of a wavelength.

The nonuniformly spaced array is characterized by spatial frequencies which are not necessarily related by integers. The spatial frequency spectrum is now unevenly distributed over a range which extends from zero to ω_M, where

$$\omega_M = 2\pi d_M \cos \Phi. \tag{3}$$

The lowest nonzero array frequency plays a major part in determining the location of the principal and minor maxima. Generally speaking, when a function is composed of slowly as well as rapidly varying functions, the slower variations will predominate. This is true since it is always possible to find some high-frequency maxima in the vicinity of a low-frequency maximum. The total number of high-frequency maxima in the vicinity of the low-frequency maximum then determines its magnitude. The major maxima differ from the minor maxima in that they represent simultaneous maxima of both the low- and high-frequency components of (2).

Unfortunately, compact expressions are not available when the argument of (2) is a nonlinear function of m. A perturbation analysis could be performed to give an indication of small nonlinear changes in element spacing. However, some of the useful properties on nonuniformly spaced arrays depend on large nonlinearities in the element spacings. A method is needed which will lend insight into the gross behavior of the nonuniformly spaced array and make it susceptible to a linear analysis. Fortunately it is possible to make a correspondence between the nonuniformly spaced and equivalent uniformly spaced array (EUA). The EUA is the best mean square representation for the original array. Some superficiality is introduced since the EUA does not physically exist. Furthermore, it will be shown that the spacing in the EUA is somewhat arbitrary. The EUA involves the transformation of higher frequency terms in (2) to a set of integral harmonic terms. The lowest nonzero superficial array frequency in the EUA is ω_1, where

$$\omega_1 = \pi R \cos \Phi. \tag{4}$$

The scale factor R determines the element spacing in the EUA. For example, the value $R=1$ corresponds to an EUA with half-wavelength spacing and $R=\frac{1}{2}$ corresponds to quarter wave spacing. The transformation to the EUA is made by finding the Fourier representation for each higher harmonic.[3] Each term in (2) is reduced to a series of integral harmonic terms with variable amplitude coefficients. For example, consider the general term in (2) given by

$$\cos \omega_M, \tag{5}$$

where

$$\omega_m = 2\pi d_m \cos \Phi.$$

Since $m>1$, $\omega_m > \omega$, (5) may be expanded in integral harmonics of the scaled variable ω_1 where

$$\omega_1 = \pi R \cos \Phi$$
$$0 < R \leq 1. \tag{6}$$

Once the lowest EUA spacing is chosen, each term in (2) must be expanded into an infinite number of uniformly spaced equivalent elements. The amplitude of the equivalent elements varies considerably across the array. Hence, for practical computations only a few terms of the expansion need be considered. Each term in (2) will have an integral harmonic cosine representation, and the individual expansions may be added term by term. When the element spacing of the EUA is decreased toward zero, only those EUA elements which are very close to the original will have an appreciable magnitude. In the limit as R approaches zero, only one term will appear in the EUA representation of the original. This will also be true of the other EUA representations for the original elements. The sum of all the uniformly spaced representations of each term will then be identical to (2).

Note that the EUA has all the general characteristics of the normal uniformly spaced array (*e.g.*, grating lobes). Different values of the scale factor R may be chosen for specific applications. From the standpoint of reproducing the actual radiation pattern, an EUA with a small value of R would give the best fit. Large values of R would yield an EUA which represents the gross pattern characteristics. The fine detail of the radiation pattern is filled in by a large number of EUA elements (*i.e.*, small values of R).

The first step in the EUA representation is to expand the mth term in (2) in an integral harmonic cosine series. When (6) is substituted in (5), the result is given by

$$\cos \omega_m = \cos \frac{2d_m}{R} \omega_1 = \cos \mu_m \omega_1, \tag{7}$$

where

$$\mu_m = 2d_m/R$$

Now the mth term may be expanded into ν integral harmonic terms by the following expansion:

[3] R. Courant, "Differential and Integral Calculus," Interscience Publishers, Inc., New York, N. Y., vol. 1, p. 444; 1955.

$$\cos \mu_m \omega_1 = \sum_{\nu=0}^{\infty} a_{m\nu} \cos \nu\omega_1, \tag{8}$$

where

$$a_{m\nu} = \frac{2}{\pi} \int_0^{\pi R} \cos \mu_m \omega_1 \cos \nu\omega_1 d\omega_1,$$

$$a_{m\nu} = \frac{2}{\pi} \left[\frac{\mu_m \sin \mu_m \omega_1 \cos \nu\omega_1 + \nu \cos \mu_m \omega_1 \sin \nu\omega_1}{\mu_m^2 - \nu^2} \right]_0^{\pi R},$$

$$a_{m\nu} = \frac{2}{\pi} \frac{\mu_m (-1)^\nu \sin \mu_m \pi}{\mu_m^2 - \nu^2}, \qquad R = 1$$

$$\mu_m \neq 0, \pm 1, \pm 2, \cdots.$$

The Fourier expansion given by (8) must be applied to each component in (2). The amplitude coefficients are added term by term to give the EUA, or

$$A = I_1 + I_2 \sum_{m=1}^{P} \left\{ \sum_{\nu=0}^{\infty} a_{m\nu} \cos \nu_{i01} \right\}$$

$$A = 1 + 2 \sum_{r=0}^{P} A_r \cos r\omega_1 \tag{9}$$

where

$$A_0 = a_{10} + a_{20} + a_{30} + \cdots$$

$$A_1 = a_{11} + a_{21} + a_{31} + \cdots, \text{ etc.}$$

Note that when μ_m is an integer, (8) may be replaced by a trivial identity. The representation given by (9) is not unique. Many choices are possible as a function of the scale factor R. However, from the least mean square error property of the Fourier expansion, each representation will be the best possible for a given ω_1.

The final form of the array factor in (9) is readily reducible to another analytical form. The reduction of (9) is performed by representing the values of A_r at P points by a Pth degree polynomial in m.[4] The array factor given in (14) is now given by a finite series of form

$$A = B + 2 \sum_{m=1}^{P} A_m \cos m\omega_1$$

$$= B + 2 \sum_{m=1}^{P} \sum_{r=0}^{P} \alpha_r m^r \cos m\omega_1$$

$$A = B + 2 \left\{ \sum_{m=1}^{P} \alpha_0 \cos m\omega_1 + \sum_{m=1}^{P} \alpha_1 m \cos m\omega_1 + \cdots + \sum_{m=1}^{P} \alpha_m m^P \cos m\omega_1 \right\}. \tag{10}$$

The individual terms in (10) may be summed exactly as sums of successive derivatives of the functions $S(\omega_1)$ and $C(\omega_1)$,[5] where

$$S(\omega_1) = \sum_{m=1}^{M} \sin m\omega_1 = \frac{\sin \frac{M}{2} \omega_1 \sin \frac{M+1}{2} \omega_1}{\sin \frac{\omega_1}{2}}, \tag{11}$$

$$C(\omega_1) = \sum_{m=1}^{M} \cos m\omega_1 = \frac{\sin \frac{M}{2} \omega_1 \cos \frac{M+1}{2} \omega_1}{\sin \frac{\omega_1}{2}}. \tag{12}$$

For example, the third term in (10) is given by

$$\sum_{m=1}^{M} \alpha_1 m \cos m\omega_1 = \alpha_1 \frac{d}{d\omega_1} S(\omega_1). \tag{13}$$

A simple approximate method for making an analysis of unequally spaced arrays may be based on the EUA and the work of Spencer.[6] The EUA may be approximated by an equivalent line source distribution by interpolating with continuous functions. These functions may be obtained empirically or by least squares fit. Note that the original form of the array factor given by (2) does not lend itself to this type of representation.

Examples

Amplitude Tapering With Equally Fed Elements

The sidelobe level and beamwidth of a uniformly spaced linear array may be controlled by varying the element driving currents. This amplitude variation corresponds to the variation of the A_r's in (9). A general result of uniformly spaced array theory is that the sidelobe level may be reduced by decreasing the current amplitudes toward the extremes of the array. This reduction is accomplished at the expense of the array beamwidth. Now it will be demonstrated that there is an analogy between amplitude tapering of a uniformly spaced array and the space variation in a nonuniformly spaced array.[7]

As a specific example, consider the array of Fig. 2.

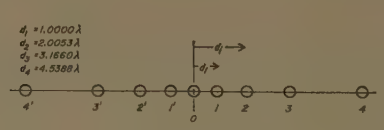

Fig. 2—Logarithmically spaced array.

[4] F. B. Hildebrand, "Introduction to Numerical Analysis," McGraw-Hill Book Co., Inc., New York, N. Y., pp. 261–269; 1956.

[5] F. B. Hildebrand, "Methods of Applied Mathematics," Prentice-Hall, Inc., New York, N. Y., p. 260; 1952.

[6] R. C. Spencer, "Fourier Integral Methods of Pattern Analysis," Mass. Inst. Tech., Cambridge, R.L. Rept. No. 762-1; January 21, 1946.

[7] This result was experimentally demonstrated during World War II at the Navy Underwater Sound Laboratory, Harvard University, Cambridge, Mass. (Prof. F. V. Hunt, Harvard University, private communication).

The elements in this array are arranged so that the d_i's increase logarithmically from the center of the array. The value of ω_1 for this discussion is chosen to be proportional to half the electrical distance to the first element, or

$$\omega_1 = \pi \cos \Phi, \qquad R = 1.$$

The EUA is readily constructed by applying (8) to each high-frequency component. The result is shown graphically in Fig. 3. The EUA may be decomposed into two arrays with one-wavelength spacing. The presence of amplitude tapering may be seen from the amplitude variation of the subarray with an odd number of elements. Since this array yields the major contribution to the radiation pattern, its effect will be more pronounced than the "even" array. The radiation pattern shown in Fig. 4 demonstrates this reduction. Note that the radiation pattern is plotted as a function of the broadbanding factor $U = R \cos \Phi$, where $R = 2$. The utility of U may be seen from the following example: consider a uniformly spaced array operating at frequency f_1 with an element spacing of one wavelength. For this case $R = 1$, and the visible range of U is $-1 \leq U \leq 1$. Now if the frequency is doubled to $2f_1$, then $R = 2$, and the visible range of U is $-2 \leq U \leq 2$. Returning to Fig. 4, note that the sidelobe level is less than 16.8 db over a ± 45 degree range, compared with 12.8 db for a uniformly spaced array of nine elements with one-wavelength spacing.

The radiation pattern shown in Fig. 4 was calculated on the basis of the original element positions. The truthfulness of the EUA representation of Fig. 3 is shown in Table I.

The error in the EUA representation is greatest at the rapidly varying portions of the radiation pattern. An increase in the number of EUA elements would improve the approximation to the actual radiation pattern shown in Fig. 4.

Broadband Property of Nonuniformly Spaced Arrays

A useful property of the nonuniformly spaced array is the reduction in the magnitude of the major principal maxima. The broad-band property of nonuniformly spaced array may be crudely explained by the division of the EUA into an even and odd array. It is well known that an array with an odd number of elements has principal maxima of the same sign, while an array with an even number of elements has alternate signs. Returning to the example of Fig. 3, the array has a comparatively large "odd" array and a smaller "even" array concentrated near the extremes. Due to the alternation in sign of the second principal maxima for the two types of subarrays, the even array increases the major maximum of the odd subarray while decreasing the height of the second principal maximum. Since the "even" array is located near the end elements, there will be an increase in the over-all sidelobe level.

The EUA for a Small Value of Element Spacing

In the limit as R becomes vanishingly small, the EUA and the original nonuniformly spaced array become equivalent. This result is demonstrated in Fig. 5. A nonuniformly spaced array of length 38.6 λ has been approximated by an EUA with 0.222 λ spacing. The geometrical equivalence between the dominant EUA elements and the original nonuniformly spaced array is clearly demonstrated.

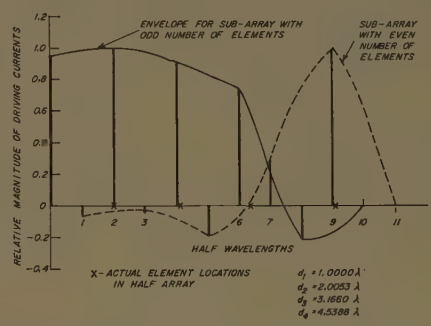

Fig. 3—Equivalent uniform array for array shown in Fig. 2.

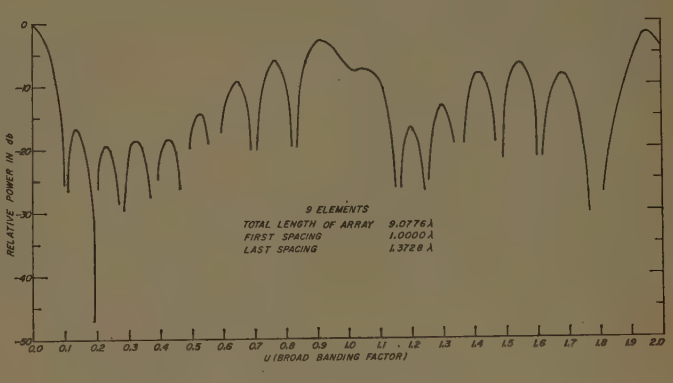

Fig. 4—Radiation pattern for array shown in Fig. 2.

TABLE I

Value of U	Relative Power Level of Original Array	Relative Power Level of EUA
0.055	− 5.0 db	− 5.6 db
0.100	−25.1 db	−23.5 db
1.000	− 6.9 db	− 7.4 db

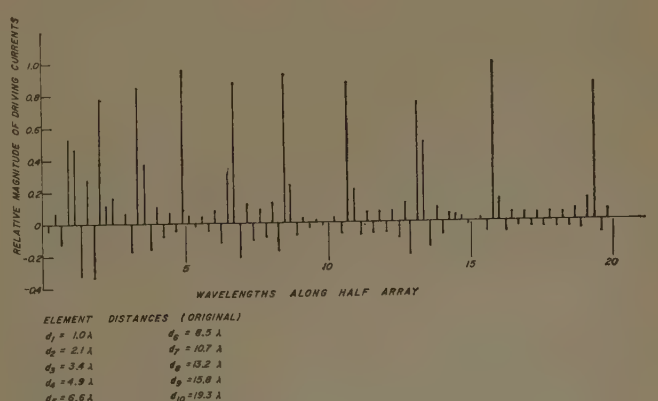

Fig. 5—Equivalent uniform array with 0.222 λ spacing.

Synthesis of Nonuniformly Spaced Arrays

The complicated nature of the A_r's in (9) does not allow a one to one correspondence between the actual element positions and the EUA driving currents. For example, if $R=1$, the following set of equations must be solved simultaneously for the element positions, given the value of A_r:

$$A_0 = \frac{\sin \mu_1\pi}{\mu_1\pi} + \frac{\sin \mu_2\pi}{\mu_2\pi} + \frac{\sin \mu_3\pi}{\mu_3\pi} + \cdots,$$

$$A_1 = \frac{2\mu_1 \sin \mu_1\pi}{\pi(\mu_1^2 - 1^2)} - \frac{2\mu_2 \sin \mu_2\pi}{\pi(\mu_2^2 - 1^2)} - \frac{2\mu_3 \sin \mu_3\pi}{\pi(\mu_3^2 - 1^2)} - \cdots,$$

$$A_2 = \frac{2\mu_1 \sin \mu_1\pi}{\pi(\mu_1^2 - 2^2)} + \frac{2\mu_2 \sin \mu_2\pi}{\pi(\mu_2^2 - 2^2)} + \frac{2\mu_3 \sin \mu_3\pi}{\pi(\mu_3^2 - 2^2)} + \cdots$$

$$\vdots$$

$$\mu_m \neq l \quad \text{where} \quad l = 1, 2, 3, \cdots.$$

Note that the number of A_r's that may be independently chosen is less than the number of original elements. Hence, if the EUA has more elements than the original array, only N uniform driving currents may be specified, where $2N+1$ is the total number of elements. If the mode of subdivision is changed to an EUA with a larger number of elements the same limitation holds true. A reasonable approach to the synthesis problem would involve an EUA having a total number of elements commensurate with the original nonuniformly spaced array.

In practice, it is rather easy to see the effect of moving an array element graphically on a representation of the type shown in Fig. 3. When the element frequency is close to a harmonic of the fundamental frequency, that harmonic will be large. When the element frequency is between two array harmonics, each adjacent harmonic will be large, though not as large as in the preceding case.

If the array elements are widely spaced, it is difficult to find the optimum distribution for supressed minor principal maxima. For example, consider the operation of a nonuniformly spaced array over a two to one frequency band. If the elements in the EUA were spaced one wavelength apart at the low-frequency range, they will be spaced two wavelengths when the frequency is doubled. It follows that it is difficult to make any rigorous mathematical statements about optimum nonuniformly spaced arrays. However, the EUA analysis may serve as a guide in specific applications. For example, consider the design of a nonuniformly spaced array with a minimum of one-wavelength spacing. The array must operate over a two to one band with no visible grating lobes. The optimum nonuniformly spaced array would be given by an element distribution which had an EUA identical to a normal uniformly spaced array with less than half-wavelength spacing (*i.e.*, $R<1$).

Acknowledgment

The EUA shown in Fig. 5 was calculated by R. Packard. The author acknowledges also the encouragement and interest of Dr. D. D. King and R. K. Thomas.

The Efficiency of Launching Surface Waves on a Reactive Half Plane by an Arbitrary Antenna*

JULIUS KANE†

Summary—**The following two-dimensional problem is considered: An arbitrary antenna is located at the origin which launches surface waves on a reactive half plane $y=0$, $x<0$. It is assumed that the other half plane, $y=0$, $x>0$, is occupied by a perfect conductor. The antenna is approximated by a distribution of multipoles easily found from the antenna's radiation pattern. With this approximation, simple algebraic expressions are obtained for the ratio of the power delivered to the surface wave as compared to the power in the radiated cylindrical field.**

* Received by the PGAP, February 27, 1960; revised manuscript received, March 26, 1960; second revised manuscript received, May 13, 1960. The research reported in this work was sponsored by the Electronics Res. Directorate, AF Cambridge Res. Center, ARDC, under Contract No. AF 19(604)5238. This material has appeared also as New York University Res. Rept. EM-159.

† Dorne and Margolin, Inc., Westbury, L. I., N. Y. Formerly with N. Y. U., N. Y., N. Y.

List of Symbols

$\delta(x)$ = dirac delta function,

$E_N(\nu) = p_N(\cos^{-1}\nu/k)$ = an entire function, a polynomial,

$H_0^{(1)}(k\rho)$ = Hankel function of the first kind of order zero (a time factor $e^{-i\omega t}$ is suppressed),

$k = |k| e^{i\delta}$ = propagation constant with a small imaginary part proportional to δ,

K = a constant proportional to the source strength,

$\sqrt{k^2-\nu^2}$ = the radical is chosen by the prescription $\sqrt{k^2} = +|k| e^{i\delta}$,

$\Lambda = \lambda/k$,

$m = \sqrt{k^2+\lambda^2}$,
$M = \sqrt{1+\Lambda^2}$,
$\nu = k \cos\varphi$ Fourier transform variables,
$p_\infty(\vartheta)$ = radiation pattern of an arbitrary antenna,
$p_N(\vartheta)$ = truncated Fourier expansion of $p_\infty(\vartheta)$,
$P(\vartheta)$ = power radiation pattern,
Π = Poynting flux,

$$\sigma(\nu) = 1 + \frac{\lambda}{i\sqrt{k^2+\nu^2}} = \frac{\sigma^+(\nu)}{\sigma^-(\nu)} = \text{Wiener-Hopf decomposition}$$

$U(\vartheta)$ = Heaviside unit function.

I. Introduction

IT IS well known that a reactive surface which supports surface waves can be represented mathematically as

$$\frac{\partial u}{\partial n} + \lambda u = 0,$$

where $\partial u/\partial n$ is the normal derivative and λ is proportional to the surface reactance [1]. In this paper we consider rigorously the excitation of surface waves on such a half plane by both a line source and an approximation to an arbitrary antenna. In Sections II–IV, we solve the problem of excitation of a surface wave by a line source. Using Kay's results [1], it is shown that the ratio of power delivered to the surface wave as compared to the radiation field is an elementary algebraic function of λ.

In Section V, we study the surface wave excitation produced by an arbitrary antenna. The antenna is approximated by a distribution of multipoles obtained from a knowledge of the antenna's radiation pattern $p_\infty(\vartheta)$ when placed on an infinite metallic plane. The excitation produced by these multipoles is then calculated. It is shown that the ratio of energy delivered to the surface wave as compared to the cylindrical field is an elementary algebraic function of $p_\infty(\vartheta)$ and λ.

We omit several details of analysis which are covered thoroughly by Kay [1] and Bazer and Karp [2].

II. Formulation and Solution

The problem (*cf.* Fig. 1) we shall solve is posed by the three equations:

$$(\nabla^2 + k^2)u(x,y) = -2\delta(x)\delta(y), \quad \text{all } x, y \geqq 0 \tag{1}$$

$$\frac{\partial u}{\partial y} + \lambda u = 0, \qquad x < 0, y = 0 \tag{2}$$

$$\frac{\partial u}{\partial y} = 0, \qquad x > 0, y = 0 \tag{3}$$

where $u(x, y)$ represents the transverse magnetic component H_z, and $H_x = H_y = 0$. For convenience, K has a small positive imaginary part $k = |k| e^{i\delta}$, and a time factor

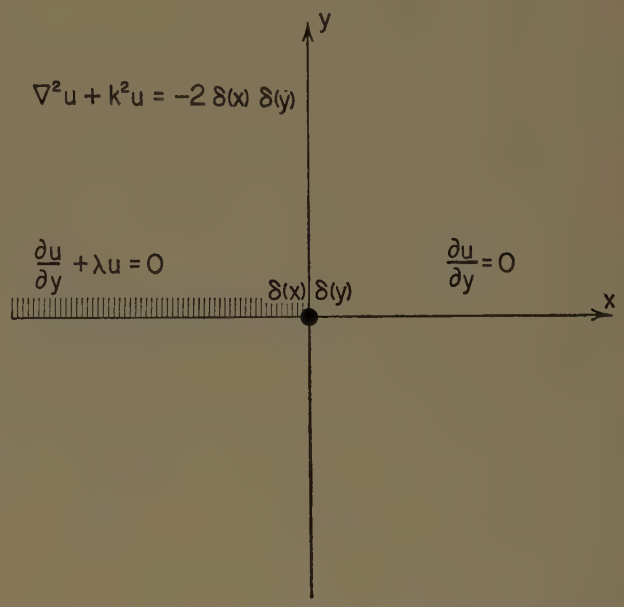

Fig. 1.

$e^{-i\omega t}$ is surpressed. Owing to the normalization[1] chosen for the source term, the free space Green's function of (1) is

$$\frac{i}{2} H_0^{(1)}(k\rho) = \frac{1}{2\pi i}\int_C \frac{e^{i\nu x + i\sqrt{k^2-\nu^2}|y|}}{\sqrt{k^2-\nu^2}}\, d\nu, \tag{4}$$

where the contour C is taken along the real axis in the ν-plane as shown in Fig. 2. Since (4) already has the correct singularity at the origin, it follows that if we seek a solution of the form

$$u(x,y) = \frac{1}{2\pi i}\int_C A^+(\nu)\, \frac{e^{i\nu x + i\sqrt{k^2-\nu^2}y}}{\sqrt{k^2-\nu^2}}\, d\nu, \tag{5}$$

where

$$A^+(\nu) = \mathcal{O}(1) \quad \text{as} \quad |\nu| \to \infty, \qquad \operatorname{Im}\nu \geqq 0, \tag{6}$$

then (1) will continue to be satisfied. At the boundary we assume that we can differentiate freely under the integral sign, and then if $A^+(\nu)$ is an analytic function in the upper ν-plane, the boundary condition (3) will be satisfied, since we can close the contour C for $x > 0$. Again, it is sufficient that if $G^-(\nu)$ defined by

$$G^-(\nu) = A^+(\nu)\left[1 + \frac{\lambda}{i\sqrt{k^2-\nu^2}}\right] \tag{7}$$

is an analytic function in the lower ν-plane and $\mathcal{O}(1)$ as $|\nu| \to \infty$, $\operatorname{Im}\nu \leqq 0$ the boundary condition (2) will be satisfied. Kay [1], and Bazer and Karp [2] show that the function $\sigma(\nu)$ can be expressed as

$$\sigma(\nu) = \left[1 + \frac{\lambda}{i\sqrt{k^2-\nu^2}}\right] = \frac{\sigma^+(\nu)}{\sigma^-(\nu)}, \tag{8}$$

[1] Recall that the usual source strength of $-4\pi\delta(x)\delta(y)$ leads to the Green's function $\pi i H_0^{(1)}(k\rho)$.

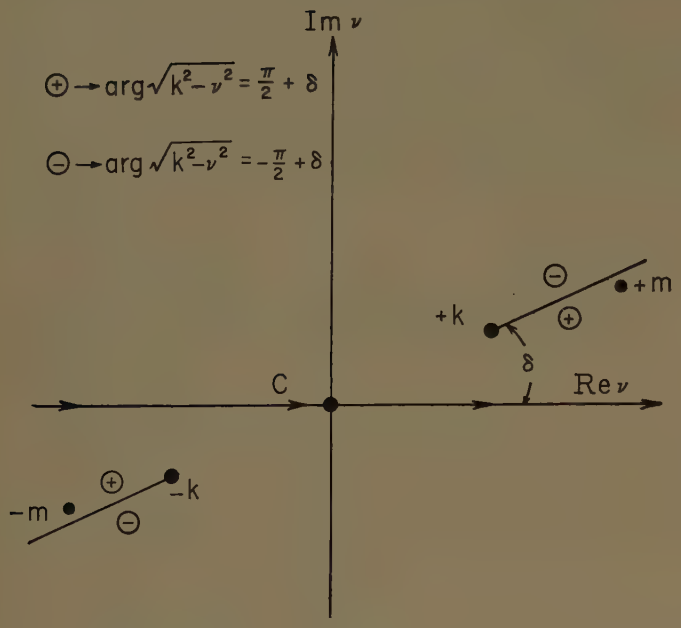

Fig. 2—Complex ν plane. The magnitude of δ is greatly exaggerated for purposes of clarity.

where $\sigma^+(\nu)$ is analytic in the upper ν-plane Im $\nu \geqq$ Im $-k$ and $\sigma^-(\nu)$ is analytic for Im $\nu \leqq$ Im $-k$. It follows that (7) can be written as

$$G^-(\nu)\sigma^-(\nu) = A^+(\nu)\sigma^+(\nu). \tag{9}$$

It can be shown[2] that $|\sigma^+(\nu)|$ and $|\sigma^-(\nu)|$ are bounded above and below by positive constants in their respective domains of analyticity. Owing to the postulated behavior of $G^-(\nu)$ and $A^+(\nu)$, the left side of (9) is bounded and analytic for Im $\nu \leqq 0$ and the right side is bounded and analytic for Im $\nu \geqq 0$, implying that each side is the analytic continuation of the other. If we invoke the Liouville theorem, we discover that each side of (9) is equal to some constant K proportional to the strength of the source, whence

$$G^-(\nu)\sigma^-(\nu) = A^+(\nu)\sigma^+(\nu) = K$$

or

$$\left.\begin{aligned} A^+(\nu) &= \frac{K}{\sigma^+(\nu)} \\ G^-(\nu) &= \frac{K}{\sigma^-(\nu)} \end{aligned}\right\}. \tag{10}$$

Observe that (10) yields kernels $A^+(\nu)$ and $G^-(\nu)$ having the required asymptotic behavior for large $|\nu|$.

The integral representation of the solution (5) is then

$$u(x, y) = \frac{K}{2\pi i}\int_C \frac{1}{\sigma^+(\nu)} \frac{e^{i\nu x + i\sqrt{k^2-\nu^2}\, y}}{\sqrt{k^2-\nu^2}}\, d\nu \tag{11}$$

or alternately by (8)

$$u(x, y) = \frac{K}{2\pi i}\int_C \frac{1}{\sigma^-(\nu)\sigma(\nu)} \frac{e^{i\nu x + i\sqrt{k^2-\nu^2}\, y}}{\sqrt{k^2-\nu^2}}\, d\nu. \tag{12}$$

[2] For example, see Bazer and Karp [2].

From (11) we observe that the poles of the integrand are the zeros of $\sigma^+(\nu)$. Since $|\sigma^+(\nu)|$ is bounded above and below in the upper half plane, these can only arise for Im $\nu \leqq$ Im k. For reference we locate the poles of the integrand of (11). We calculate that

$$\frac{1}{\sigma^+(\nu)} = \frac{1}{\sigma^-(\nu)\sigma(\nu)} = \frac{1}{\sigma^-(\nu)} \frac{i\sqrt{k^2-\nu^2}}{i\sqrt{k^2-\nu^2}+\lambda}$$

$$= \frac{1}{\sigma^-(\nu)} \frac{i\sqrt{k^2-\nu^2}(\lambda - i\sqrt{k^2-\nu^2})}{(\sqrt{\lambda^2+k^2}-\nu)(\sqrt{\lambda^2+k^2}+\nu)}.$$

The only pole that can arise in the lower ν-plane is at ν_0 given by

$$\nu_0 = -\sqrt{k^2+\lambda^2} \tag{13}$$

The corresponding residue of (11) is found to be

$$\frac{K}{\sigma^-(-\sqrt{k^2+\lambda^2})} \frac{\lambda}{\sqrt{\lambda^2+k^2}} e^{-i\sqrt{k^2+\lambda^2}x - \lambda y}, \tag{14}$$

which represents the surface wave contribution.

III. The Far Field

Introduce the transformations

$$\nu = k\cos\varphi \tag{15}$$

and

$$x = \rho\cos\vartheta, \qquad y = \rho\sin\vartheta \tag{16}$$

so that (11) becomes

$$u(\rho, \vartheta) = -\frac{K}{2\pi i}\int_P \frac{1}{\sigma^+(k\cos\varphi)} e^{ik\rho\cos(\varphi-\vartheta)}\, d\varphi \tag{17}$$

in which the contour C has been transformed into the path P (Fig. 3). If we transform the alternate representation (12) to the φ-plane, we obtain

$$u(\rho, \vartheta) = -\frac{K}{2\pi i}\int_P \frac{ik\sin\varphi\, e^{ik\rho\cos(\varphi-\vartheta)}\, d\varphi}{\sigma^-(k\cos\varphi)(ik\sin\varphi+\lambda)} \tag{18}$$

from which it is seen that the pole at ν_0 which generates the surface wave now arises for φ_0 given by

$$\sin\varphi_0 = -\frac{\lambda}{ik} \quad \text{or} \quad \cos\varphi_0 = -\sqrt{1+(\lambda/k)^2}. \tag{19}$$

An asymptotic development of (17) or its equivalent (18) is readily obtained by deforming the path P into the steepest descents contour $S(\vartheta)$. For a given ϑ this contour is defined as the locus of points in the φ-plane which satisfy the equation

$$\cos(\varphi - \vartheta) = 1 + is^2, \tag{20}$$

with s as a real parameter. It is easily established that $S(\vartheta)$ originates at Re $\varphi = \vartheta - \pi/2$, Im $\varphi = \infty$, passes through the saddle point $\varphi = \vartheta$ on the real axis, and terminates at infinity Re $\varphi = \vartheta + \pi/2$, Im $\varphi = -\infty$. Inspection of Fig. 3 reveals that for $0 \leqq \vartheta < \pi/2$ we can deform C freely to $S(\vartheta)$ without picking up the residue

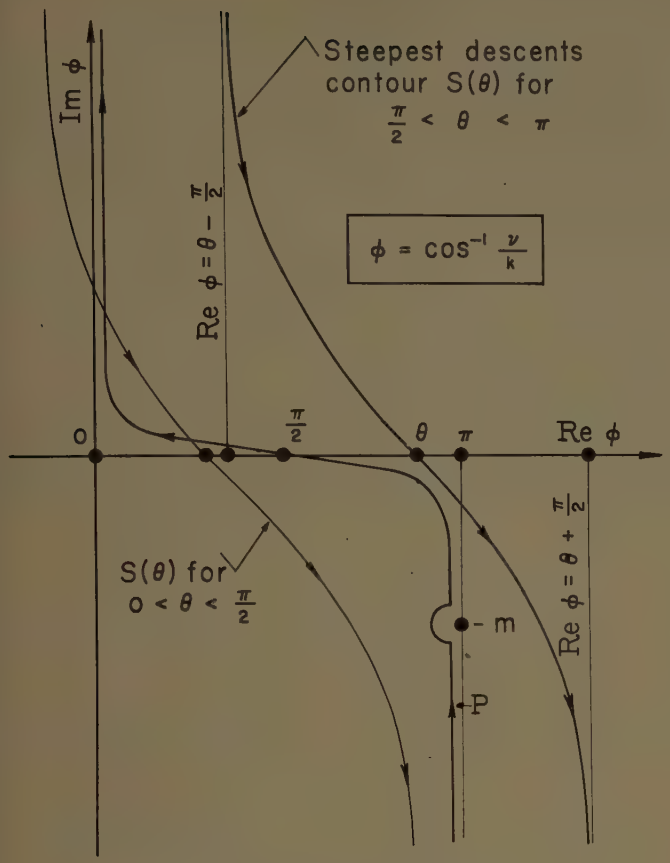

Fig. 3—Complex ϕ plane.

of φ_0, and for some ϑ in the interval $\pi/2<\vartheta\leqq\pi$ we pick up the residue. With the aid of (19) and (20) it is established by comparing the real parts of (20) that this critical angle ϑ_c is given by

$$\vartheta_c = \cos^{-1}\left(\frac{1}{\sqrt{1+(\lambda/k)^2}}\right), \tag{21}$$

where $\pi/2\leqq\vartheta_c\leqq\pi$, so that we only obtain the surface wave on the left for $x<0$.

For $k\rho\gg1$, we obtain the far-field behavior

$$\lim_{\rho\to\infty} u(\rho,\vartheta) = K\left[\frac{e^{-imx-\lambda y}}{\sigma^-(-m)m}\,U(\vartheta-\vartheta_c) + \frac{e^{i(k\rho+\pi/4)}}{\sigma^+(k\cos\vartheta)\sqrt{2\pi k\rho}}\right] + \mathcal{O}[(k\rho)^{-3/2}], \tag{22}$$

where

$$m = \sqrt{k^2+\lambda^2} \tag{23}$$

and $U(\vartheta)$ is the Heaviside unit function. The result (22) should be modified somewhat if $\lambda\sim0$ to allow for a pole in the vicinity of the saddle point for $\vartheta=\pi$. This detail is fully discussed in [2] and [4] where the procedure for isolating the pole is explained.

Apart from terms $\mathcal{O}[(k\rho)^{-3/2}]$, we see that the radiation field contains a cylindrical wave $p(\vartheta)e^{ik\rho}/\sqrt{k\rho}$ with a pattern function $p(\vartheta)$ proportional[3] to

$$\frac{1}{\sigma^+(k\cos\vartheta)} = \sigma^-(-k\cos\vartheta). \tag{24}$$

and in addition a surface wave field whose amplitude is proportional to

$$\frac{1}{\sigma^-(-m)}\,. \tag{25}$$

For each field the power carried off to infinity varies as the absolute square of these coefficients. As Kay and Lurye have observed, it is an extraordinary occurrence in that the absolute squares of (24) and (25) are simple elementary functions. From Kay's paper (66), we obtain in our notation:

$$|\sigma^-(-k\cos\vartheta)|^2 = \frac{\cos\vartheta+1}{\cos\vartheta+\sqrt{1+(\lambda/k)^2}}, 0\leqq\vartheta\leqq\pi, \tag{26}$$

and

$$|\sigma^-(-m)|^2 = |\sigma^-(-\sqrt{k^2+\lambda^2})|^2 = \frac{\sqrt{k^2+\lambda^2}+k}{2\sqrt{k^2+\lambda^2}} = \frac{m+k}{2m}\,. \tag{27}$$

Note that our λ corresponds to Kay's a.

IV. The Energy Distribution

In this section we shall obtain an explicit expression for the ratio of the power delivered to the surface wave field as compared to the cylindrical radiation field. From (22) we see that the surface wave is

$$u_{\text{surf}}(x,y) = \frac{\lambda K}{m\sigma^-(-m)}\,e^{-i\sqrt{k^2+\lambda^2}\,x-\lambda y}U(\vartheta-\vartheta_c). \tag{28}$$

The Poynting flux Π transported by this field is readily calculated if we recall that $u(x,y)$ represents the transverse magnetic component H_z.

$$\Pi_{\text{surf}} = \int_0^\infty [E_y\cdot H_z^*]_{\text{surf}}\,dy = \frac{1}{i\omega\epsilon}\int_0^\infty\left[\frac{\partial u}{\partial x}\,u^*\right]_{\text{surf}}dy = \frac{\lambda}{2m\omega\epsilon}\left|\frac{K}{\sigma^-(-m)}\right|^2.$$

If we use Kay's results, our (26) and (27), then

$$\Pi_{\text{surf}} = \frac{\Lambda|K|^2}{\omega\epsilon(\sqrt{1+\Lambda^2}+1)} = \tanh\left(\tfrac{1}{2}\sinh\Lambda\right) \tag{29}$$

where $\Lambda=\lambda/k$.

In the same fashion we can compute the radiated power of the cylindrical field by using (12),

$$u_{\text{cyl}} = \frac{K}{\sigma^+(k\cos\vartheta)\sqrt{2\pi k\rho}}\,e^{i(k\rho+\pi/4)+} + \mathcal{O}[(k\rho)^{-3/2}], \tag{30}$$

[3] Since $\sigma(\nu)$ is even in ν, we have $\sigma^+(\nu)=1/\sigma^-(-\nu)$, [2].

whence

$$\Pi_{cyl} = \int_0^\pi [E_\vartheta \cdot H_z^*]_{cyl}\, \rho d\vartheta$$
$$= \frac{1}{i\omega\epsilon}\int_0^\pi [u_\rho u_z^*]_{cyl}\, \rho d\vartheta$$
$$= \frac{|K|^2}{2\pi\omega\epsilon}\int_0^\pi \frac{d\vartheta}{|\sigma^+(k\cos\vartheta)|^2}$$
$$= \frac{|K|^2}{2\pi\omega\epsilon}\int_0^\pi \frac{\cos\vartheta + 1}{\cos\vartheta + \sqrt{1+(\lambda/k)^2}}\, d\vartheta.$$

The integral that appears in this expression is evaluated in Appendix I; we find

$$\Pi_{cyl} = \frac{|K|^2}{2\omega\epsilon}\left[2 + \frac{\Lambda - \sqrt{1+\Lambda^2} + 1}{\Lambda(\Lambda - \sqrt{1+\Lambda^2})}\right]. \tag{31}$$

The ratio Π_{surf}/Π_{cyl} represents the efficiency of launching the surface wave. With the aid of (4) and (31) we obtain

$$\frac{\Pi_{surf}}{\Pi_{cyl}} = \frac{\Lambda}{(1+\sqrt{1+\Lambda^2})}\left[\frac{\Lambda(\Lambda - \sqrt{1+\Lambda^2})}{2\Lambda(\Lambda - \sqrt{1+\Lambda^2}) + \Lambda - \sqrt{1+\Lambda^2} + 1}\right]. \tag{32}$$

For $\Lambda \gg 1$, the bracketed expression behaves like 2Λ so that

$$\lim_{\Lambda\to\infty} \frac{\Pi_{surf}}{\Pi_{cyl}} = \mathcal{O}(\Lambda). \tag{33}$$

Consequently, *even without using a directive source, the major portion of the radiated energy is apportioned to the surface wave as we increase the surface reactance* Λ.

It is perhaps of greater use to compare the surface wave energy to the total radiated energy

$$\Pi_{total} = \Pi_{cyl} + \Pi_{surf}.$$

If we use (4) and (31) a little manipulation reveals

$$\Pi_{total} = \frac{|K|^2}{\omega\epsilon}\left[\frac{\Lambda}{M+1} + \frac{\Lambda - M + 1}{2\Lambda(\Lambda - M)} + 1\right], \tag{34}$$

where $M = \sqrt{1+\Lambda^2}$ so that

$$\frac{\Pi_{surf}}{\Pi_{total}} = \frac{\Lambda}{1+\sqrt{1+\Lambda^2}}\left[\frac{\Lambda}{M+1} + \frac{\Lambda - M + 1}{2\Lambda(\Lambda - M)} + 1\right], \tag{35}$$

which is plotted in Fig. 4 (opposite) as a function Λ.

V. Arbitrary Excitation

In actual practice one would not excite a surface wave structure by a line source. We would use a directive antenna $\mathfrak{A}$ such as an exponential horn to focus the maximum energy into the surface wave. How can we obtain the excitation produced by such a radiator? If we replace the surface wave structure by a metallic plane, then the antenna $\mathfrak{A}$ will produce some radiation pattern $p_\infty(\vartheta)$ which will characterize the antenna. The pattern $p_\infty(\vartheta)$ is known for $0 \leqq \vartheta \leqq \pi$, so that it is a simple matter (Appendix II) to approximate it arbitrarily by a cosine polynomial

$$p_\infty(\vartheta) \sim p_N(\vartheta) = \sum_{n=0}^{N} a_n (k\cos\vartheta)^n, \tag{36}$$

since the cosine functions $\cos n\vartheta$ or $\cos^n\vartheta$ are complete on the interval $0 \leqq \vartheta \leqq \pi$. In particular, the sine functions $\sin n\vartheta$ are expressible as infinite series of cosine functions for $0 \leqq \vartheta \leqq \pi$. We observe then that

$$u(x,y) = \frac{1}{2\pi i}\int_C \sum_{n=0}^{N} a_n \nu^n \frac{e^{i\nu x + i\sqrt{k^2-\nu^2}\,y}}{\sqrt{k^2-\nu^2}}\, d\nu \tag{37}$$

is a function which possesses the approximate far-field behavior (36). It is also clear that (37) satisfies the wave equation (*cf.* Fig. 5)

$$(\nabla^2 + k^2)u(x,y) = -2\sum_{n=0}^{N} \frac{a_n}{i^n}\delta^{(n)}(x)\delta(y), \qquad y \geqq 0, \tag{38}$$

where $\delta^{(n)}(x) = \partial^n/\partial x^n\, \delta(x)$, and the boundary condition

$$\frac{\partial u}{\partial y} = 0 \tag{39}$$

at $y=0$.

Eq. (38), reveals that what we have done is to replace the antenna by an approximate equivalent—a distribution of multipoles. We shall assume that the a_n are real, which corresponds to feeding the multipoles in phase intervals of $\pi/2$. One need only solve (38) subject to the two-part boundary condition

$$\left.\begin{aligned} \frac{\partial u}{\partial y} &= 0 \qquad y = 0,\ x > 0 \\ \frac{\partial u}{\partial y} + \lambda u &= 0 \qquad y = 0,\ x < 0, \end{aligned}\right\} \tag{40a, 40b}$$

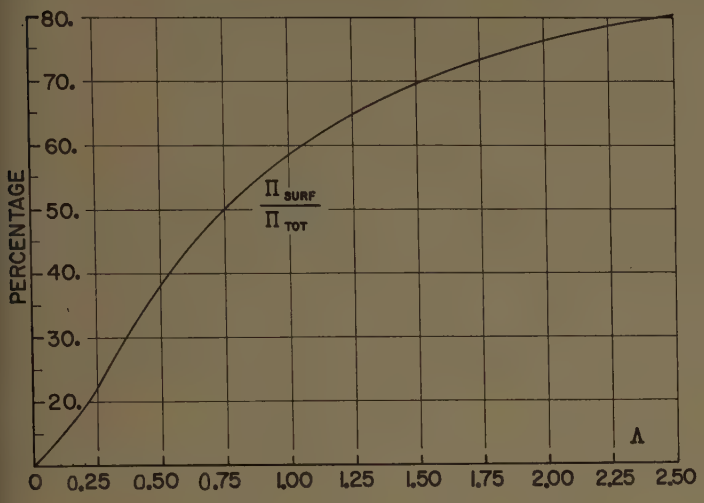

Fig. 4.

TABLE I

Λ	Π_{surf}/Π_{tot}	Π_{cyl}/Π_{tot}	Π_{cyl}/Π_{surf}
0.00	0.0000	1.0000	∞
0.02	0.0198	0.9802	49.5050
0.04	0.0392	0.9608	24.5100
0.06	0.0582	0.9418	16.1816
0.08	0.0768	0.9232	12.0200
0.10	0.0950	0.9050	9.5249
0.12	0.1128	0.8872	7.8632
0.14	0.1302	0.8698	6.6777
0.16	0.1473	0.8527	5.7897
0.18	0.1639	0.8361	5.1002
0.20	0.1802	0.8198	4.5495
0.22	0.1961	0.8039	4.0998
0.24	0.2116	0.7884	3.7258
0.26	0.2268	0.7732	3.4101
0.28	0.2415	0.7585	3.1401
0.30	0.2560	0.7440	2.9067
0.32	0.2700	0.7300	2.7031
0.34	0.2838	0.7162	2.5239
0.36	0.2972	0.7028	2.3650
0.38	0.3102	0.6898	2.2234
0.40	0.3230	0.6770	2.0963
0.42	0.3354	0.6646	1.9817
0.44	0.3475	0.6525	1.8779
0.46	0.3593	0.6407	1.7834
0.48	0.3708	0.6292	1.6971
0.50	0.3820	0.6180	1.6180
0.60	0.4338	0.5662	1.3052
0.70	0.4793	0.5207	1.0862
0.80	0.5194	0.4806	0.9254
0.90	0.5546	0.4454	0.8030
1.00	0.5858	0.4142	0.7071
1.25	0.6492	0.3508	0.5403
1.50	0.6972	0.3028	0.4343
1.75	0.7344	0.2656	0.3616
2.00	0.7639	0.2361	0.3090
2.25	0.7878	0.2122	0.2694
2.50	0.8074	0.1926	0.2385
2.75	0.8238	0.1762	0.2138
3.00	0.8377	0.1623	0.1937
4.00	0.8769	0.1231	0.1404
5.00	0.9010	0.0990	0.1099
6.00	0.9172	0.0828	0.0902
8.00	0.9377	0.0623	0.0664
10.00	0.9501	0.0499	0.0525

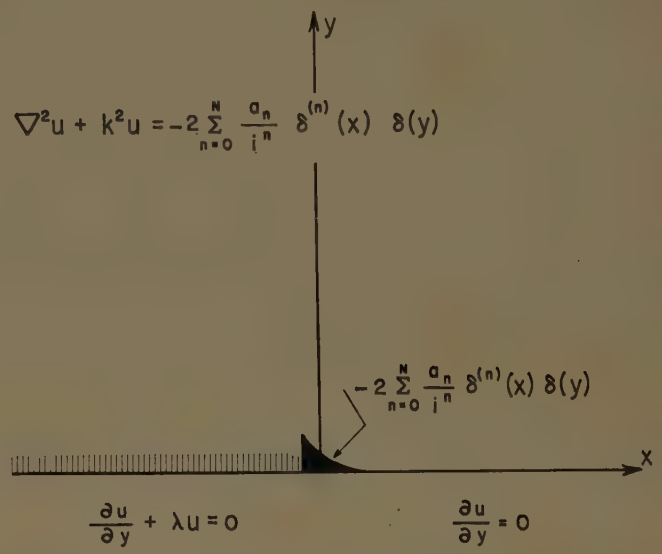

Fig. 5—Approximation to an arbitrary surface wave launcher.

to obtain the effect of introducing the surface wave structure in the left half plane.

Our procedure is to choose

$$u(x, y) = \frac{1}{2\pi i} \int_C A^+(\nu) E_N(\nu) \frac{e^{i\nu x + i\sqrt{k^2-\nu^2}\, y}}{\sqrt{k^2 - \nu^2}}\, d\nu, \qquad (41)$$

where $E_N(\nu)$ is a known entire function of ν, *i.e.*, a Tchebycheff polynomial approximation defined by

$$\left.\begin{aligned} E_N(\nu) &= \sum_{n=0}^{N} a_n \nu^n \\ E_N(k \cos \vartheta) &= p_N(\vartheta) \end{aligned}\right\}. \qquad (42)$$

If $A^+(\nu)$ is an analytic function of ν for Im $\nu \geqq 0$, the boundary condition (40a) will be satisfied. In addition, if

$$A^+(\nu) = \mathcal{O}(1), \qquad |\nu| \to \infty, \qquad (43)$$

then (41) will have the singularity at the origin demanded by (19). For $x<0$, $y=0$ we observe that if

$$G^-(\nu) = A^+(\nu) E(\nu) \left[1 + \frac{\lambda}{i\sqrt{k^2 - \nu^2}}\right] \qquad (44)$$

is an analytic function of algebraic order in the lower ν-plane, (40b) will be satisfied. If we assume (43), then we see by (44) that

$$G^-(\nu) = \mathcal{O}(\nu^n), \qquad |\nu| \to \infty. \qquad (45)$$

Use of (8) yields by (44)

$$G^-(\nu)\sigma^-(\nu) = A^+(\nu) E(\nu) \sigma^+(\nu). \qquad (46)$$

Once again we repeat the argument that each side of (46) is analytic in a half plane with a common region (at least the real axis) of analyticity and hence is the analytic continuation of the other. Owing to the assumed growths, we obtain by an appeal to the Liouville theorem that each side is equal to a polynomial $\mathcal{P}^N(\nu)$ of

order N, hence

$$A^+(\nu)E(\nu)\sigma^+(\nu) = \mathcal{P}^N(\nu)$$

or

$$A^+(\nu)\sigma^+(\nu) = \frac{\mathcal{P}^N(\nu)}{E(\nu)}. \tag{47}$$

Since $E_N(\nu)$ is a polynomial with real coefficients, its zeros are either on the real axis or conjugate pairs. Unless $\mathcal{P}^N(\nu) = K\,E_N(\nu)$, where K is some constant, the zeros of $E_N(\nu)$ in the right side of (47) will contradict the analyticity of $A^+\sigma^+$ for Im $\nu \geqq 0$, whence

$$A^+(\nu) = \frac{K}{\sigma^+(\nu)}, \tag{48}$$

or

$$u(x, y) = \frac{K}{2\pi i}\int_C \frac{E(\nu)}{\sigma^+(\nu)}\,\frac{e^{i\nu x + i\sqrt{k^2-\nu^2}\,y}}{\sqrt{k^2-\nu^2}}\,d\nu, \tag{49}$$

$$\frac{\Pi_{\text{surf}}}{\Pi_{\text{cyl}}} = \frac{2\pi\Lambda}{1+\sqrt{1+\Lambda^2}}\,|\,E(-m)\,|^2\int_0^\pi |\,p(\vartheta)\,|^2\,\frac{\cos\vartheta+1}{\cos\vartheta+\sqrt{1+\Lambda^2}}\,d\vartheta \tag{56}$$

and again the constant K is proportional to the strength of the source. A straightforward application of the method of saddle points yields

$$\lim_{\rho\to\infty} u(\rho, \vartheta) = u_{\text{surf}}\,U(\vartheta - \vartheta_c) + u_{\text{cyl}} + \mathcal{O}[(k\rho)^{-3/2}], \tag{50}$$

where the surface wave field u_{surf} is

$$u_{\text{surf}}(x, y) = \frac{\lambda K}{m}\,\frac{E(-m)}{\sigma^-(-m)}\,e^{-i\sqrt{k^2+\lambda^2}\,x - \lambda y}, \tag{51}$$

and the cylindrical field u_{cyl} is

$$u_{\text{cyl}} = \frac{K\,p_N(\vartheta)}{\sigma^+(k\cos\vartheta)}\,\frac{e^{i(k\rho+\pi/4)}}{\sqrt{2\pi k\rho}}. \tag{52}$$

The power pattern $P(\vartheta)$ of the cylindrical field is distributed as a function of ϑ by

$$P(\vartheta) = |\,p_N(\vartheta)\,|^2\,\frac{\cos\vartheta+1}{\cos\vartheta+\sqrt{1+(\lambda/k)^2}}. \tag{53}$$

It is interesting to observe that *this expression is* $|\,p_N(\vartheta)\,|^2$ *modulated by the previous power pattern function of the line source.*

The Poynting flux Π transported by each field can be readily calculated; we find first

$$\begin{aligned}\Pi_{\text{surf}} &= \frac{1}{i\omega\epsilon}\int_0^\infty \left[\frac{\partial u}{\partial x}\,u^*\right]_{\text{surf}} dy \\ &= \frac{|\,K\,|^2}{\omega\epsilon}\,\frac{\lambda}{m+k}\,|\,E(-m)\,|^2.\end{aligned} \tag{54}$$

From (21) we have

$$E(-m) = p_N\left(\cos^{-1}\frac{m}{k}\right) = p_N\left(\cos^{-1}\sqrt{1+\Lambda^2}\right)$$

so that the amplitude of the surface wave is proportional to the reactive power delivered by the antenna to the complex angle $\vartheta = \cos^{-1}\sqrt{1+\Lambda^2}$. Secondly, the cylindrical radiated power becomes

$$\Pi_{\text{cyl}} = \frac{1}{i\omega\epsilon}\int_0^\pi u_\rho u^*\,d\vartheta = \frac{|\,K\,|^2}{2\pi\omega\epsilon}\int_0^\pi \left|\frac{p_N(\vartheta)}{\sigma^+(k\cos\vartheta)}\right|^2 d\vartheta,$$

or

$$\Pi_{\text{cyl}} = \frac{|\,K\,|^2}{2\pi\omega\epsilon}\int_0^\pi |\,p_N(\vartheta)\,|^2\,\frac{\cos\vartheta+1}{\cos\vartheta+\sqrt{1+\Lambda^2}}\,d\vartheta, \tag{55}$$

and then

In Appendix I we evaluate integrals of the form

$$I_n = \int_0^\pi \cos^n\vartheta\,\frac{\cos\vartheta+1}{\cos\vartheta+\sqrt{1+\Lambda^2}}\,d\vartheta,$$

which materially eases the labor in computing (56) for any specified radiation pattern.

Appendix I

Evaluation of the integral I_0 where $M = \sqrt{1+(\lambda/k)^2}$:

$$I_0 = \int_0^\pi \frac{\cos\vartheta+1}{\cos\vartheta+M}\,d\vartheta = \frac{1}{2}\int_0^{2\pi}\frac{\cos\vartheta+1}{\cos\vartheta+M}\,d\vartheta,$$

$$|\,M\,| > 1.$$

This integral can be evaluated very simply by residues; define the complex variable

$$z = e^{i\vartheta},$$

whence

$$dz = iz\,d\vartheta$$

$$\cos\vartheta = \frac{1}{2}\left(z+\frac{1}{z}\right),$$

so that I_0 becomes

$$I_0 = \frac{\pi}{2\pi i}\oint_{|z|=1}\frac{z^2+2z+1}{z^2+2Mz+1}\,\frac{dz}{z}.$$

The denominator can be readily factored

$$(z^2 + 2Mz + 1) = (z - \alpha)(z - \beta),$$

where

$$\alpha = -M + \sqrt{M^2 - 1}, \quad \beta = -M - \sqrt{M^2 - 1},$$

and since $|M| > 1$, clearly $|\alpha| < 1$, $|\beta| > 1$. If we add the residues at $z = 0$ and $z = \alpha$, we obtain

$$I_0 = \pi\left[\frac{\alpha^2 + 2\alpha + 1}{\alpha(\alpha - \beta)} + \frac{1}{\alpha\beta}\right]$$

or in terms of $\Lambda = \lambda/k$

$$I_0 = \pi\left[2 + \frac{\Lambda - \sqrt{1 + \Lambda^2} + 1}{\Lambda(\Lambda - \sqrt{1 + \Lambda^2})}\right].$$

It is a simple matter to note that $I_0 \to 0$ as $\Lambda \to \infty$, and $I_0 \to \pi$ as $\Lambda \to 0$.

If the integral is of the form

$$I_n = \int_0^{\pi} \cos^n \vartheta \frac{\cos\vartheta + 1}{\cos\vartheta + M}\, d\vartheta,$$

the same procedure yields

$$I_n = \frac{1}{2\pi i}\frac{\pi}{2^n}\oint_{|z|=1} \frac{z^2 + 2z + 1}{z^2 + 2Mz + 1} \frac{\left(z + \frac{1}{z}\right)^n}{z}\, dz.$$

Observe that if $n = 1$

$$\frac{1}{z}\left(z + \frac{1}{z}\right)^1 = 1 + \frac{1}{z^2},$$

$$\text{if } n = 2 \quad \frac{1}{z}\left(z + \frac{1}{z}\right)^2 = z^2 + \frac{2}{z} + 1,$$

and in general for n odd the coefficient of $1/z$ vanishes for the factor $(z + 1/z)^n/z$, whereas for n even, the coefficient of $1/z$ is

$${}_nC_{n/2} = \frac{\Gamma(n + 1)}{\Gamma^2\left(\frac{n}{2} + 1\right)}.$$

Hence for n odd, the only pole of the integrand is at $z = \alpha$; we find

$$I_n = I_0\left(\frac{\Lambda^2 - 2\Lambda\sqrt{1 + \Lambda^2} + 1}{\Lambda - \sqrt{1 + \Lambda^2}}\right)^n, \qquad n \text{ odd},$$

$$I_n = I_0\left(\frac{\Lambda^2 - 2\Lambda\sqrt{1 + \Lambda^2} + 1}{\Lambda - \sqrt{1 + \Lambda^2}}\right)^n + \frac{\pi\Gamma(n + 1)}{\Gamma^2\left(\frac{n + 2}{2}\right)}, \qquad n \text{ even}.$$

Appendix II

First, observe that the $\cos n\vartheta$ functions form a complete set on the interval $0 \leqq \vartheta \leqq \pi$. Expand $p_\infty(\vartheta)$ as a Fourier cosine series

$$p_\infty(\vartheta) = \sum_{n=0}^{\infty} \alpha_n \cos n\vartheta \tag{57}$$

in the interval $0 \leqq \vartheta \leqq \pi$ either from an analytic knowledge of $p_\infty(\vartheta)$ or numerically [3] from a measured radiation pattern. Truncate the series at some $n = N$ and express $\cos n\vartheta$ as a polynomial of order n in $\cos\vartheta$, *e.g.*,

$$\cos 4\vartheta = 8\cos^4\vartheta - 8\cos^2\vartheta + 1.$$

A collection of terms in (57) will yield

$$p_N(\vartheta) = \sum_{n=0}^{N} \alpha_n' \cos^n \vartheta, \tag{58}$$

or as a function of $\nu = k\cos\vartheta$

$$E_N(\nu) = \sum_{n=0}^{N} \alpha_n' \left(\frac{\nu}{k}\right)^n. \tag{59}$$

The expression (59) corresponds to a Tchebycheff approximation [3] of $E_\infty(\nu)$ in the interval $|\nu/k| \leqq 1$ by a polynomial of order N.

Acknowledgment

The author gratefully acknowledges the many helpful remarks and suggestions of Prof. S. N. Karp of New York University.

References

[1] A. F. Kay, "Scattering of a surface wave by a discontinuity in reactance," IRE Trans. on Antennas and Propagation, vol. AP-7, pp. 22–33; January, 1959.
[2] J. Bazer and S. N. Karp, "Propagation of Plane Electromagnetic Waves Past a Shoreline," Inst. Math. Sci., New York University, New York, N. Y., Res. Rept. No. EM-46; July, 1952.
[3] C. Lanczos, "Applied Analysis," Prentice Hall, Inc., New York, N. Y.; 1956.
[4] B. L. Van der Vaerden, "On the method of saddle points," *Appl. Sci. Res.* vol. B-2, pp. 33–45; 1951.

Surface-Wave Luneberg Lens Antennas*

C. H. WALTER†, SENIOR MEMBER, IRE

Summary—**It is demonstrated that a surface-wave structure having isotropy in the plane of the structure can be operated as a lens. The index of refraction is given for a dielectric slab on a ground plane, a bed of metal posts on a ground plane and a parallel-plate structure with one plate filled with holes. The necessary radial variations in index for several Luneberg-type lenses are given. These include the conventional Luneberg lens, Gutman's modification, the rim-fed Luneberg adapted to a spherical surface and a modification adapted to a spherical surface and collimation of the rays at an arbitrary angle with respect to the plane on which the lens is mounted. An approximate analysis of surface-wave lenses based on optics is described.**

THEORETICAL work by Luneberg[1] on the optics in a medium of variable index of refraction resulted in a type of lens that has many applications in microwave antennas. In the spherical Luneberg lens, an image on a sphere in a region with spherically symmetric index is focussed diametrically opposite onto a concentric inner sphere. Usually the outer sphere is taken to be at infinity. In the cylindrical lens the spheres are replaced by cylinders in a region having cylindrically symmetric index. The electromagnetic theory of the Luneberg lens has been worked out by Jasik[2] for the cylindrical lens and by Wilcox[3] and Tai[4] for the spherical lens. Eaton[5] has considered some extensions of Luneberg-type lenses, and recently Morgan[6] presented a general analysis of the Luneberg lens.

Another basic study that has been applied to microwave antennas is that of surface-wave propagation. An electromagnetic surface wave can be defined as an electromagnetic wave that propagates along an interface between two media. The earliest work on this subject appears to be that of Sommerfeld,[7] who discussed the propagation of a transverse magnetic surface wave along an infinitely long cylindrical wire of finite conductivity. Important contributions have been made by Cutler[8] with his work on electromagnetic waves guided by corrugated conducting surfaces, Goubau[9] with his work on electromagnetic waves guided by a dielectric coated wire, and Attwood[10] with his work on surface-wave propagation over a dielectric coated plane conductor. A good summary and extensive bibliography on surface waves have been presented by Zucker.[11]

It is the purpose of this paper to show that a surface-wave structure can be made to perform as a two-dimensional Luneberg-type lens. By definition, the index of refraction η of the lens is given by

$$\eta = c/v, \tag{1}$$

where c is the velocity of light in free space, and v is the phase velocity of a wave in the medium under consideration. In this case v is the phase velocity of the surface wave. Surface-wave structures consisting of both natural and artificial dielectrics will be considered.

Surface-Wave Structures

A surface-wave Luneberg lens is a two-dimensional lens. Lens action is achieved by varying the phase velocity of the surface wave in the proper manner. The surface-wave structure must be isotropic in the plane of the structure.

Examples of surface wave structures having the necessary isotropy are dielectric sheet on a ground plane, bed of metal posts on a ground plane, and parallel plate structure with holey top plate.

A. Dielectric Sheet on Ground Plane

This problem has been treated by many authors.[10–13] A sketch of the dielectric sheet structure is shown in Fig. 1. Both transverse magnetic (TM) and transverse electric (TE) surface waves are possible. A TM mode will produce polarization perpendicular to the ground plane, whereas a TE mode will produce polari-

* Received by the PGAP, April 1, 1960. This work was performed under Contracts AF 33(616)-3353 and AF 33(616)-6211 between Wright Air Dev. Center and The Ohio State University Research Foundation.

† Antenna Lab., The Ohio State University, Columbus, Ohio.

[1] R. K. Luneberg, "The Mathematical Theory of Optics," Brown University Press, Providence, R. I., pp. 208–213; 1944.

[2] H. Jasik, "The Electromagnetic Theory of the Luneberg Lens," AF Cambridge Res. Center, Bedford, Mass., Rept. No. TR 54-121; November, 1954.

[3] C. H. Wilcox, "The Refraction of Plane Electromagnetic Waves by a Luneberg Lens," Lockheed Aircraft Corp., Van Nuys, Calif., Rept. No. MSD 1802; June, 1956.

[4] C. T. Tai, "The Electromagnetic Theory of the Spherical Luneberg Lens," Antenna Lab., The Ohio State University Research Foundation, Rept. No. 667–17; August, 1956.

[5] J. E. Eaton, "An Extension of the Luneberg-Type Lenses," Naval Res. Lab., Washington, D. C., Rept. No. 4110; February, 1953.

[6] S. P. Morgan, "General solution of the Luneberg lens problem," *J. Appl. Phys.*, vol. 29, pp. 1358–1368; September, 1958.

[7] A. Sommerfeld, "Fortpflanzung Electrodynamischer Wellen an Einem Zykindrischen Leiter," *Ann. Phys. Chem.*, vol. 67, p. 233; 1899.

[8] C. C. Cutler, "Electromagnetic Waves Guided by Corrugated Conducting Surfaces," Bell Telephone Labs., New York, N. Y., Rept. No. MM-44-160-218; 1944.

[9] G. Goubau, "Surface waves and their applications to transmission lines," *J. Appl. Phys.*, vol. 21, pp. 1119–1128; November, 1950.

[10] S. S. Attwood, "Surface wave propagation over a coated plane conductor," *J. Appl. Phys.*, vol. 22, pp. 504–509; April, 1951.

[11] F. J. Zucker, "The guiding and radiation of surface waves," *Proc. Symp. on Modern Advances in Microwave Techniques*, Polytechnic Inst. of Brooklyn, Brooklyn, N. Y., pp. 403–436; November, 1954.

[12] C. H. Walter, "Surface-Wave Luneberg Lens Antenna," Antenna Lab., The Ohio State University Research Foundation, Rept. No. 667–32; May, 1957.

[13] J. H. Richmond, "Surface Waves on Plane Dielectric Sheets and Sandwiches," Antenna Lab., The Ohio State University Research Foundation, Rept. No. 786-10; September, 1958.

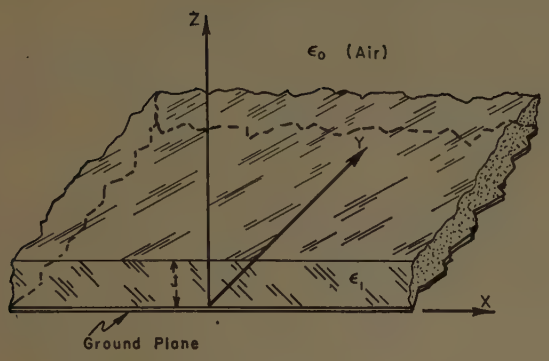

Fig. 1—Infinite dielectric sheet of thickness t and dielectric constant ϵ_1 on an infinite perfectly conducting ground plane. The sheet is assumed to be lossless, isotropic and homogeneous.

zation parallel to the ground plane. The index depends on the mode, the thickness, t, of the sheet, and the relative dielectric constant. For TM modes, the index for a sheet of dielectric of infinite extent is obtained from the equations

$$\beta_0^2 = k_0^2 + k_x^2, \tag{2}$$

$$\epsilon_r\beta_0^2 = k_1^2 + k_x^2, \tag{3}$$

and

$$\epsilon_r k_0 = k_1 \tan k_1 t, \tag{4}$$

where

$\beta_0 = 2\pi/\lambda_0$ = free space propagation constant,
λ_0 = free space wavelength,
k_0 = propagation constant in z direction in ϵ_0,
k_1 = propagation constant in z direction in ϵ_1,
k_x = propagation constant in x direction,
$\epsilon_r = \epsilon_1/\epsilon_0$.

Eq. (4) may be obtained by the usual boundary value solution or by application of a transverse resonance method.[11]

Eqs. (2) and (3) reduce to

$$\eta^2 = 1 + \left(\frac{k_0}{\beta_0}\right)^2 \tag{5}$$

and

$$\eta^2 = \epsilon_r - \left(\frac{k_1}{\beta_0}\right)^2 \tag{6}$$

respectively.

Eliminating k_0 gives

$$\eta = \sqrt{1 + \left(\frac{k_1}{\beta_0\epsilon_r}\tan k_1 t\right)^2}, \tag{7}$$

which is a convenient form for comparison with the metal post structure to be described later. Elimination of both k_0 and k_1 gives

$$\epsilon_r\sqrt{\eta^2 - 1} = \sqrt{\epsilon_r - \eta^2}\tan\left[\beta_0 t\sqrt{\epsilon_r - \eta^2}\right]. \tag{8}$$

If the required index is known, the thickness t is given by

$$t/\lambda_0 = \frac{1}{2\pi\sqrt{\epsilon_r - \eta^2}}\tan^{-1}\left[\frac{\epsilon_r\sqrt{\eta^2 - 1}}{\sqrt{\epsilon_r - \eta^2}}\right]. \tag{9}$$

The use of (9) assumes that the variation in t will be sufficiently gradual so that at any point on the lens the index is the same as it would be for a sheet of that thickness and dielectric constant and of infinite extent.

For TE modes the index is obtained from (2) and (3) and

$$k_0 = -k_1 \cot k_1 t. \tag{10}$$

Again, if the index is known, the thickness t is given by

$$t/\lambda_0 = \frac{1}{2\pi\sqrt{\epsilon_r - \eta^2}}\cot^{-1}\left[\frac{-\sqrt{\eta^2 - 1}}{\sqrt{\epsilon_r - \eta^2}}\right]. \tag{11}$$

Higher-order modes are possible for both TM and TE propagation. The lowest-order TM mode degenerates into a TEM wave as t goes to zero. The lowest-order TE mode, however, has a cutoff. For a given dielectric there is a critical value of t/λ_0, below which TE surface-wave propagation is not possible for the structure in Fig. 1. This does not mean that the structure of Fig. 1 is not suitable for a TE surface wave Luneberg lens; it merely means that such a lens would have finite thickness at the rim.

In practice it may be most convenient to keep ϵ_r constant and obtain the necessary variation in η by varying t. However, this makes η a function of λ_0. Satisfactory operation of a 45 λ_0 diameter lens has been obtained over a 10 per cent band in this manner. Operation over greater bandwidths may be achieved by increasing t to reduce the effect of λ_0 and varying ϵ_r to obtain the necessary index.

B. Bed of Metal Posts on a Ground Plane

The metal post structures illustrated in Fig. 2 may be considered as sheets of artificial dielectric. Such structures will support the dominant TM surface-wave mode.[14,15] Furthermore, these structures are very nearly isotropic. The index depends on the post size and spacing and the height h. An exact analysis is not readily obtained. An approximate analysis based on a transverse resonance solution gives[15]

$$\eta = \sqrt{1 + (W\tan kh)^2}, \tag{12}$$

[14] A. F. Kay, "Excitation Efficiency of Surface Waves Over Corrugated Metal and Doubly Corrugated Metal and in Dielectric Slabs on a Ground Plane," Technical Research Group, New York, N. Y., Scientific Rept. No. 5; December, 1956.

[15] H. B. Querido, "Surface Wave Fields and Phase Velocity Variations of Grounded Dielectric Sheets and of Periodic Structures of Metal Posts on a Ground Plane," Antenna Lab., The Ohio State University Research Foundation, Rept. No. 667-46; November, 1958.

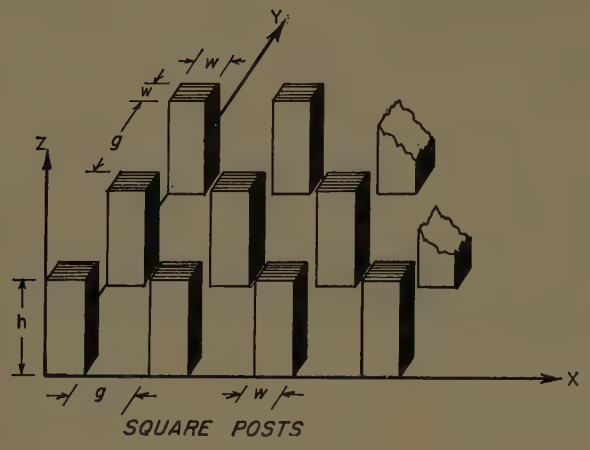

(a)

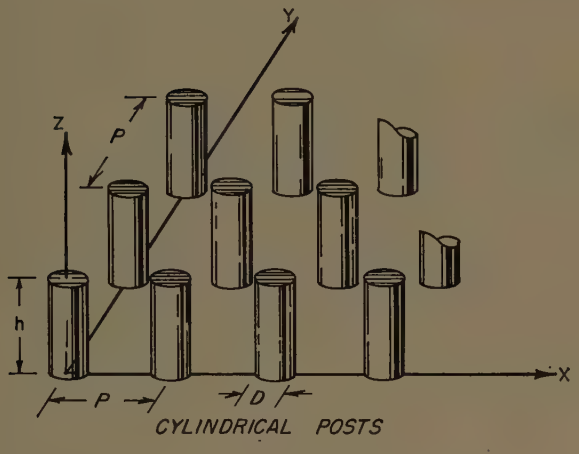

(b)

Fig. 2—Metal post surface-wave structures.

where $k \cong 1.05\beta_0$ = propagation constant in the direction parallel to the posts in the post region,

W = weighting factor

$$= \frac{g}{g+w} \text{ for square posts}$$

$$= \frac{PD - \pi D^2/4}{PD} \text{ for circular posts.}$$

Eq. (12) is found to be a good approximation for structures with five or more posts per wavelength.

C. Holey-Plate Structure

A holey-plate surface-wave structure capable of providing an index from nearly zero to a value approaching the square root of the dielectric between the plates is illustrated in Fig. 3. This structure gives horizontally polarized radiation (electric field parallel to the surface). An approximate expression for the index may be obtained by assuming that the holey-plate structure is composed of stacked TE_{01} waveguides with holes in a narrow wall of each of the guides. Since the electric

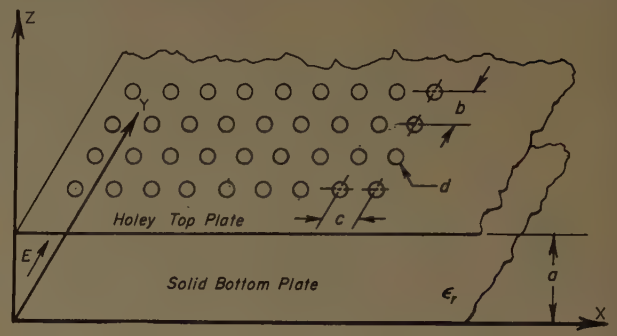

Fig. 3—Holey-plate surface-wave structure.

field would be everywhere normal to the common walls, these walls may be removed to form the structure in Fig. 3. An expression for the index may be obtained by using a transverse resonance procedure.[16] The resulting equations are given by

$$b[\kappa^2 - (\epsilon_r - 1)\beta_0^2] - j\frac{12bc}{d^3} - j2\kappa \cot \kappa a = 0 \quad (13)$$

and

$$k_x = \sqrt{\epsilon_r\beta_0^2 - \kappa^2} = \beta - j\alpha, \quad (14)$$

where

κ = propagation constant in z direction in parallel plate region

$$\cong \frac{\pi}{a},$$

$\beta = \beta_0\eta$,

α = attentuation constant of wave traveling in x direction.

By a perturbation method the index is given approximately by

$$\eta \cong \frac{\lambda_0}{\lambda_g}\left[1 + \frac{\lambda_g^2 X'}{4\pi a^2}\right], \quad (15)$$

where

$$\lambda_g = \frac{\lambda_0}{\sqrt{\epsilon_r - \left(\frac{\lambda_0}{2a}\right)^2}}$$

$$X' = \frac{B'}{G'^2 + B'^2}$$

G' = normalized aperture conductance

$$= \frac{b}{2\kappa}[\kappa^2 - (\epsilon_r - 1)\beta_0^2]$$

B' = normalized aperture susceptance

$$= \frac{6bc}{\kappa d^3}.$$

[16] L. O. Goldstone, and A. A. Oliner, "Leaky Wave Antennas I: Rectangular Waveguides," Polytechnic Institute of Brooklyn, Brooklyn, N. Y., Rept. No. R-606-57, PIB 534; August, 1957.

The structure is assumed to be lossless. However, for indexes less than unity a wave supported by such a structure is attenuated due to radiation. The attenuation constant in nepers per wavelength is given by

$$\alpha \cong \frac{\lambda_g}{2a^2} R' \tag{16}$$

where

$$R' = \frac{G'}{G'^2 + B'^2}.$$

Eqs. (15) and (16) become very poor approximations for operation in the region near cutoff. For such operation it is necessary to find an exact solution for (13) and (14). In all cases the use of the above equations is restricted to $c<\lambda/2$ and $d<b$. For isotropy, b is made equal to c.

Lens Design

The surface-wave lenses that have been considered to date are of the Luneberg type having a radially symmetric index. A typical rimfed lens is shown in Fig. 4. The diameter of the lens will be determined by the desired azimuth beamwidth (lens assumed to be horizontal). The sidelobe level in the horizontal plane may be controlled by proper choice of feed pattern.[17] The vertical beam is not easily controlled. Its shape and position are influenced by the shape and extent of the lens and ground plane as well as the location and extent of the lens feed. For surface-wave lenses with indexes equal to or greater than unity, the vertical pattern is essentially that of an end-fire line source with a nonuniform phase velocity. The effect of ground plane shape and extent is very pronounced for the case of vertical polarization.[18] For lenses 15 to 60 wavelengths in diameter and approximately equal extent of ground plane, the vertical beam maximum ranges from 12° to 6° with respect to the ground plane, respectively. Higher elevation angles for the vertical beam maximum may be obtained by using lenses with indexes less than unity. One may also control the vertical beam position by partially covering the aperture to form a rim radiating lens as illustrated in Fig. 5. In principle, the vertical beam position for a ring radiator may be controlled by means of the phase distribution around the ring. This would be achieved by the proper selection of index. The radial variations in index for various lenses are given below.

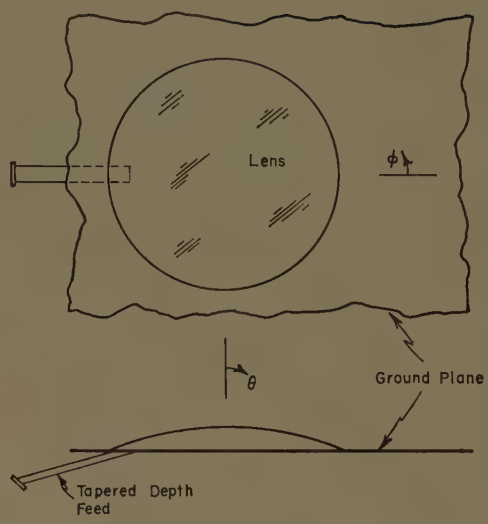

Fig. 4—Sketch showing a TM surface-wave lens on a ground plane.

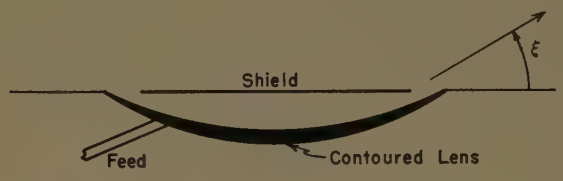

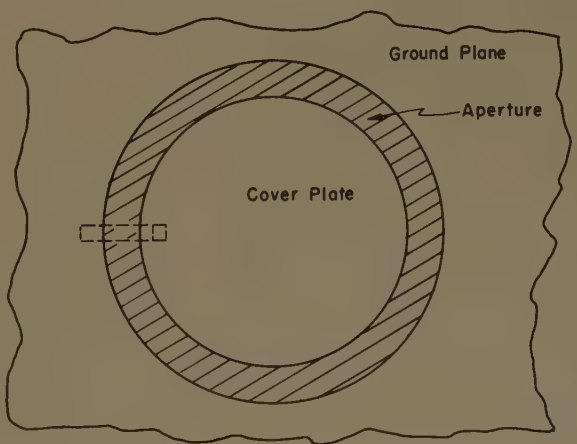

Fig. 5—Sketch of a rim radiating lens.

A. Conventional Luneberg Lens

In the conventional Luneberg lens an incident plane wave is focussed at a point on the rim diametrically opposite from the incident wave. The index is given by the relation

$$\eta(r) = \sqrt{2 - r^2}, \tag{17}$$

where r is the normalized radius. Eq. (17) is not the only index variation producing focus at the rim,[6] but it is perhaps the most practical.

[17] G. D. M. Peeler and D. H. Archer, "A Two-Dimensional Microwave Luneberg Lens," Naval Res. Lab., Washington, D. C., Rept. No. 4115; March, 1953.

[18] B. T. Stephenson and C. H. Walter, "Endfire slot antennas," IRE Trans. on Antennas and Propagation, vol. AP-3, pp. 81–86; April, 1955.

B. Luneberg Lens with Internal Focus

There is no unique index variation for focussing a plane wave at a point within the lens. The problem has been considered by many authors.[5,6,19,20] One of the simplest relations is that obtained by Gutman[20] in which the index for a lens of unit radius with focus at r_1 is given by

$$\eta(r) = \frac{\sqrt{1 + r_1^2 - r^2}}{r_1}. \tag{18}$$

C. Spherical Cap Lens

A solution to the problem of a lens capping a spherical dome on a ground plane has been obtained.[21] Such a structure is shown in Fig. 6. However, the analysis will apply also for a spherical depression, such as the one shown in Fig. 5. A plane wave traveling parallel to the ground plane and striking the spherical surface will focus diametrically opposite at the intersection of the sphere and ground plane. The index variation is given by

$$\eta(r) = \frac{A\sqrt{2R^2 - A^2r^2}}{R^2}, \tag{19}$$

where

$$A = 1 + \sqrt{1 - \frac{1}{a^2}}$$

$$R = 1 + \sqrt{1 - \left(\frac{r}{a}\right)^2}.$$

In the limit as the radius of the sphere becomes infinite (19) reduces to (17) for the conventional Luneberg lens.

If the lens is covered to restrict radiation to the rim as in Fig. 5, an index variation for a feed at $r_1 \leq 1$ and rays collimated at an angle ξ with respect to the ground plane may be obtained from the analyses in footnotes 6 and 21. A resulting expression that reduces to Luneberg's relation [see (17)] for $a = \infty$, $r_1 = 1$ and $\xi = 0$ is given by

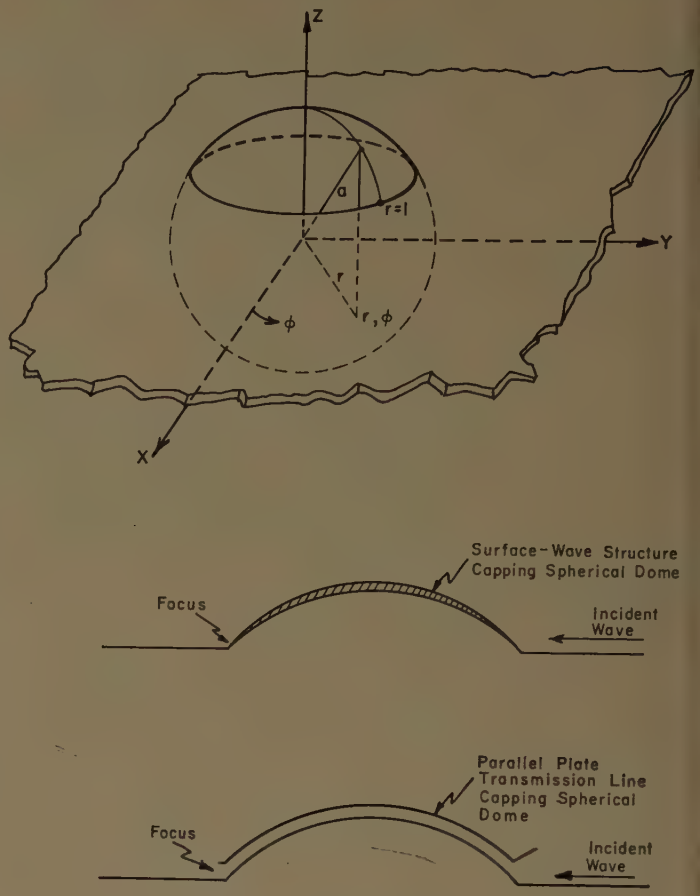

Fig. 6—Spherical cap lenses.

where

$$\rho = \eta r$$

$$\Omega(\rho) = \frac{1}{\pi}\int_{r_1}^{1} \tan^{-1}\left[\frac{\cos^2\xi - \rho^2}{\rho^2(r) - \cos^2\xi}\right]^{1/2} \frac{a}{r\sqrt{a^2 - r^2}}\,dr,$$

and $P(r)$ is arbitrary except for the restrictions

$$P(r) = \rho(r) \geq \cos\xi \qquad r_1 \leq r \leq 1$$

$$\frac{\pi}{2} \geq a\cos\xi\int_{r_1}^{1} \frac{1}{r\sqrt{a^2 - r^2}\sqrt{\rho^2(r) - \cos^2\xi}}\,dr.$$

$$\eta = \frac{\cos\xi(\cos\xi + \sqrt{\cos^2\xi - \rho^2})(a + \sqrt{a^2 - r_1^2})^2 + \rho^2 r_1^2 e^{2\Omega(\rho)}}{2ar_1\sqrt{\cos\xi}(\cos\xi + \sqrt{\cos^2\xi - \rho^2})^{1/2}(a + \sqrt{a^2 - r_1^2})e^{\Omega(\rho)}}, \tag{20}$$

Measurements

Surface-wave lenses have been constructed for both TM and TE operation at X-band, K_u-band and K_a-band with diameters from 15 to 60 wavelengths in order to show that lens action is indeed achieved. When the

[19] J. E. Brown, "Microwave wide-angle scanner," *Wireless Eng.*, vol. 30, pp. 250–255; October, 1953.

[20] A. S. Gutman, "Modified luneberg lens," *J. Appl. Phys.*, vol. 25, pp. 855–859; July, 1954.

[21] S. Adachi and C. H. Walter, "A Spherical Cap Lens," Antenna Lab., The Ohio State University Research Foundation, Rept. No. 903-3; April, 1959.

lens is fed by a point source at the focus, the beamwidth and sidelobe level are very close to the expected values. A point source feed, however, may produce an excessive interference pattern in the vertical plane. For TM dielectric-sheet lenses a tapered-depth source[18] as illustrated in Fig. 7 has been found to work quite well. The aperture of the antenna in Fig. 7 has the necessary field components for TM surface-wave excitation and the velocity ratio c/v (the index) along the aperture may be controlled by varying the width and depth. The antenna may be placed under the lens and its phase velocity adjusted to match that of the lens at the point of focus. For the TE case, however, a comparable tapered-depth feed is equivalent to a magnetic current source and produces a strong cross-polarized component in the far-field pattern of the lens antenna.

Patterns of a 60 λ_0 diameter TM dielectric sheet lens of the conventional Luneberg type with tapered-depth feed are shown in Fig. 8. Polystyrene dielectric was used and the necessary thickness vs radius was obtained from (9) and (17). Measured patterns for a 15 λ_0 diameter lens with feed at $r_1=0.65$ are shown in Fig. 9 (next page). This lens was designed from (9) and (18).

Measured patterns of a metal post lens designed from (12) and (17) are shown in Fig. 10. An open ended waveguide positioned at the rim of the lens provided the feed in this case.

These results and additional measurements which included TE lenses demonstrate that surface-wave structures can be made to operate as lenses. The vertical pattern (plane normal to ground plane) is that of a traveling wave source with a nonuniform phase velocity and with significant influence from the ground plane for TM modes. Cross sections of the beam show the lens action. Although there is some defocussing due to the use of an extended source the lens operation compares quite favorably with that of conventional two-dimensional lenses.[17] In some cases there may be significant deterioration in lens action due to direct radiation from the feed.

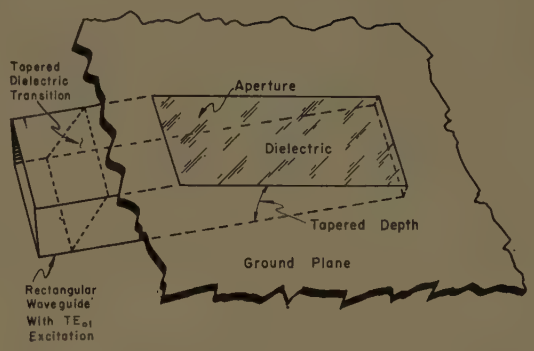

Fig. 7—A tapered-depth antenna suitable as a feed element for a TM surface-wave lens.

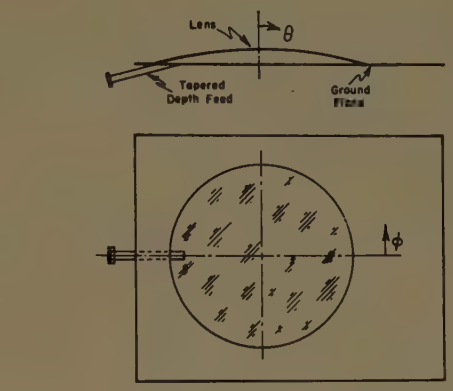

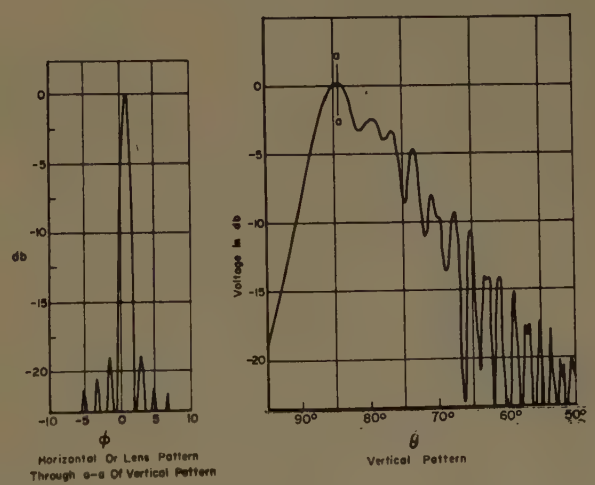

Fig. 8—Measured patterns at 35 kmc of a 60 λ diameter TM surface-wave Luneberg lens with 2 λ_0 tapered-depth feed. The ground plane extends approximately 60 λ_0 beyond the lens.

Analysis of Surface-Wave Lenses

The radiation patterns of a surface-wave lens may be obtained by application of Huygens' principle. By Huygens' principle the electromagnetic waves generated in a source free region by any set of sources can be generated by a sheet of electric currents of surface density $\overline{J}=\bar{n}\times\overline{H}$ and a sheet of magnetic currents of surface density $\overline{M}=\overline{E}\times\bar{n}$ spread over the surface S which surrounds the sources, where $\overline{E}$ and $\overline{H}$ are the electric and magnetic fields, respectively, and $\bar{n}$ is a unit vector normal to S and pointing into the source free region. Two vector potentials may be defined in the usual manner,[22]

$$\overline{A}=\frac{\mu}{4\pi}\int_S\int\frac{\overline{J}e^{-jkR}dS}{R} \tag{21}$$

and

$$\overline{F}=\frac{\epsilon}{4\pi}\int_S\int\frac{\overline{M}e^{-jkR}dS}{R} \tag{22}$$

[22] A. B. Bronwell and R. E. Beam, "Theory and Application of Microwaves," McGraw-Hill Book Co., Inc., New York, N. Y., 1st ed.; 1947.

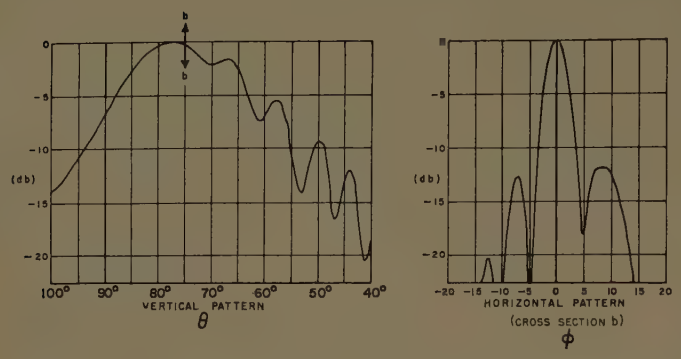

Fig. 9—Measured patterns at 10 kmc of a 15 λ_0 diameter TM surface-wave Luneberg lens with Gutman modification. A 2 λ_0 tapered-depth feed was matched to the lens at $r_1 = 0.65$.

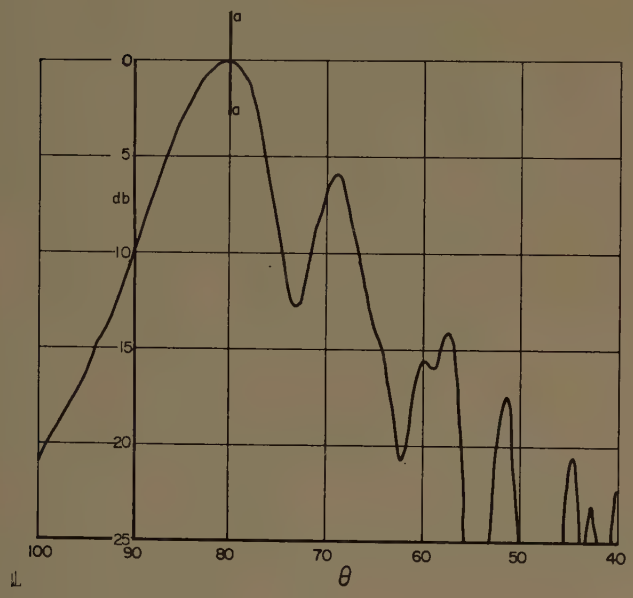

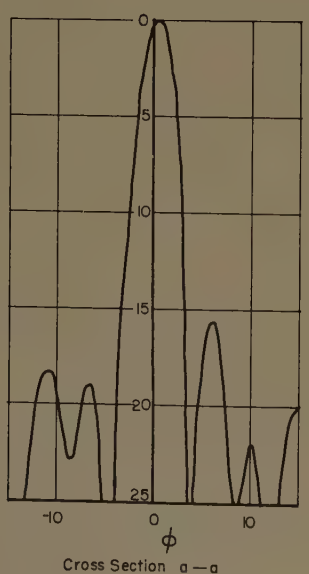

Fig. 10—Measured patterns at 10 kmc of a 15 λ_0 diameter cylindrical metal post lens. The ground plane extends approximately 15 λ_0 beyond the lens.

where

k = propagation constant,
μ = permeability,
ϵ = dielectric constant,
R = distance from a point on S to point of observation.

The electric field on the source free side of S is given by[22]

$$\overline{E} = -\frac{1}{\epsilon}\nabla \times \overline{F} - \frac{j}{\omega\mu\epsilon}\nabla \times \nabla \times \overline{A}, \qquad (23)$$

where ω is the angular frequency of the source.

It is usually most convenient to take S as the surface of the structure and in most cases a satisfactory approximation is obtained by assuming that the currents on the rear surface are negligible compared to those on the front surface where the lens is located.

Tangential E and H over the lens and ground plane may be found approximately by optical methods. Referring to Fig. 11, one can assume that all of the energy

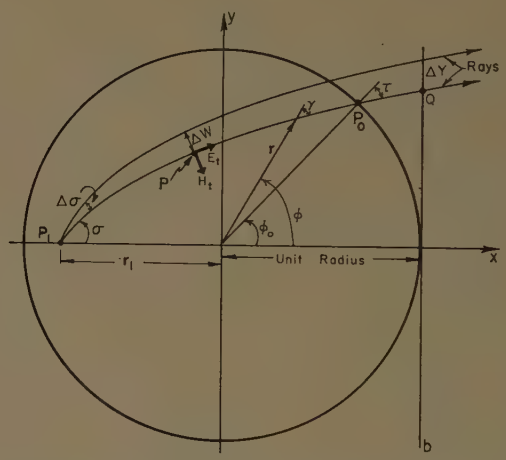

Fig. 11—Coordinate system used in approximate analysis of surface-wave Luneberg lens antenna.

in an incremental angle $\Delta\sigma$ at the source, which is assumed to be located at a point P_1, travels as a surface wave between two surfaces designated as rays in the figure. If the lens is focused at infinity, the angles τ and ϕ_0 are equal. From Fermat's principle and the application of the calculus of variations to a radially symmetric medium, the ray paths are found to satisfy the relation

$$\eta r \sin \gamma = \sin \tau. \qquad (24)$$

This is a generalization of Snell's law. An equivalent equation in differential form is

$$\eta r = \sqrt{1 + \frac{1}{r^2}\left(\frac{dr}{d\phi}\right)^2} \sin \tau. \qquad (25)$$

The optical approximation enables one to find the relative surface-wave amplitude, from which the relative tangential electric fields, E_t, and magnetic fields, H_t, can be found for a particular surface wave structure. The relative phase, ψ, of the fields at any point P on the surface with respect to the feed point P_1 may be obtained from the relation

$$\psi = 360 r_\lambda \int_{P_1}^{P} \eta ds, \tag{26}$$

where ds is an element of path length along the ray through P_1 and P and r_λ is the radius of the lens in wavelengths.

If only the lens pattern of a slow wave ($\eta > 1$) lens is desired, a good approximation is to replace the lens by an equivalent line source such as line b in Fig. 11. Assuming no z variation (direction out of page) conservation of energy gives

$$U(\sigma)\Delta\sigma = U_b(y)\Delta y, \tag{27}$$

where

$U(\sigma)$ = energy distribution per unit angle in the pattern of the feed,
$U_b(y)$ = energy distribution per unit length along b.

If the lens is focused at infinity the phase is constant along b and

$$E_b^2(y) = \frac{E^2(\sigma)}{\eta_1 r_1 \cos\sigma} = \frac{E^2(\sigma)}{\sqrt{\eta_1^2 r_1^2 - y^2}}, \tag{28}$$

where

$E(\sigma)$ = electric field pattern of the feed,
$E_b(y)$ = electric field amplitude along b,
η_1 = index at point of feed.

If the lens is used as a ring radiator, the amplitude and phase at the rim of the lens may be found by the above methods.

ACKNOWLEDGMENT

It is a pleasure to acknowledge the help given by D. M. Brown, R. St. Clair, D. Wilford, R. Adler and other members of The Ohio State University Antenna Laboratory Staff.

Correction

E. J. Martin, Jr., author of "Radiation Fields of Circular Loop Antennas by a Direct Integration Process," which appeared on pp. 105–107 of the January, 1960, issue of these TRANSACTIONS, has called the following to the attention of the *Editor*.

In (1), the subscripts P should be lower case, in order to be consistent with the text; thus, (1) should read

$$r = r_p - a \sin\theta_p \cos(\phi - \phi_p).$$

In (2), (4), and (6), the r components at the vectors should be proportional to $\sin\theta_p$, rather than $1/\sin\theta_p$.

In the second sentence of the last paragraph, the symbol ∇ appears inverted in three places. These relations should read

$$E = (1/j\omega\mu\epsilon)\nabla(\nabla \cdot A) - j\omega A$$

and

$$H = 1/\mu(\nabla \times A).$$

communications

Phenomenological Concepts in Beyond-the-Horizon Tropospheric Propagation*

B. J. STARKEY†

THE PAPER by Bullington[1] gives an excellent comprehensive survey, but one rather puzzling aspect of the author's approach is a somewhat confusing vagueness with which he treats the phenomenological issues involved.

A reader anxious to interpret the relevant part of the paper in a more definite way would have to draw the following conclusions:

1) The theory generally used by radio engineers in their beyond-the-horizon tropospheric propagation work is the one based on the assumption that scatter of EM waves caused by atmospheric "blobs" is the principal mechanism involved.
2) It appears that a so-called "reflection" approach might provide a rather easier explanation of experimental results.
3) Nevertheless, let us forget about the physical mechanism of the phenomena involved, keep on using equations "that fit the experimental results" (which in this context seems to mean equations of the "scatter" theory conveniently manipulated to "come into reasonable agreement" with experiment) and "minimize the fine shades of meaning in the interpretation of the equations." The historical fact that Isaac Newton discovered a formula that accounted for the motion of the planets, but did not explain the mechanism of gravitation, is quoted as a good precedent for such attitude.

Of course, Newton explained a large number of complex phenomena by means of a single one, gravity, which was left unexplained. It is rather difficult to place tropospheric propagation in the same category of basic concepts as gravitation. An unreserved application of Dr. Bullington's recommendation in this respect to other fields of scientific endeavor might lead to rather unexpected results.

The paper also tends to create an impression that the difference between the concepts of "reflection" and "scattering" can be regarded simply as a difference between the "layman" and the "physicist" interpretation

* Received by the PGAP, April 5, 1960.
† Dept. of National Defence, Ottawa, Ont., Can. Formerly with RAE, Farnborough, England.
[1] K. Bullington, "Status of tropospheric extended range transmission," IRE TRANS. ON ANTENNAS AND PROPAGATION, vol. AP-7, pp. 439–440; October, 1959.

of the same phenomenon. Certainly, there is more to it than that! Physical factors behind this difference in the case of tropospheric propagation have been discussed elsewhere.[2]

Reply to Starkey's Discussion[3]

I agree with Mr. Starkey that an understanding of the physical mechanism is a worthwhile objective. However, until that goal is reached, it seems important to describe the experimental results with a minimum of theoretical interpretation.

Since my paper[1] was the opening address of a symposium, its principal purpose was to describe the general characteristics and usefulness of tropospheric beyond-horizon transmission without taking sides on the controversial question of the theoretical explanation. The vagueness to which Starkey refers was caused in part by the neutral purpose of the paper and in part by my own reluctance to accept the scattering theories because of the arbitrary parameters involved. The generalized equation used in the paper was intended to represent experimental data. The use of the angle θ does not necessarily imply scattering, since it is possible and in some cases convenient to describe diffraction and reflection, as well as scattering, in this way.

K. Bullington
Bell Telephone Labs.
Murray Hill, N. J.

[2] B. J. Starkey, W. R. Turner, S. R. Badcoe, and G. F. Kitchen, "The effects of atmospheric discontinuity layers up to and including the tropopause on beyond-the-horizon propagation phenomena," *Proc. IEE*, vol. 105, pt. B, suppl. 8, pp. 97–105; January, 1958.

[3] Received by the PGAP, April 20, 1960.

The Magneto-Ionic Theory for Drifting Plasma*

H. UNZ†

A PAPER titled as above will be published on a later date. However, it is felt that one of the main results should be mentioned as early as possible. It has been found that the refractive index n of the magneto-ionic medium, for the case of plasma drifting with a constant velocity $\bar{v}_0$, is given by the following algebraic equation:

$$C[A^2 - Y_L^2(n^2-1)^2] - A[Y_T^2(n^2-1)^2 + \beta_T^2 X^2 n^2 (1-n\beta_L)^2] - 2XY_L(\bar{\beta}_T \cdot \bar{Y}_T)n(1-n\beta_L)(n^2-1)^2 = 0; \quad (1a)$$

$$A = (n^2-1)(1-iZ) + X(1-n\beta_L)^2; \text{ and} \quad (1b)$$

$$C = (n^2-1)(1-X-iZ) + n^2 X \beta_T^2, \quad (1c)$$

where

$$\beta_T = \frac{v_{0T}}{c}, \quad \beta_L = \frac{v_{0L}}{c}, \qquad v_{0T} \text{ and } v_{0L}$$

are the transverse and the longitudinal components of the constant drift velocity vector of the plasma. All the rest of the symbols are defined as in the classical monograph by Ratcliffe.[1]

In the particular case of stationary plasma, *i.e.*, $\beta_T = \beta_L = 0$, the solution of (1) will give the classical Appleton-Hartree equation[1] of the magneto-ionic theory. Several other more complicated cases have been solved explicitly from (1). The above theory has been applied to emissions generated in the earth exosphere,[2] whistler propagation,[3,4] etc. The results will be published soon.

* Received by the PGAP, April 25, 1960. This work has been supported in part by contract No. DA-44-009-ENG-3769 at the Midwest Research Institute, Kansas City, Mo.

† Elec. Engrg. Dept., University of Kansas, Lawrence, Kans.

[1] J. A. Ratcliffe, "The Magneto-Ionic Theory and Its Applications to the Ionosphere," Cambridge University Press, Cambridge, England; 1959.

[2] R. M. Gallet, "The very low frequency emissions generated in the Earth Exosphere," Proc. IRE, vol. 47, pp. 211–231; February, 1959.

[3] R. A. Helliwell and M. G. Mogran, "Atmospheric whistlers," Proc. IRE, vol. 47, pp. 200–208; February, 1959.

[4] R. E. Barrington, "Whistler propagation in the presence of ion Streams," (Abstract) IRE Trans. on Antennas and Propagation, vol. AP-7, pp. 287; July, 1959.

An Endfire Array Continuously Proximity-Coupled to a Two-Wire Line*

GEORGE R. FORBES†

IN THE new type of VHF-UHF communication antenna designed by Sletten and Forbes in 1957,[1] radiating dipoles are capacitively coupled to a two-wire transmission line. The degree of coupling is a function of the angle that the dipole makes with the axis of the transmission line, and is maximum at an angle of approximately 20°. The broadside antenna developed with dipoles spaced $\lambda/2$ apart along the axis of the two-wire line and alternately making an angle of $+20°$ and $-20°$ with the axis is excellent for VHF communication application, since it requires no individual dipole feed lines.

The principle of this broadside antenna has been applied to develop an endfire array of proximity-coupled dipoles. Fig. 1 shows $\lambda/2$ radiating dipoles, spaced $\lambda/4$ apart, capacitively coupled to a two-wire line. Each dipole is transversely perpendicular to the axis of the line. When the coupling between the dipoles and two-wire line is small (dipoles spaced $\lambda/4$ or less apart), the phase velocity along the line approximates that of free space and the currents induced in the dipoles produce a single beam in the direction of propagation of the traveling wave. (Spacing of $\lambda/2$ produces a bidirectional pattern.)

Although the coupling of a dipole perpendicular to the axis is considerably less than that of a dipole inclined to the axis, it is sufficient for use with an array 7.5 λ long (30 dipoles spaced $\lambda/4$ apart).[2] The coupling depends on the spacing between the two wires of the line, the length of the dipole, and especially on the height of the dipoles above the line.

In testing the admittance of a single dipole shunted across the transmission line, it was not possible to obtain a purely resonant load. This condition was also found by Seshardri and Iizuka.[3]

Fig. 2 shows the measured conductance of a $\lambda/2$ dipole plotted against the height of the dipole above the transmission line. To determine impedance characteristics, an equivalent circuit was derived for the dipole [see Fig. 3(a)].[4] Each wire couples to the dipole by a

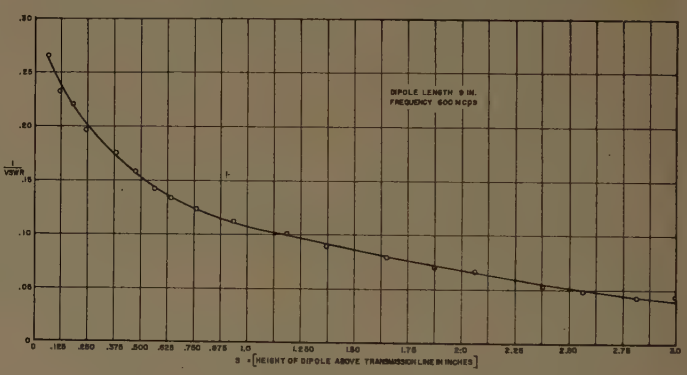

Fig. 2—Reciprocal of VSWR vs height of dipole above transmission line.

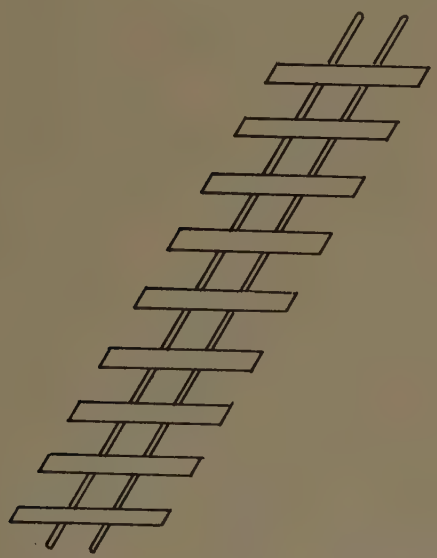

Fig. 1—$\lambda/2$ radiating dipoles spaced $\lambda/4$ apart capacitively coupled to a two-wire line.

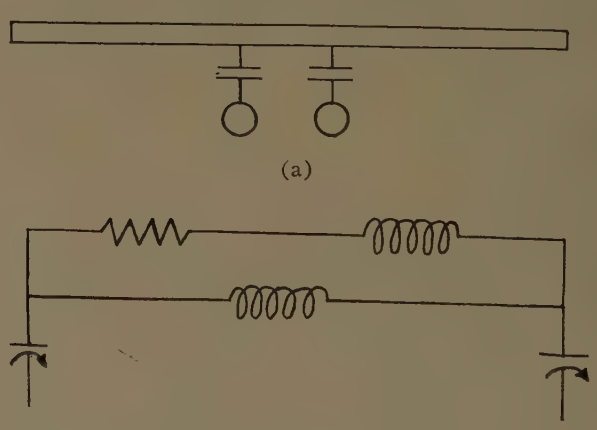

Fig. 3—Equivalent circuit of a dipole coupled to a two-wire line.

* Received by the PGAP, April 12, 1960.

† Electromagnetic Rad. Lab., AF Cambridge Res. Ctr., Bedford, Mass.

[1] C. J. Sletten and G. R. Forbes, "A New Antenna Radiator for VHF-UHF Communications," AF Cambridge Res. Ctr., Tech. Rept. No. AFRC-TR-57-114; June, 1957.

[2] G. R. Forbes, "An Endfire Array Continuously Proximity-Coupled," AF Cambridge Res. Ctr., Tech. Rept. No. AFCRC-TR-59-368; December, 1959.

[3] S. R. Seshardri and K. Iizuka, "A Dipole Antenna Coupled Electromagnetically to a Two-Wire Transmission Line," Cruft Lab., Harvard University, Cambridge, Mass., Tech. Note No. AFCRC-TN-58-594, Contract AF19(604)-786, Scientific Rept. No. 21; October 31, 1958.

[4] Fig. 3(a) and 3(b) and the mathematical analysis are due to J. Ruze, Consultant to the Electromagnetic Radiation Laboratory.

capacitive reactance $X_c/2$. The two capacitors are shorted by an inductive strip created by the radiating dipole, the impedance X_L of the dipole coupling electromagnetically with the strip. With this coupled impedance denoted as R_D+jX_D, the equivalent circuit is as shown in Fig. 3(b). The input impedance Z is

$$Z = -jX_c + \frac{jX_L(R_D + jX_D)}{R_D + j(X_D + X_L)}$$

$$Z = \frac{R_D X_L^2}{R^2_D + (X_D + X_L)^2} + jX_L \frac{[R^2_D + X_D(X_D + X_L)]}{R^2_D + (X_D + X_L)^2} - jX_c.$$

When $X_c \gg X_L$ (small coupling and short strip),

$$Z = \frac{R_D X^2_L}{R^2_D + (X_D + X_L)^2} - jX_c.$$

The series resistance is then small and the reactance capacitive; reactance cannot be tuned out by changing the dipole length.

Fig. 5 shows typical radiation patterns of the array, both terminated and unterminated. Patterns measured over a range of frequencies from 580 to 670 mc showed very little change in their basic characteristics. From the results of these measurements, it is apparent that the effective phase velocity along the array is slower than the velocity of the light since the Hansen-Woodyard condition is approximately fulfilled.

Radiation from the line, checked by removing all the dipole elements, is about 17 db below the beam peak when the line is terminated. The level can be lowered by decreasing the spacing between the wires.

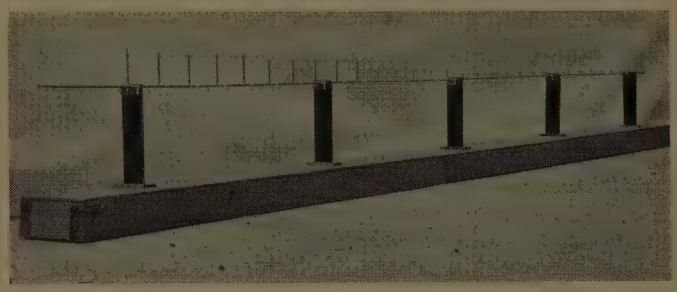

Fig. 4.

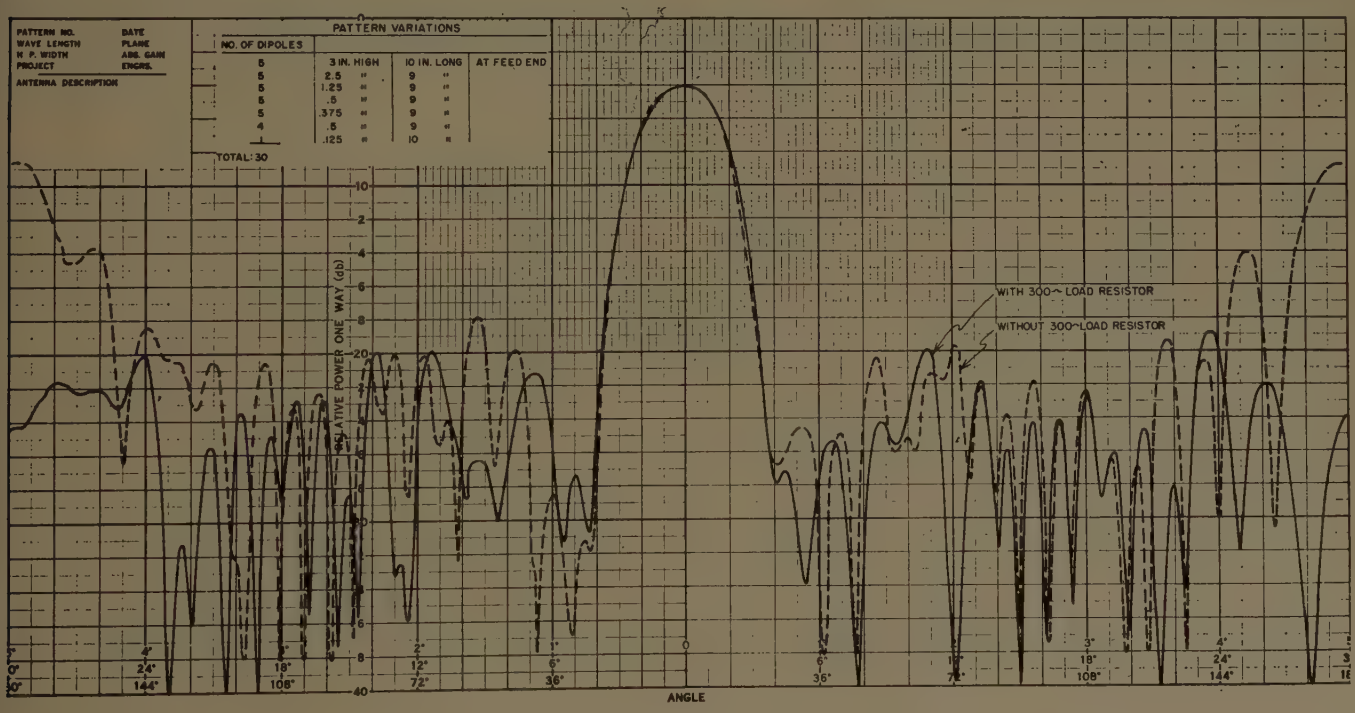

Fig. 5—Thirty-element endfire array with 25-db taper.

When the impedance of the entire array was measured, it was found that the array was not coupling as much energy as expected, probably because mutual coupling between parallel dipoles is high in an endfire array.

At an operating frequency of 600 mc the most practical length for an antenna of this type is the 7.5 λ (13-foot) array constructed of 30 dipoles (see Fig. 4). The amplitude distribution is effectively tapered by varying the height of the dipoles above the two-wire line.

Arrays of the type in Fig. 1 were used to study "modulated" surface wave antennas,[5] in which two surface waves—one along the two-wire line and one along the array of dipoles—are coupled in an attempt to control the aperture illumination. This approach differs from the one described in both design philosophy and results.

[5] D. K. Reynolds and R. A. Gigelmann, "Research on Traveling Wave Antennas," AF Cambridge Res. Ctr., Tech. Rept. No. AFCRC-TR-59-160 (ASTIA Document No. AD217821), Final Rept. Contract AF19(604)-4052; June, 1959.

Direction Finding in a Two-Component Field*

D. N. TRAVERS†, MEMBER, IRE, AND W. M. SHERRILL†, MEMBER, IRE

IT is well known that high-frequency radio direction finding is sometimes severely complicated by re-radiated secondary signals of frequency equal to that of the primary, but of different azimuth, amplitude, and phase. An example of considerable practical importance is naval shipboard direction finding. A method for analyzing a two-component field, using a twin-channel receiver and crossed loops, has been proposed by Gabler.[1] The method makes use of the fact that the phase difference between the primary and secondary components varies throughout the resultant field, and provides a means of displaying both azimuth and relative amplitudes of the components incident on the antenna in the form of an envelope of ellipses. The purpose of this note is to show that the use of a twin-channel receiver and indicator is not essential to achieve a display which provides the same information for a two-component field. A spinning loop antenna, or crossed loops and goniometer with a single-channel receiver, can be used to analyze a two-component field and display both the azimuths and the relative amplitudes of the two incident waves.

Consider two spinning simple loop antennas, A and B, of radius r, small with respect to the wavelength of two incident plane waves arriving from infinitely distant sources. Let the antennas be located about a coordinate center, point O, from which phase in the resultant field of the incident waves is measured. The radial distances, ρ_A and ρ_B, from the origin to the loops are arbitrary.

Let two vertically polarized plane waves of equal frequency, but of arbitrary amplitudes E_1 and E_2, phases ϕ_1 and ϕ_2, and azimuths δ_1 and δ_2, arrive at horizontal incidence upon the spinning loops as shown in Fig. 1. Since the sources of the incident waves are remote, their azimuths are the same for each of the two spinning loop antennas. Thus the only difference between the signals induced in the two loops is a phase difference.

The total signal (V_T) induced in either of the loops may be derived in the following manner:

$$V_T = -jh_e\{E_1 \sin [\beta_0 r \sin (\theta_{A,B} - \delta_1)] \cdot e^{j[\omega t - \beta_0 \rho_{A,B} \cos (\delta_1 - \tau_{A,B}) + \phi_1]} + E_2 \sin [\beta_0 r \sin (\theta_{A,B} - \delta_2)] \cdot e^{j[\omega t - \beta_0 \rho_{A,B} \cos (\delta_2 - \tau_{A,B}) + \phi_2]}\}, \quad (1)$$

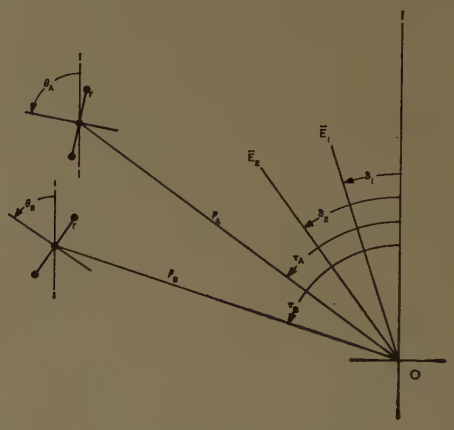

Fig. 1—Geometry for a single channel direction finder in a two-component field.

where h_e is effective height, E is field strength, $\phi + \omega t$ is the field phase at point O, and $\beta_0 = \omega/c$.

Since the wavelength is much greater than the loop dimensions, it can be assumed that

$$\sin [\beta_0 r \sin (\theta_{A,B} - \delta_{1,2})] = [\beta_0 r \sin (\theta_{A,B} - \delta_{1,2})]$$

and

$$V_T = -jh_e\beta_0 r\{E_1 \sin (\theta_{A,B} - \delta_1) e^{-j[\beta_0 \rho_{A,B} \cos (\delta_1 - \tau_{A,B}) - \phi_1]} + E_2 \sin (\theta_{A,B} - \delta_2) e^{-j[\beta_0 \rho_{A,B} \cos (\delta_2 - \tau_{A,B}) - \phi_2]}\} e^{j\omega t}. \quad (2)$$

Let the relative phase between the two component voltages induced in either loop be $\phi_{d(A,B)}$, so that

$$V_T = -jh_e\beta_0 r\{E_1 \sin (\theta_{A,B} - \delta_1) + E_2 \sin (\theta_{A,B} - \delta_2) e^{j\phi_d(A,B)}\} \cdot e^{j[\omega t - \beta_0 \rho_{A,B} \cos (\delta_1 - \tau_{A,B}) + \phi_1]}, \quad (3)$$

where

$$\phi_{d(A,B)} = \beta_0 \rho_{A,B}[\cos (\delta_1 - \tau_{A,B}) - \cos (\delta_2 - \tau_{A,B})] + (\phi_2 - \phi_1).$$

The two patterns displayed by the two loops are

$$|V_T'|_A = [E_1^2 \sin^2 (\theta_A - \delta_1) + E_2^2 \sin^2 (\theta_A - \delta_2) + 2E_1E_2 \sin (\theta_A - \delta_1) \sin (\theta_A - \delta_2) \cos \phi_{dA}]^{1/2},$$

$$|V_T'|_B = [E_1^2 \sin^2 (\theta_B - \delta_1) + E_2^2 \sin^2 (\theta_B - \delta_2) + 2E_1E_2 \sin (\theta_B - \delta_1) \sin (\theta_B - \delta_2) \cos \phi_{dB}]^{1/2}, \quad (4)$$

where $|V_T'|$ includes the constant $-jh_e\beta_0 r$ and the transmission characteristics of the receiver.

The polar display of either antenna pattern is of the form

$$x = |V_T'| \cos \theta$$
$$y = |V_T'| \sin \theta. \quad (5)$$

* Received by the PGAP, April 12, 1960.

† Dept. of Electronics and Elec. Engrg., Southwest Res. Inst., San Antonio, Tex.

[1] H. Gabler, and M. Wachtler, "A new method of determining the components of radio bearings from coherent waves," *Elektrotech. Z. (ETZ)*, vol. 79A, pp. 385–388; June, 1958. National Research Council of Canada Technical Translation 819.

In order to use a single-channel receiver it is necessary either to switch between antennas A and B so as to allow θ_A and θ_B each to move through 2π radians separately, or to use the same antenna at positions A and B at different times. The two patterns will intersect at a common value of θ, say θ_i. At this intersection the amplitudes $|V_T'|_A$ and $|V_T'|_B$ are equal so that

$$\sin(\theta_i - \delta_1)\sin(\theta_i - \delta_2)(\cos\phi_{dA} - \cos\phi_{dB}) = 0. \quad (6)$$

Therefore,

$\sin(\theta_i - \delta_1) = 0$, that is $\theta_1 = \delta_1, \delta_1 + \pi$

$\sin(\theta_i - \delta_2) = 0$, that is $\theta_1 = \delta_2, \delta_2 + \pi$

$\cos\phi_{dA} = \cos\phi_{dB}$, that is the patterns are coincident.

In the case of coincident patterns, there may be more than one condition which allows $\phi_{dA} = \phi_{dB}$ to be obtained; however, a necessary condition for determining the bearings is $\phi_{dA} \neq \phi_{dB}$. Thus, the intersection azimuths θ_i are the directions of the field components with a 180° ambiguity. Furthermore, when $\theta_i = \delta_1$,

$$|V_T'|_{\theta_i=\delta_1} = |E_2 \sin(\delta_1 - \delta_2)|$$

and when $\theta_i = \delta_2$,

$$|V_T'|_{\theta_i=\delta_2} = |E_1 \sin(\delta_2 - \delta_1)|.$$

Since

$$|\sin x| = |\sin(-x)|,$$

the display amplitudes at these points are proportional to E_1 and E_2, the field amplitudes.

Experimental Comparison of Image Line Radiators and Polyrod Antennas*

S. P. SCHLESINGER†, MEMBER, IRE, AND A. VIGANTS†

Summary—**Experimental comparison is made for some polyrod antennas and the corresponding HE_{11} excited dielectric image line radiators on a finite image surface, dipole and reflector launched. There is a sufficient amount of correspondence in the radiation intensities to justify the use of polyrod design data in design of image line antennas. The amount of back radiation is smaller for the image line antennas.**

THE polyrod antenna[1–4] has an analog in a finite section of an HE_{11} excited dielectric image line.[5] It is instructive to compare the practical cases of a polyrod antenna launched from the end of a waveguide and an image line antenna on a finite image surface launched from a dipole with a reflector.

In this investigation the polyrod antennas were launched from windows at the end of RG-96/U waveguide into which the dielectric rods were fitted except in the case of a large diameter rod of relative dielectric constant 1.67 which was launched from a window at the end of a small horn. A cross section of the image line radiator is shown in Fig. 1. The reflector is located $\lambda_0/4$ behind the dipole where λ_0 denotes the free space wavelength. The reflector diameter is about 0.9 λ_0 and the image surface size is about 32 λ_0 by 18 λ_0 with the long dimension parallel to the rod and the dipole at the center of the image surface. The frequency in all cases was 34.86 kmc. The length of the rod L is the distance from the window to the end of the rod for the polyrod antennas and it was arbitrarily taken to be the distance from the center of the dipole to the end of rod

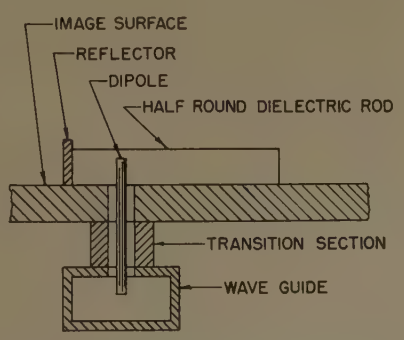

Fig. 1—Cross section of HE_{11} excited dielectric image line radiator.

* Received by the PGAP, April 20, 1960. This work was supported by the AF Cambridge Res. Center, Cambridge, Mass., under Contract No. AF 19(604)3879.

† Dept. of Elec. Engrg., Columbia University, New York, N. Y.

[1] G. E. Mueller, and W. A. Tyrell, "Polyrod antennas," *Bell Sys. Tech. J.*, vol. 26, pp. 837–851; October, 1947.
[2] D. G. Kiely, "Dielectric Aerials," John Wiley and Sons, Inc., New York, N. Y.; 1953.
[3] J. Brown, and J. O. Spector, "The radiating properties of end-fire aerials," *Proc. IEE*, pt. B, vol. 104, pp. 27–34; January, 1957.
[4] L. W. Mickey, and M. G. Chadwick, "Closely spaced high dielectric constant polyrod arrays," 1958 IRE NATIONAL CONVENTION RECORD, pt. 1, pp. 213–224.
[5] S. P. Schlesinger, and D. D. King, "Dielectric image lines," IRE TRANS. ON MICROWAVE THEORY AND TECHNIQUES, vol. MTT-6, pp. 291–299; July, 1958.

for the image line radiators. The radiation patterns were taken with a horn polarized to detect the electric field vector in the E plane of the exciting waveguide for the polyrod antennas and in the plane formed by the rod axis and the dipole axis for the image line radiators.

Three sets of radiation patterns obtained in the manner described in the previous paragraph are shown in Fig. 2. The angle θ is measured from the rod axis and ϵ and $2a$ denote the relative dielectric constant and diameter of the rods. Since there are diffraction effects in the main lobes of the image line radiator patterns, an arbitrary basis for comparison is arrived at by matching first sidelobes of corresponding image line and polyrod patterns. Masking and diffraction due to launching mechanisms can be seen to begin at about 90° with masking more pronounced for the image line radiators. There is a sufficient amount of correspondence between the radiation patterns to justify the use of polyrod design procedures for image line antennas. An attractive feature of the dipole and reflector launched image line section is the reduced level of back radiation as compared to the polyrod antenna.

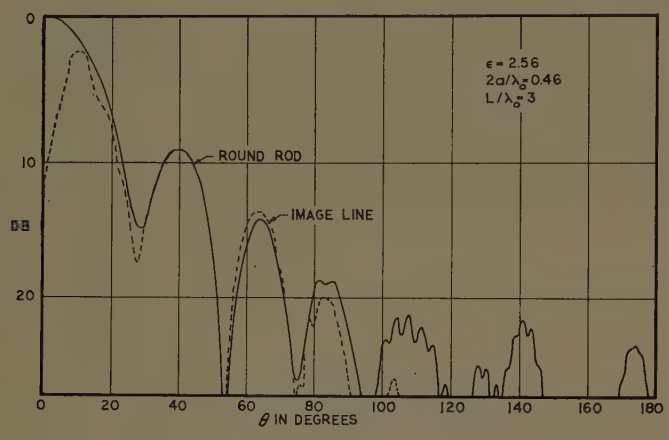

(a)

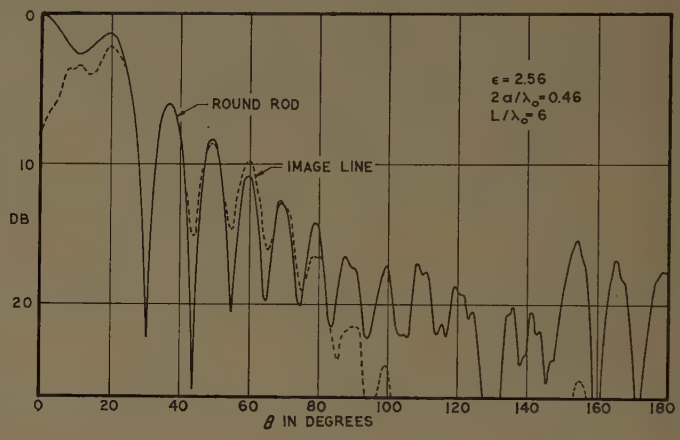

(b)

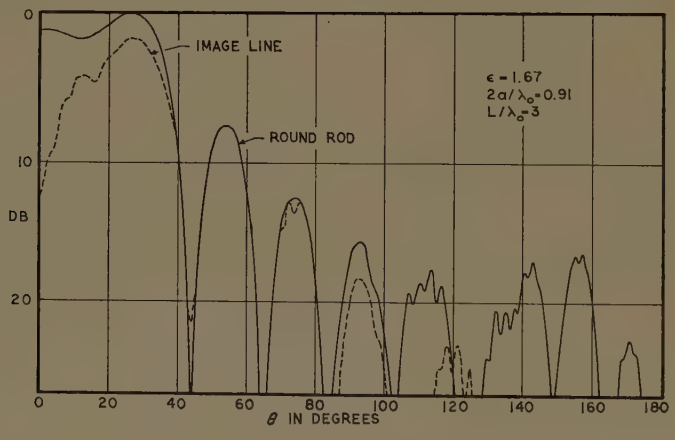

(c)

Fig. 2—Comparison of radiation intensities for HE_{11} excited dielectric image line and polyrod antennas.

Horn Antennas for HF Long-Range Communication*

H. BRUECKMANN†, FELLOW, IRE, AND B. G. HAGAMAN‡, SENIOR MEMBER, IRE

THE well-known pyramidal horn antennas with a rectangular aperture whose sides are parallel to those of the rectangular waveguide feed section produce radiation patterns with relatively strong sidelobes in the *E*-plane. This undesirable characteristic is explained by the fact that the amplitude distribution of the electric field in the aperture parallel to the *E*-plane is essentially uniform. In the *H*-plane the amplitude distribution is sinusoidal and the sidelobes are much weaker. B. G. Hagaman has proposed a simple modification[1] which reduces greatly the sidelobes of horn antennas. It has been investigated under a contract sponsored by the U. S. Army Signal Research and Development Laboratories, Fort Monmouth, N. J., which was guided in the direction of technical effort by the co-author. Independently, G. F. Koch has also made a proposal along similar lines for reflector type antennas.[2] Hagaman proposed to align the diagonals, rather than the sides, of the aperture parallel to the sides of the waveguide feed section, and to shape properly the aperture.

The accompanying change of the amplitude distribution in the aperture was measured using the unsymmetrical configuration shown in Fig. 1. For the sake of brevity, this configuration was named TAHA, short for Tapered Aperture Horn Antenna. The lower corner of the aperture was cut off in order to keep its vertical dimension to a minimum. This is a modification of practical importance, as will be discussed later, but has no bearing on the TAHA principle. Disregarding this detail the aperture is a rhombic with an acute angle of about 60 degrees. The function of the peculiar shape of the aperture and the particular alignment of its excitation is explained in Fig. 2, if only qualitatively. It shows the lines of the electric field across the aperture as one would expect them to flow, from a theoretical consideration of the conducting boundaries and the chosen excitation parallel to the long diagonal. Obviously, the vertical components of the electric field vectors above and below the long diagonal symmetrical to it have opposite directions and essentially cancel with respect to radiation. The horizontal components, however, have the same directions and add with respect to radiation broadside to the aperture. Moreover, Fig. 2 allows realizing qualitatively that the integral of the excitation over a vertical narrow strip tapers from a maximum at the center gradually to zero at the ends of the long diagonal. The results of measurements at three different frequencies shown in Fig. 3 confirm this explana-

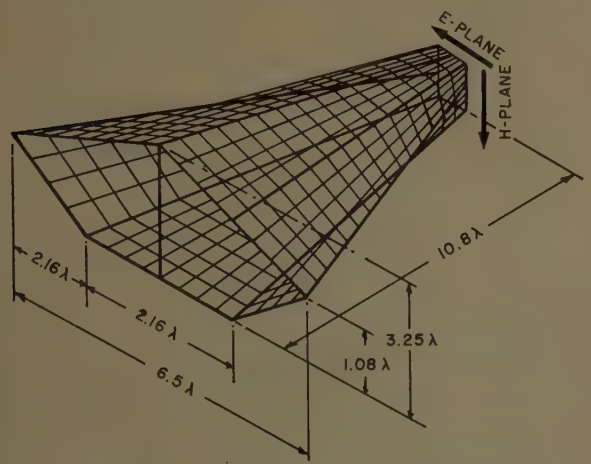

Fig. 1—Dimensions of model TAHA at 2000 mc (160:1 model).

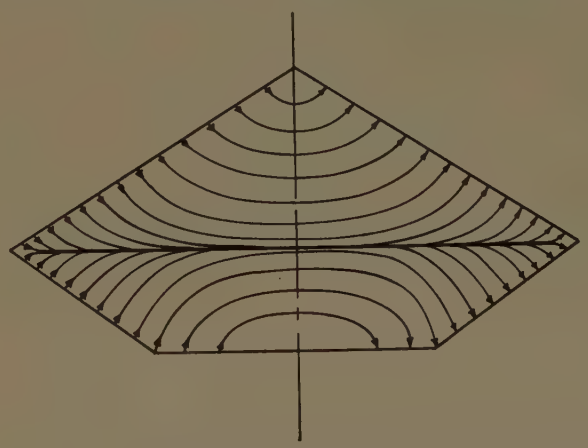

Fig. 2—Assumed *E*-field distribution of TAHA aperture.

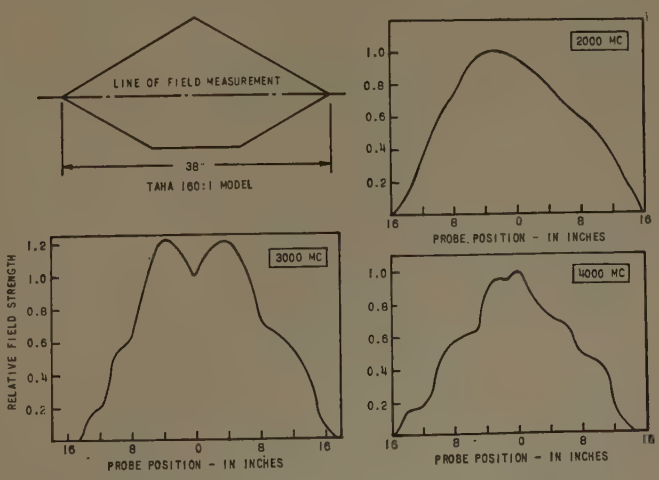

Fig. 3—Measured *E*-field distribution of TAHA aperture.

* Received by the PGAP, May 6, 1960. This paper is the substance of a presentation to the NTG, Prof. Group "Antennas" (a German professional society of electrical engineers), Munich, Germany, on April 29, 1960. The complete paper will be published in the *NTG Journal*.

† U. S. Army Signal Res. and Dev. Lab., Ft. Monmouth, N. J.
‡ Developmental Engrg. Corp., Ft. Evans Lab., Leesburg, Va.

[1] B. G. Hagaman, U. S. Patent No. 2,851,686, filed June 28, 1956.

[2] G. F. Koch, "Richtantennen mit besonderen Aperturformen," *Nachrichtentech. Z.*, vol. 70, pp. 175–186; April, 1957. Also, "Flüchenstrahler mit kleinen Nebenmaxima," *Fernmelde tech. Z.*, vol. 7, pp. 498–509; October, 1954.

tion and also prove that the effect is little dependent on frequency.

It might be argued that the explanations and evidence given for the *E*- and *H*-planes do not preclude strong new sidelobes arising in directions between the two principal planes. This argument is disproved by the experimental evidence presented in Fig. 4, which shows contour map plots of the radiation in the entire forward hemisphere over a wide range of frequency. The radiation plotted is the resultant of the field strength components measured separately in orthogonal planes of polarization. In calculating the resultant it was arbitrarily assumed that these components are in phase. This is the most unfavorable phase relation possible from the viewpoint of sidelobe suppression. The actual resultant may be up to 3 db weaker, which occurs when the phase difference is 90°. Note that all sidelobes are more than 20 db down from the peak of the main lobe. The sidelobes of an optimum-design TAHA made of sheet metal are actually in the order of 30 db down over a frequency range of more than 1:3.

An immediate practical application of TAHA has

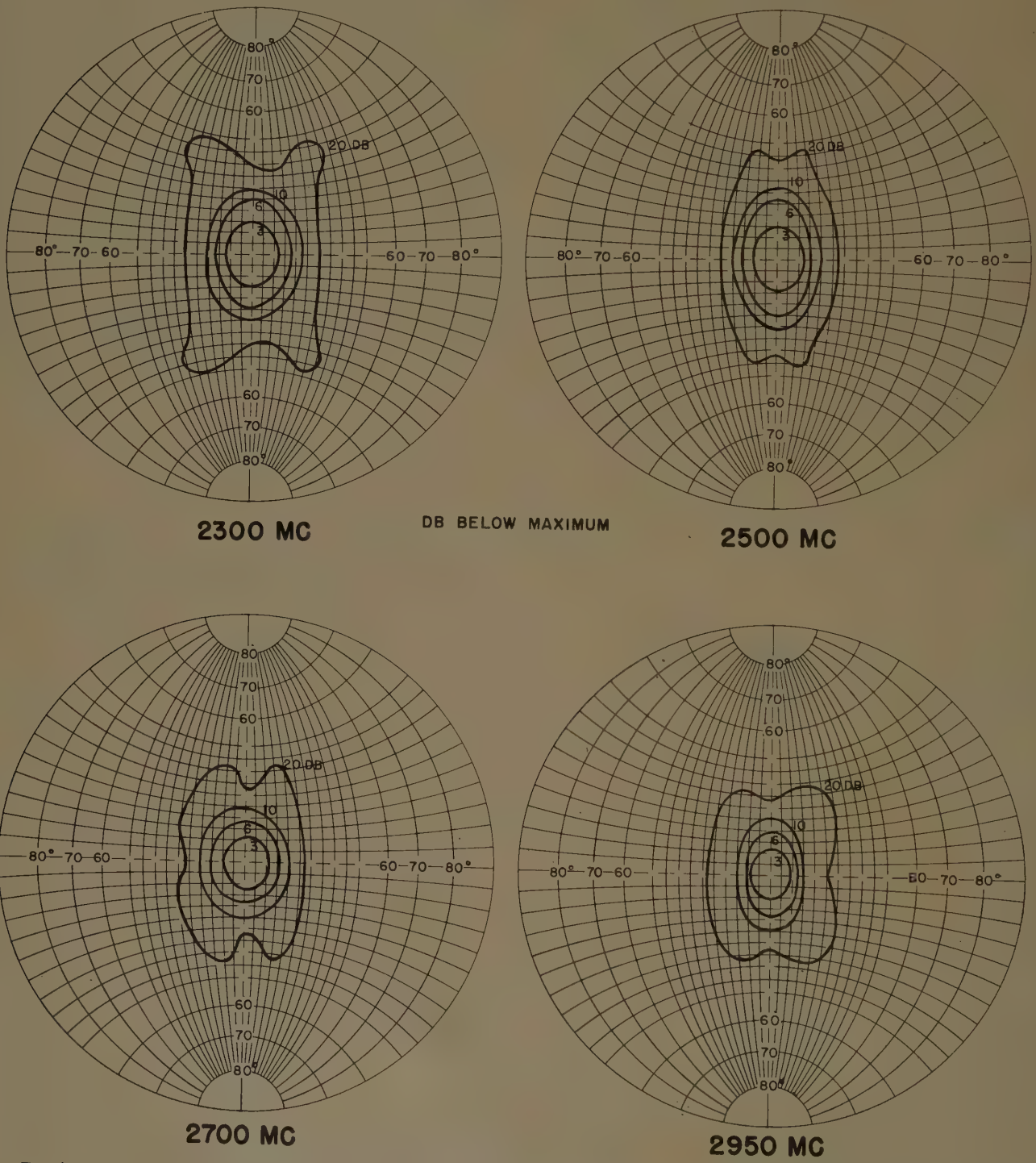

Fig. 4—Resultant radiation pattern of experimental symmetrical TAHA. Shown are all contour lines for −20 db field strength level and above.

been found as a receiving antenna for HF long-range communication systems, making use of the reflection of electromagnetic waves at the ionosphere. A simple and effective solution for the design of the feed section was found in the so-called ridge type waveguide depicted in Fig. 5. The two ridges taper gradually into the throat of the horn. The cone between them is isolated at its tip and represents the output terminal. Another difficult design problem, if not the most difficult, is the design of the wire grids which replace the sheet metal walls of conventional horns for obvious practical reasons.

The electrical performance of the completed antenna, a photograph of which is shown in Fig. 6, conformed essentially to the expectations derived from model measurements. The major dimensions are given in the sketch of Fig. 7. A SWR of 4:1 can be tolerated in receiving applications because it corresponds to a mismatch loss of only 2 db. Using this criterion, the frequency range covered is 6.5 to 23 mc. Fig. 8 shows a sample of radiation patterns measured by means of a helicopter.[3] Fig. 9 summarizes the pattern measurements as to directivity gain and half-power beamwidth in azimuth and elevation vs frequency.

[3] H. Brueckmann, "Helicopter measures antenna patterns," *Electronics*, vol. 28, pp. 134–136; November, 1955.

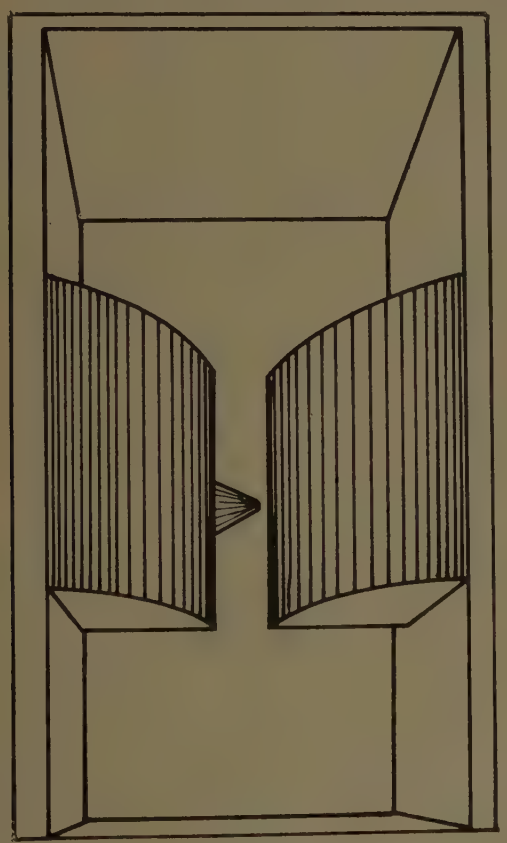

Fig. 5—Ridge waveguide feed system. (Perspective view.)

Fig. 6—Full-scale TAHA.

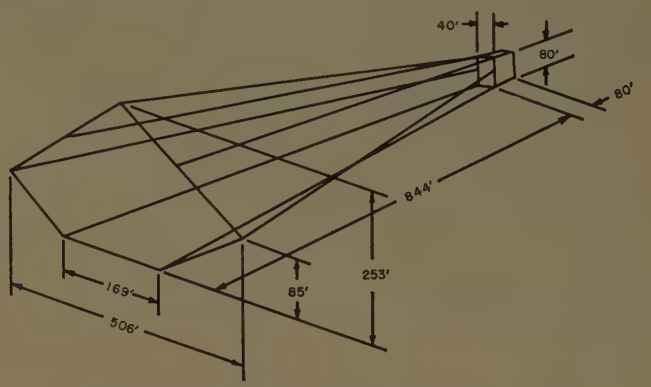

Fig. 7—Major dimensions of high-frequency TAHA.

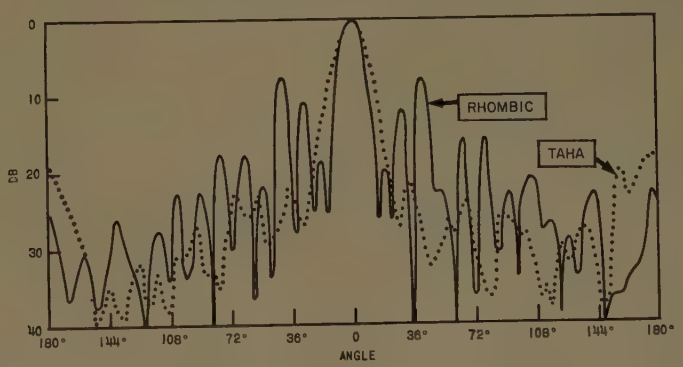

Fig. 8—Comparison of measured patterns of the TAHA and of the rhombic at 12 mc. ——— Azimuthal pattern of rhombic (E_ϕ); envelope of patterns for $\psi = 6°, 9.2°, 14.0°$. ····· Azimuthal pattern of TAHA (E_ϕ); envelope of patterns for $\psi = 5.5°, 11.2°, 15.5°$.

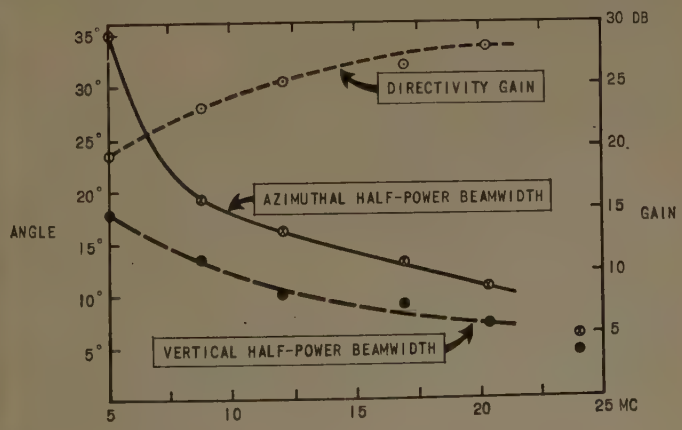

Fig. 9—Characteristics of TAHA vs frequency.

Fig. 10 illustrates a certain pattern characteristic of TAHA which distinguishes it favorably from most other type antennas, including rhombics. The characteristic referred to is the change of the elevation angle of the main lobe maximum vs frequency. Usually, this angle is about inversely proportional to frequency. Such a strong dependance on frequency is not desirable from the viewpoint of adaptation to normal ionospheric propagation. The "angle of fire" of TAHA depends less strongly on frequency and comes closer to an optimum dependence. The reason is that the center of gravity of the excitation in the aperture decreases in height above ground with increasing frequency. The main advantage of TAHA over a rhombic of equal gain lies, of course, in the much lower sidelobes which differ by a factor of 10 to 15 db.[4] The disadvantage is the higher cost of construction. The experience with the first full-scale antenna has uncovered a number of possibilities to reduce the cost; for example, by arranging the supporting towers differently. Others are being investigated, such as shortening of the horn. A current model investigation of horns for dual-polarization employing the TAHA principle shows promise of success. This would permit substituting one horn antenna operated in polarization diversity reception for two large rhombic antennas operated in space diversity reception.

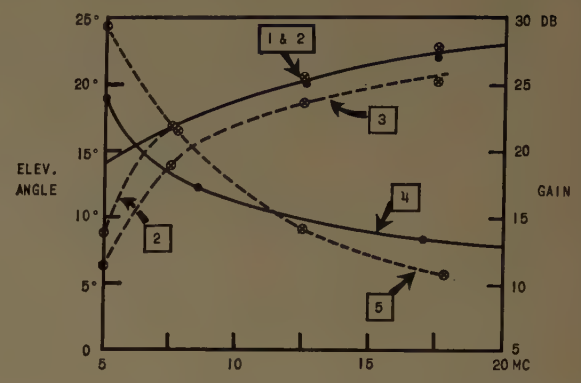

Fig. 10—Comparison of TAHA vs rhombic. Measured gain: 1) TAHA directivity. 2) Rhombic directivity. 3) Rhombic power. Elevation angle: 4) TAHA major lobe. 5) Rhombic major lobe. Rhombic referred to has leg length of 400 feet, tilt angle of 71° and height of 130 feet.

[4] H. Brueckmann," Suppression of undesired radiation from directional HF antennas and associated feed lines," PROC. IRE, vol. 46, pp. 1510–1516; August, 1958.

The Measurement of Self and Mutual Impedances*

E. ALTSHULER†

Summary—**There are two well-known methods which can be used to measure the self and mutual impedances of identical, parallel antennas, the symmetric-antisymmetric method, and the open circuit-short circuit method.[1] In principle, these methods are quite simple and straightforward. In practice, however, major difficulties arise in both methods. In this paper, it is shown that by using a part of each method, the self and mutual impedances can be measured quite easily and to a good degree of accuracy.**

CONSIDER the set of linear equations which relate the driving voltages, input currents, and self and mutual impedances of identical antennas.

$$V_{10} = (Z_{S1} + Z_{L1})I_{10} + Z_{12}I_{20}$$
$$V_{20} = Z_{21}I_{10} + (Z_{S2} + Z_{L2})I_{20}.$$

Z_{L1} and Z_{L2} are impedances which may be placed in series with Z_{S1}, or Z_{S2}. Since the antennas are identical, $Z_{S1}=Z_{S2}$. Since the antennas constitute a reciprocal network, $Z_{12}=Z_{21}$.

In the symmetric-antisymmetric method, both antennas are driven with equal voltages, first in phase (symmetric), then 180° out of phase (antisymmetric), and the corresponding symmetric and antisymmetric input impedances are measured. $Z_{L1}=Z_{L2}=0$.

Symmetric case:

$$V_{10} = Z_{S1}I_{10} + Z_{12}I_{20}$$
$$V_{10} = Z_{12}I_{10} + Z_{S1}I_{20}.$$

It follows,

$$Z^S = \frac{V_{10}}{I_{10}} = Z_{S1} + Z_{12}.$$

* Received by the PGAP, May 19, 1960.
† Gordon McKay Lab., Harvard University, Cambridge, Mass.
[1] R. W. P. King, "The Theory of Linear Antennas," Harvard University Press, Cambridge, Mass., pp. 346–347; 1956.

Antisymmetric case:

$$V_{10} = Z_{S1}I_{10} + Z_{12}I_{20}$$

$$-V_{10} = Z_{12}I_{10} + Z_{S1}I_{20}.$$

It follows,

$$Z^a = \frac{V_{10}}{I_{10}} = Z_{S1} - Z_{12}.$$

Therefore,

$$Z_{S1} = \frac{Z^S + Z^a}{2}$$

$$Z_{12} = \frac{Z^S - Z^a}{2}.$$

This procedure is in general quite difficult to carry through experimentally, especially if identical antennas are not driven by identical transmission lines. Probably one of the best methods that can be used to determine whether the antennas are driven 180° out of phase is to place a small auxiliary probe midway between them and then adjust the phase and amplitude of one of the driving voltages until a null is detected by this probe. This is an indication that the fields midway between the antennas cancel and therefore the input currents as well as the driving voltages are 180° out of phase. Since the null is very sharp, the antisymmetrical condition can be obtained quite precisely. The phase and amplitude of one of the driving voltages can be varied quite easily by inserting a line stretcher and variable attenuator in one of the transmission lines driving the antenna. A similar procedure cannot be used to obtain the symmetric condition since a broad maximum exists at the auxiliary probe. In order to obtain this condition, the line stretcher could be changed by 180° from the antisymmetric condition, but in general there are small reflections associated with line stretchers, thereby making it difficult to produce an accurate 180° shift without also slightly changing the amplitude. Naturally, it is not impossible to drive two antennas symmetrically. However, it is quite difficult to accomplish this precisely.

In the open circuit-short circuit method, one antenna is driven while the other remains parasitic; therefore, $V_{20}=0$. For the driven antenna, $Z_{L1}=0$.

With the input terminals of the parasitic antenna open circuited, the input impedance of the driven antenna is measured.

$$Z_{\text{O.C.}} = \frac{V_{10}}{I_{10}} = Z_{S1}; \qquad Z_{L2} = \infty; \qquad I_{20} = 0.$$

Thus, the self impedance of the antenna is simply the input impedance of the driven antenna with the parasite open circuited. The open circuit condition is obtained by locating a small current probe at the input of the parasite and then adjusting the position of a short circuit on the transmission line which feeds the parasite so that a null appears at the input. The input impedance of the driven antenna is then measured with the parasite short circuited.

$$Z_{\text{S.C.}} = \frac{V_{10}}{I_{10}} = Z_{S1} - \frac{Z_{12}^2}{Z_{S1}}; \qquad Z_{L2} = 0.$$

The short circuit condition is most easily obtained by simply short circuiting the input terminals of the parasite. Solving for Z_{12},

$$Z_{12} = \pm \sqrt{Z_{S1}(Z_{S1} - Z_{\text{S.C.}})}.$$

As can be seen, there exists an ambiguity in the sign of the mutual impedance. In order to determine the correct sign, an additional measurement is required. The principal limitation of this method is that it cannot be used to measure small mutual impedances accurately. The determination of the mutual impedance depends on the difference of the input impedances of the driven antenna when the parasite is open and short circuited. This difference, which is usually quite small, is then multiplied by the self impedance, which is relatively large. In this process, the accuracy of the mutual impedance is reduced.

By using a part of each of the previous methods, the self and mutual impedances can be measured quite easily and to a good degree of accuracy. As has been stated earlier, the self impedance of an antenna is simply the input impedance of the driven antenna when the parasite is open circuited. This measurement is quite exact. The antisymmetric impedance which can also be measured quite precisely is by definition:

$$Z^a = Z_{S1} - Z_{12}.$$

Therefore, the mutual impedance is simply the difference between Z^a and Z_{S1}.

An Island as a Natural Very-Low-Frequency Transmitting Antenna*

M. G. MORGAN†, SENIOR MEMBER, IRE

IN thinking about how to generate whistlers artificially, it has occurred to me that an island of suitable size and shape, extending through the conducting sea, may constitute a naturally resonant, VLF slot antenna of high quality. Following this line of reasoning, I thought first of the annular Pacific atolls, but knowing of the fresh-water lenses in them, rejected them as being too pervious to water to be satisfactory insulators. Also, of course, they are not found in suitable latitudes for generating whistlers. The Pacific atolls are built upon submerged volcanic cones and this led me to think of Deception Island (Fig. 1, opposite) in the SubAntarctic, a remarkable, similarly shaped, volcanic island in which the volcanic rock extends above the surface; and which is located in the South Shetland Islands where the rate of occurrence of natural whistlers has been found to be very great. Deception Island is a thin annulus surrounding a lagoon which has a single narrow entrance through the ring. The length of the island is about 30 km which is a half-wavelength at 5 kc, a frequency at which natural whistlers are very strong. To a rough approximation, the radiation pattern would be that of a vertical monopole, that is, proportional to the sine of the zenith angle.

Taking the conductivity of sea water to be 4 mhos/meter and the relative dielectric constant to be 80, one calculates the ratio of conduction current density to displacement current density ($\sigma/\omega\epsilon$) at 5 kc to be 1.8×10^5, so that the sea is certainly a good conductor. The "depth of penetration" ($\sqrt{2/\omega\mu\sigma}$) is only 3.5 meters so that depths in the lagoon, which run from 110 meters near the shore to 165 in the middle, appear to be adequate. The entrance, called Neptune's Bellows, is 635 meters wide. For half of this width, the water is only 3 to 4 meters deep, but there is a channel about 150 meters wide which is 25 meters deep. The salinity in the lagoon does not differ significantly from that of the outside sea.

The island appears to be constituted mainly of massive tuff, a geological material and form which could be very favorable to its being a good insulator. The quality of the insulator most likely depends entirely upon the water content due to porosity, stratification, and fracturing. It would be a relatively simple matter to make an *in situ* measurement of the driving point impedance of the proposed island antenna over a range of frequency and this would give a decisive answer to the critical question of the quality of the island as an insulator. The highest impedance across a half-wave resonant slot is found at its center which, for the island antenna, would be between the outside sea and the lagoon at a point opposite to the entrance to the lagoon, a point aptly named Telefon Bay.

At Telefon Bay, it is 2 km across the island to the outside so that from the middle the connecting lines to the sea terminals would each be 1 km long. The inductive reactance of these leads will not be negligible. Inasmuch as the current will not return in the ground directly under the wires if the quality of the island as an insulator is sufficiently good (the wires should be insulated from the moist surface), we use the expression $(\mu/\pi)\ \ln\ (b/a)$ for the inductance per unit length of a parallel wire transmission line of conductor separation b and radius a. We take $b=2l$ where l is the length from the center of the island to a point along either wire and obtain the total inductance as

$$\frac{\mu}{\pi}\int_0^l \ln\frac{2l}{r}\,dl = \frac{\mu}{\pi}\,l\left(\ln\frac{2l}{r}-1\right).$$

For $l=1$ km, $r=1$ mm (approximately No. 12 American wire gauge), and $\mu=4\pi\times10^{-7}$, the inductance is 5.4 mh which leads to a reactance of 170 ohms at 5 kc.

The inductance of the connecting wires can be reduced by running multiple wires in parallel. For uniformally spaced wires, the inductance is given by

$$\left[\frac{L+(n-1)M}{n}-lk\times10^{-7}\right]$$

where L is the inductance without the added conductors, M is the mutual inductance of any pair of adjacent conductors, n is the number of conductors on each side, and k is given by

n	2	4	6	8	10
k	0	0.621	1.18	1.66	2.05.

M is given by

$$2l\times10^{-7}\left[\ln\frac{2l}{d}-1\right]$$

* Received by the PGAP, June 8, 1960.
† Thayer School of Engrg., Dartmouth College, Hanover, N. H

Fig. 1—Deception Island. There are fumaroles on the beach at Whalers Bay and De Mayo Bay. In 1930 an earthquake occurred at Whalers Bay, lowering the bottom nearly 5 metres.

where d is the separation of adjacent wires. The following calculations show that the inductive reactance can be lowered to 35 ohms by using 10 wires, 10 meters apart, which would certainly be practical.

$d=5$ meters

n	2	4	6	8	10	20
L (mh)	3.20	2.04	1.62	1.38	1.20	0.90
X (ohms at 5 kc)	101	64	51	43	38	28

$d=10$ meters

n	2	4	6	8	10
L (mh)	3.13	1.93	1.50	1.25	1.11
X (ohms at 5 kc)	98	60	47	39	35

The resistance of the wires will be negligible and the connections to the sea present no problems either. To investigate the latter point, we make use of the fact that if the capacitance between two electrodes is C, the resistance between them when immersed in a medium of conductivity σ and dielectric constant ϵ, is $\epsilon/\sigma C$. The capacitance of an isolated sphere of radius r is $4\pi\epsilon r$ giving the resistance to a surrounding, boundless, conducting medium as $1/4\pi\sigma r$. For $\sigma=4$, the resistance is 1 ohm for $r=1/16\pi$ or a sphere whose area is but fifty square centimeters which is less than the surface area of one-meter of wire of 1 mm radius. Thus, though the configuration has been idealized, it is obvious that it will suffice to run each wire out a few meters from shore.

Acknowledgment

I am especially grateful to Prof. E. C. Jordan of the University of Illinois for the stimulation which produced this idea, and for his help and encouragement in analyzing it.

Notes

1) For a general description of Deception Island, see "Sailing Directions for Antarctica," U. S. Navy Hydrographic Office, pp. 101–104, 1943, and supplement of 1959; or "The Antarctic Pilot," U. K. Admiralty Hydrographic Dept., pp. 164–166, 1948.

For a detailed scientific description, see "Contribucion al Conocimiento del Sector Anartico Argentino," Instituto Antartico Argentino, publ. no. 1, 1955; and "Contribucion a la Geologia de la Antartida Occidental," Instituto Antartico Argentino, publ. no. 2, 1956.

2) MKS rationalized units are used. The formula for the reduction of inductance by using multiple wires, is from *Circular 74*, U. S. National Bureau of Standards, p. 249; 1924 (reprinted 1937).

Contributors

Wallace L. Anderson (M'58) was born in Adams, N. D., on September 2, 1922. During World War II, he served as an officer in the Airways Communications System of the Air Force. He received the B.S.E.E. degree from the University of North Dakota, Grand Forks, in 1948, and the M.A. degree in physics from Rice Institute, Houston, Tex., in 1957.

W. L. Anderson

He worked for the McCollum Exploration Company, Houston, for several years, doing field and research work. He is presently a research associate in the Electrical Engineering Division of the University of New Mexico Station, and is a doctoral candidate in the Department of Electrical Engineering.

Mr. Anderson is a member of the Society of Exploration Geophysicists, Sigma Tau, and Sigma Xi.

❖

Norman J. Beyers was born in Pana, Ill., on February 12, 1929. He received the B.S. degree in meteorology and climatology from the University of Washington, Seattle, in 1956.

N. J. Beyers

From 1948 to 1952, he served in the United States Navy and worked in naval aerology. He joined the United States Army, White Sands Signal Agency, White Sands, N. M., in 1956, and has been engaged in research in microwave propagation and atmospheric electricity.

Mr. Beyers is a member of the El Paso Chapter of the American Meteorological Society.

❖

Jon W. Eberle was born in Chillicothe, Ohio, on August 28, 1934. He received the B.S.E.E. and M.S.E.E. degrees in 1957 and 1960, respectively, from The Ohio State University, Columbus.

J. W. Eberle

Since 1957, he has been employed as a Research Associate at the Antenna Laboratory of The Ohio State University Research Foundation, where he has been engaged in research in reflectivity studies and antennas.

Mr. Eberle is a member of Sigma Xi.

❖

Peter Foldes (M'58) was born in Budapest, Hungary, on April 8, 1928. He received the B.S.E.E. degree from the Technical University of Budapest in 1950.

P. Foldes

From 1950 to 1956, he was a research engineer at the Hungarian Telecommunication Research Institute, and from 1953–1956, on a part-time basis, was also a lecturer on antennas at the Technical University of Budapest. In 1957, he joined RCA Victor Co., Ltd., Montreal, Canada. His work has been mostly in the field of antenna, propagation, and system engineering studies. Since 1958, he has been responsible for the theoretical aspects of the microwave subsystem in a wide band microwave communication equipment.

❖

Robert C. Hansen (S'47–A'49–M'55–SM'56) was born on August 3, 1926, in St. Louis, Mo. He attended the Missouri School of Mines and Metallurgy, Rolla, from which he received the B.S.E.E. degree in 1949. He received the M.S. and Ph.D. degrees in 1950 and 1955, respectively, from the University of Illinois, Urbana.

R. C. Hansen

While at the University of Illinois, he worked at the Antenna Laboratory on ferrite loops and streamlined airborne antennas. From 1955 to 1959, he was at the Microwave Laboratory of Hughes Aircraft Company, Culver City, Calif., where, as senior staff engineer, he worked on surface-wave antennas, slot arrays, and related fields. In 1959, he became senior staff engineer in the Telecommunications Laboratory of Space Technology Laboratories, Los Angeles Calif., where he is at present.

Dr. Hansen is a member of the American Physical Society, Commission VI of URSI, Tau Beta Pi, Sigma Xi, Eta Kappa Nu, and Phi Kappa Phi.

❖

Julius Kane was born on January 23, 1935, in Vorozenh, Russia. He received the B.A. degree from Brooklyn College, Brooklyn, N. Y. in 1954, majoring in physics.

Following graduation he was employed as a radiation physicist in cancer research. Subsequently, he spent a summer at Sylvania Electric Products, Bayside, L. I., N. Y., as a research physicist, working on problems of electroluminescent displays. He was a lecturer in physics at the College of the City of New York, and has done post-graduate work at New York University, New York, N. Y., where he received the Ph.D. degree in applied mathematics. Currently, he is a staff consultant with Dorne and Margolin, Inc., Westbury, L. I., N. Y., engaged in research on antennas and propagation. In July, 1960, he became an associate professor of Electrical Engineering at the University of Rhode Island, Kingston.

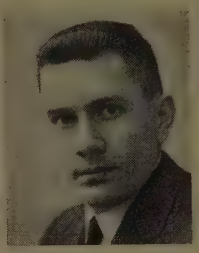

J. Kane

Dr. Kane is a member of the American Physical Society and the American Mathematical Society.

❖

Aharon A. Ksienski (S'53–M'58) was born on June 24, 1924, in Warsaw, Poland. He received the M.S. degree in 1952 and the Ph.D. degree in 1958, both in electrical engineering from the University of Southern California, Los Angeles.

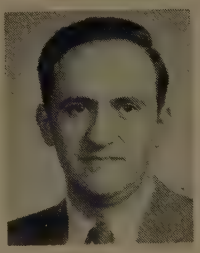

A. A. Ksienski

From 1948 to 1951, he was in charge of an Aircraft Electrical School in the Israeli Air Force. From 1951 to 1952, he attended the University of Southern California as a graduate student and a part time member of the teaching staff. Between 1953 and 1955, he was with Wiancko Engigineering Company, Pasadena, Calif., engaged in developing instrumentation systems for the measurement of various flight parameters and in the design of electromechanical transducers. In 1955, he returned to the University of Southern California as a lecturer in mathematics and electrical engineering, and continued graduate research in the field of antennas. After graduating in 1958, he joined the Antenna Research Department in the Microwave Laboratory of Hughes Aircraft Company, Culver City, Calif., where he is presently a senior staff engineer engaged in research in the field of antennas and antenna systems.

Dr. Ksienski is a member of Phi Kappa Phi, Tau Beta Pi, Eta Kappa Nu, and Sigma Xi.

Curt A. Levis (S'48–A'52–M'57–SM'59) was born in Berlin, Germany, on April 16, 1926. During World War II he served in the U. S. Navy as an electronic technician and subsequently studied electrical engineering at Case Institute of Technology, Cleveland, Ohio, where he received the B.S. degree in 1949. During this time he was also employed as studio engineer at Radio Station WSRS.

C. A. Levis

He was a Gerard Swope Fellow at Harvard University and received the M.A. degree in engineering science and applied physics there in 1950, and the Ph.D. in electrical engineering at The Ohio State University, Columbus, in 1956.

Since 1950, Dr. Levis has been employed at the Antenna Laboratory of The Ohio State University. His present position is associate supervisor of the Antenna Laboratory and associate professor of electrical engineering.

❖

Donald R. McCoy (A'54–M'58) was born in Burkeburnette, Tex., on August 30, 1920. He attended The Ohio State University, Columbus, from which he received the B.S.E.E. degree in 1951 and the M.S. degree in 1956.

D. R. McCoy

He was an instructor in the Signal Corps Radar schools from 1942 to 1945, and worked with the Signal Corps Engineering Laboratory Development Detachment from 1945–1946. He was with the Antenna Laboratory of The Ohio State University Research Foundation from 1949–1956. He joined the General Electric Company, Syracuse, N. Y., in 1956, and is presently engaged in Systems Engineering.

Mr. McCoy is a member of Sigma Xi.

❖

Ralph J. Rainey (S'59) was born in Albuquerque, N. M. on April 18, 1931. He received the B.S.I.A. degree in 1953 and the B.S.E.E. degree in 1959, both from the University of New Mexico, Albuquerque. He served as a rated officer in the Air Force for three years from 1953 to 1956.

R. J. Rainey

Since September, 1958, he has been employed in the Electrical Engineering Division of the Engineering Experiment Station, University of New Mexico, where he is engaged in tropospheric propagation studies.

Mr. Rainey is a member of Sigma Tau and an associate member of Sigma Xi.

❖

Sheldon S. Sandler, for a photograph and biography, please see p. 453 of the July, 1960 issue of these Transactions.

❖

Howard E. Shanks was born in Los Angeles, Calif., on January 28, 1933. He attended Pasadena City College, Pasadena, Calif., from 1950 to 1952, and then transferred to the California Institute of Technology, Pasadena, where he received the B.S.E.E. degree in 1954. In 1956, he received the M.S. degree in physics from the University of California at Los Angeles under the Hughes Fellowship program.

He was with the Antenna Research Department of the Hughes Aircraft Company, Culver City, Calif., for six years and contributed to research in the areas of UHF-VHF antennas, scattering cross sections, circular-aperture antennas, flush-mounted radar antennas, arbitrarily polarized radiators, advanced antenna techniques, and pattern synthesis methods. He joined American Systems, Inc., Inglewood, Calif., in March, 1960. He is the author of numerous technical reports and journal articles, and has seven patent applications in the field of antennas and microwave devices. He is a lecturer in electrical engineering at the University of Southern California, Los Angeles.

H. E. Shanks

Mr. Shanks is a member of Tau Beta Pi and RESA.

❖

Carlton H. Walter (S'48–A'51–M'56–SM'59) was born at Willard, Ohio, on July 22, 1924. He received the B.E.E. degree at The Ohio State University, Columbus, in June, 1948, at which time he joined the staff of The Ohio State University Antenna Laboratory. He did graduate work while employed at the Antenna Laboratory and received the M.S. degree in physics in March, 1951 and the Ph.D. in electrical engineering in June, 1957.

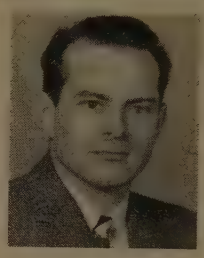

C. H. Walter

He is now an associate supervisor at The Ohio State University Antenna Laboratory and an assistant professor in the Electrical Engineering Department.

Dr. Walter is a member of Sigma Xi, Tau Beta Pi, Eta Kappa Nu, and Sigma Pi Sigma, and a Registered Professional Engineer in Ohio.

FOR INFORMATION CONCERNING ADVERTISING RATES

Contact

MR. DELMER C. PORTS
Jansky and Bailey, Inc.
1339 Wisconsin Avenue N.W.
Washington 7, D.C.

Telephone: Federal 3-4800

INSTITUTIONAL LISTINGS

The IRE Professional Group on Antennas and Propagation is grateful for the assistance given by the firms listed below, and invites application for Institutional Listing from other firms interested in the field of Antennas and Propagation.

AERO GEO ASTRO CORP., 1200 Duke St., Alexandria, Va.
Research and Development; Antennas; Transponders; Command Receivers; Augmenters; Telemetry-Radar.

ANDREW CORPORATION, P.O. Box 807, Chicago 42, Ill.
Antennas, Antenna Systems, Transmission Lines, Development and Production.

ANTLAB, INC., 6330 Proprietors Rd., Worthington, Ohio
Antenna Pattern Range Systems—Recorders & Mounts, & Telemetry Servo Pedestals.

BLAINE ELECTRONETICS, INC., 14757 Keswick St., Van Nuys, Calif.
Antennas, Paraboloids, Scale Models, Antenna Radiation Pattern Measurement Towers.

GABRIEL ELECTRONICS, Division of The Gabriel Company, Main & Pleasant Sts., Millis, Mass.
Research, Engineering and Manufacture of Antenna Equipment for Government and Industry.

HUGHES AIRCRAFT COMPANY, Florence and Teale Sts., Culver City, Calif.
Res., Dev., Mfg.: Radar Systems & Components; Antennas, Tubes, Radomes, Solid-State Devices.

I-T-E CIRCUIT BREAKER CO., Special Products Div., 601 E. Erie Ave., Philadelphia 34, Pa.
Design, Development and Manufacture of Antennas, and Related Equipment.

JANSKY & BAILEY, INC., An Affiliate of Atlantic Research Corp.,
1339 Wisconsin Ave., N.W., Washington, D. C.
Complete Engineering Services for Antennas and Propagation Programs.

MARK PRODUCTS CO., 5439 W. Fargo Ave., Skokie, Ill.
Antennas for Two-Way Communications, Grid Parabolas, Research & Development.

TECHNICAL APPLIANCE CORP., 1 Taco St., Sherburne, N. Y.
Des., Dev., & Mfg.: Antennas & Antenna Systems for Communications, Telemetry, & Tracking.

WEINSCHEL ENGINEERING COMPANY, INC., Kensington, Md.
Antenna Pattern Receivers; Bolometer Amplifiers; Modulated Microwave Sources;
Insertion Loss Measuring Systems.

WHEELER LABORATORIES, INC., Great Neck, N. Y.; Antenna Lab., Smithtown, N. Y.
Consulting Services, Research and Development, Microwave Antennas and Waveguide Components.

The charge for Institutional Listing is $25 for one issue or $100 for six consecutive issues (one year). Application may be made to the Technical Secretary, The Institute of Radio Engineers, 1 East 79th Street, New York 21, N. Y.